UNITED STATES DEPARTMENT OF THE INTERIOR

GEOLOGICAL SURVEY

Geometry, Emplacement History, Petrography, and Chemistry of a Basaltic Intrusive Complex, San Rafael and Capitol Reef Areas, Utah

Anne E. Gartner[1]

Open-File Report 86-81

1. U.S. Geological Survey, Menlo Park, CA. 94025

UNITED STATES DEPARTMENT OF THE INTERIOR

DONALD PAUL HODEL, Secretary

GEOLOGICAL SURVEY

Dallas L. Peck, Director

For additional information write to:

U.S. Geological Survey
IGP Branch, Room 2153A MS 910
345 Middlefield Road
Menlo Park, CA 94025

Copies of this report can be purchased from:
Open-File Services Section
U.S. Geological Survey
Box 25425, Federal Center
Denver, CO 80225

Call (303) 236-7476

TABLE OF CONTENTS

LIST OF ILLUSTRATIONS

Inside Back Cover:

Plate 1. Map of Intrusive Complex, San Rafael and Capitol Reef area, Utah

LIST OF TABLES

ABSTRACT

This report describes the geometry, emplacement history, petrography, and chemistry of a basaltic intrusive complex in the San Rafael and Capitol Reef areas, Utah. The complex consists of diabasic dikes, breccia bodies, and diabasic and syenitic sills exposed in Jurassic sedimentary strata of the San Rafael Group on the northwest edge of the Colorado Plateau between the San Rafael and Waterpocket monoclines. The complex is 60 km long in a N. 20° E. direction and has a maximum width of 22 km. Thickness of cover at the time of emplacement determined from stratigraphic relations was no more than 2.5 km, but likely considerably less. K-Ar radiometric dates of a diabase (3.8±0.2 m.y.) and a syenite (4.6±0.2 m.y.) from the complex are similar in age to a nearby basalt flow (3.8±0.2 m.y.), indicating that the complex may have been the plumbing system of a now-eroded volcanic terrane.

Relative order of mineral abundances of diabase in the dikes are: augite, labradorite, olivine, biotite, orthoclase, and kearsutite. Accessory and alteration minerals include analcite, apatite, titano-magnetite, thomsonite, natrolite, and varying amounts of serpentine, chlorite, calcite, and clay minerals. Hydrothermal alteration is extensive throughout the complex.

The intrusions are resistant to erosion, and details of dike morphology are remarkably well preserved. Field data include numerous measurements of dike thickness (average 120 cm), outcrop length (highly variable and map-scale dependent), strike (typically between N. 25° W. and N. 15° E., average N. 13° W.), local dike-propagation direction (50 percent range between 0° and 25° of horizontal), occurrences of breccias, and strikes of systematic joints in the host rock. Outcrop patterns of the 153 dikes identified at the map-compilation scale of 1:48,000 are discontinuous and composed of about 1200 smaller dike segments.

Dike emplacement may have occurred as either magma flow into, and dilation of, preexisting fractures or flow into cracks both opened and guided by the pressure of magmatic injection relative to principal stress orientations. In the study area evidence exists for emplacement by both processes. The en echelon geometry of the dikes can occur when an initial crack, propagating in a principal stress plane, becomes rotated about an axis parallel to the propagation direction. The en echelon cracks can then grow along twisting surfaces into a new plane also roughly normal to the minimum principal stress. The pattern of dike emplacement provides a reference frame for interpretation of stress fields in the transition region between the Colorado Plateau and the Basin and Range Province during a part of Pliocene history.

INTRODUCTION

Scope of the Investigation

This report describes the geometry, distribution, and emplacement history of a basaltic intrusive complex in east-central Utah, and provides a framework for the interpretation of its petrography and geochemistry. Work is in progress to obtain K-Ar radiometric ages, major and minor element data, and to characterize processes of magma evolution in a continental crustal setting. Petrographic and geochemical interpretations included in this report are based on data available at the time of compilation and are, accordingly, preliminary.

Mapping, geochronology, and chemical data necessary for detailed interpretation of the geometry and emplacement history of the San Rafael and Capitol Reef areas intrusive complex are the goal of this study. The following sections are based on present field studies and the literature, where available, in an attempt to synthesize the state of knowledge at the time of this writing.

Previous Work

Early geologic surveys of the Colorado Plateau by Gilbert (1877), Dutton (1880), and Powell (1875) describe the San Rafael Swell and the high plateaus and desert to the south and west. Subsequent work was undertaken to investigate mineral resources of the area (Lupton, 1913; Gilluly and Reeside, 1928; Gilluly, 1929; Smith and others, 1963; and Hawley and others, 1968); these studies mention only briefly the intrusive rocks that form the subject of this report.

Gilluly (1927) was the first to provide a general description of the chemistry, mineralogy, and petrology of the dikes, sills, and plugs. He noted that the diabases of the dikes and sills are macroscopically and microscopically similar, and concluded from the field associations that they are essentially comagmatic and contemporaneous in age. Gilluly (1927) also described the syenite of the sills and concluded that it was a product of a second injection of magma. Gilluly (1929) and Gilluly and Reeside (1928) described and interpreted the stratigraphy and correlated strata of the region with rocks elsewhere on the Colorado Plateau. Wilshire (1967) collected and analyzed rock samples from a dike and sill near Hebes Mountain (fig. 1) and a second sill near Cedar Mountain (fig. 1). Williams (1983) described the petrology and chemistry of a 29-meter-thick composite sill at Cedar Mountain (fig. 1). He concluded that the igneous assemblage was produced by in-situ differentation and the interaction of silicate-liquid immiscibility and liquid fractionation.

Smith and others (1963) investigated the regional geology and stratigraphy of the Capitol Reef area. They state that the dikes strike within 15 degrees of north, paralleling a prominent joint trend in the host rock. The igneous intrusive rocks of the Capitol Reef area are mineralogically and chemically similar to the analcite diabase of the San Rafael Swell area (Gilluly, 1927). Billingsley and others (1981) published a 1:62,500-scale geologic map of the Capitol Reef National Park and vicinity, Utah. This map was compiled from previous work and a photogeologic interpretaion of the area. E. H. McKee (written communication, 1984) has provided K-Ar ages of five selected basaltic rocks from the San Rafael and Capitol Reef areas in Utah.

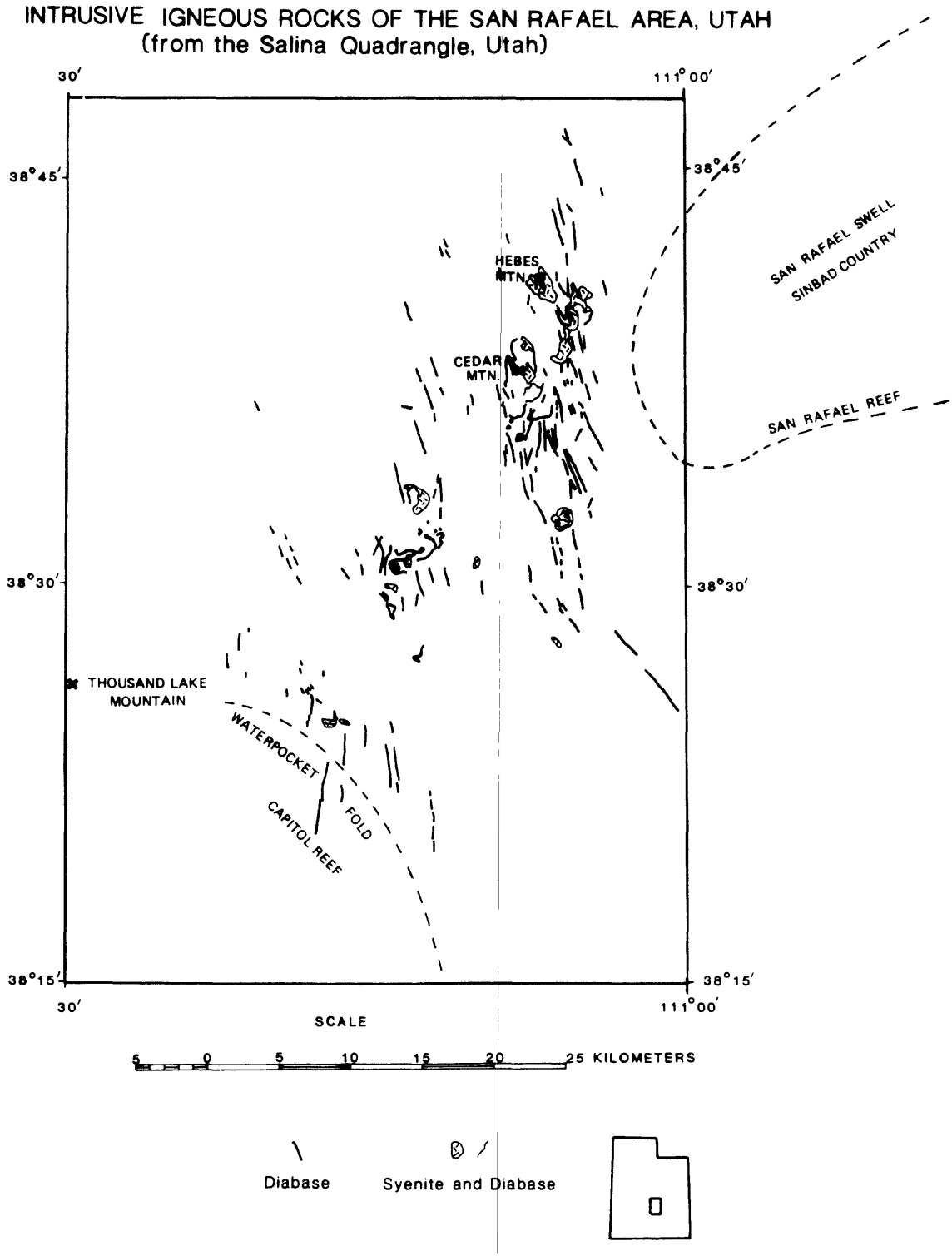

Figure 1. Location of the intrusive complex in south central Utah. Dashed lines represent the edges of the San Rafael Swell and Waterpocket Fold modified from Williams and Hackman (1971), 1:250,000 map scale.

Location

The basaltic intrusive complex is located approximately 230 km southeast of Salt Lake City, Utah, between 38°20'00" and 38°50'00" N. latitude and 111°00'00" and 111°26'00" W. longitude (fig. 1). The area is approximately 1200 km² with elevations ranging from 1500 to 2000 m. The complex consists of diabasic dikes and breccia bodies and related diabasic and syenitic sills exposed within eroded Jurassic sedimentary strata on the northwest edge of the Colorado Plateau, west of the San Rafael monocline and straddling the Waterpocket monocline. The intrusive complex is 60 km long in a direction N. 20° E and has a maximum width of 22 km. Because the intrusive rocks are relatively resistant to erosion, and vegetation is minimal in the semi-arid climate, exposures are excellent.

The northern boundary of the study area can be reached from Salina, Utah, by driving east on Highway 70 for 43 miles, then south approximately 3 miles on a maintained dirt road. The remainder of the study area is accessible with a 4-wheel-drive vehicle on semi-maintained dirt roads and jeep trails.

Definitions

Dikes are tabular, commonly vertical or steeply dipping igneous intrusions that cut across the bedding or foliation of country rock, whereas sills are tabular igneous intrusions that parallel the planar structure of the surrounding rock. In the San Rafael and Capitol Reef areas the regional bedding is nearly horizontal.

Some terms used to describe tabular bodies are illustrated in figure 2. Many sheet intrusions, particularly near their peripheries, are composed of discrete fingers of igneous rock pointing in the direction of propagation (Pollard and others, 1975). Fingers (dike segments) grow in a plane perpendicular to the least principal compressive stress. Offset dike segments can develop as the intrusive body moves through a region where the stress changes orientation. As the dike grows, the offset segments coalesce, leaving a step on the dike wall. Offsets in dikes form parallel to the finger lengths and, therefore, are also parallel to the direction of propagation. Figure 2 (insert) illustrates the offset of dike segment fingers and the local propagation direction. In map view, dike thickness is measured along the lesser dimension, and segment length is measured along the greater dimension of the segment. Dike emplacement length is measured along the dominant magma transport direction. Offset is measured between segments in the direction perpendicular to segment strike, and separation (or overlap) is measured parallel to strike. Outcrop distance (length) is the total length of all segments of a specific dike. Dike segments form en echelon patterns when viewed either at the scale of the outcrop or from the air (see Plate 1). Thick, bulbous masses that form along dike segments are termed buds (Wentworth and Jones, 1940). The term plug is a cylindrical body rather than a tabular body. Volcanic necks may represent plugs that lead upward towards the surface. Commonly, breccia is associated with buds and plugs. Breccia consists of angular broken fragments that usually include sedimentary host rock as well as intrusive igneous dike material. Breccia composes bodies or continuous zones usually of circular to elongate topographic form that trend along the strike of the dikes; in most cases the dikes may radiate from and cut breccia bodies.

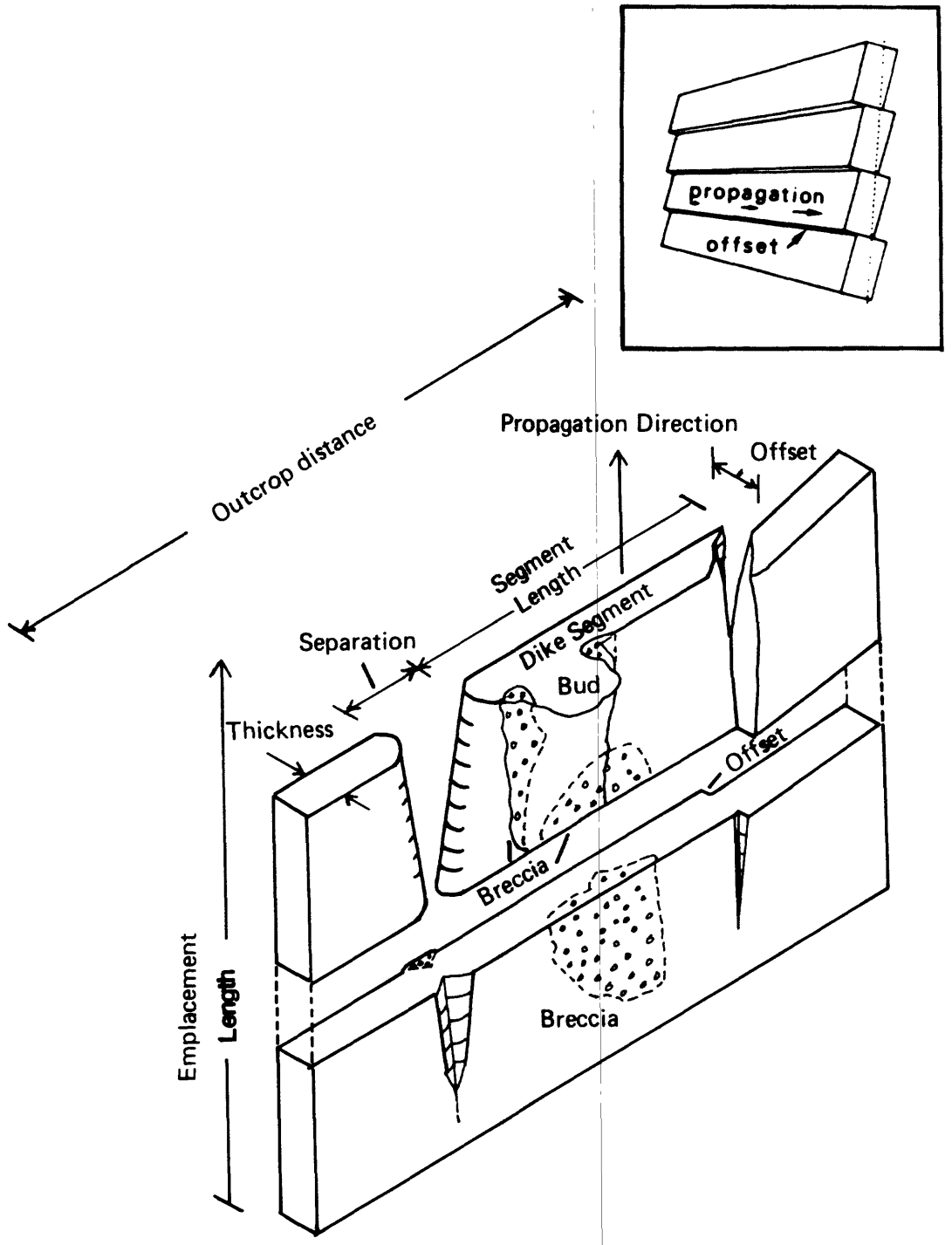

Figure 2. Idealized diagram of a dike and associated structures (modified after Delaney and Pollard, 1981). Terms on the diagram are defined in the text. Insert illustrates propagation direction with respect to offset (from Pollard and others, 1975).

A classification of igneous rocks based on combined modal mineralogical and chemical data is used in this study. According to the classification based on total alkalies versus silica (Cox and others, 1979), the igneous intrusive dike rocks of the San Rafael Swell fall into the alkali olivine basalt category. Silica content (recalulated to 100 wt. % anhydrous) ranges from 44 to 50 wt. %. Gilluly (1927) described the melanocratic rocks from the area as analcite diabase and the lighter-colored sill rocks as alkaline syenite. Diabase, as used in this study, refers to the intrusive rocks which have a distinctive medium-grained, typically subophitic texture and whose main components are labradorite and pyroxene (augite).

Field and Laboratory Methods

Black and white and color aerial photographs at scales of 1:20,000, 1:24,000, and 1:34,000, and orthophoto quadrangle maps at a scale of 1:24,000 were used as the basis for field mapping. Data collected in the field were recorded directly onto the aerial photographs and orthophoto quadrangle maps.

Field measurements include dike thicknesses, strikes, local propagation directions, occurrences of breccias, strikes of systematic joint sets in the host rock, and presence of alteration minerals. Appendix 1 provides a complete listing of all measurements taken during this study.

Dike thicknesses were measured at the thickest part of the dike segment along the most continuous length of dike outcrop. Thickness measurements were recorded where the contact with the host rock was sharp and distinct.

Field data were transcribed onto 1:48,000-scale topographic base map. Outcrop-length and dike-segment length data were measured directly on the orthophoto quadrangle maps using a digital display linear measuring probe with a resolution and accuracy of 1.9 m at a scale of 1:48,000.

Dike orientations were measured directly on the 1:48,000-scale map using a protractor. For dikes with variable strikes (see #1, Appendix 1), the strike for each distinct part of the segment was measured, and then the strikes were numerically averaged to represent one overall strike.

Local propagation directions (as defined on fig. 2) on the dike walls at the tips of the dike segments, where evident in the field, were also measured and recorded on the aerial photographs.

Occurrence of breccias also were noted and recorded on the aerial photographs and orthophoto quadrangle maps in the field. Breccia body length and thickness data were measured directly on the orthophoto quadrangle maps and noted in the tabulation of field measurement data (Appendix 1).

Strikes of systematic joints in the host rock (San Rafael Group) also were measured and noted during field work. Strikes of joints were taken and averaged over a single outcrop. If joint orientations were within a 10 degree range, they were used to define a systematic joint set at the outcrop scale. Relative ages of one joint set to another were recorded. Joints were considered to be systematic if the set was continuous for 20 to 40 m laterally and could be traced through the beds of the formation outcrop.

In some localites sedimentary rocks on the Colorado Plateau typically display systematic joints oriented parallel to the dikes (Delaney and others, written communication). Narrowly spaced dike-parallel joints are closely associated with dike emplacement, and the frequency of joints decreases with perpendicular distance from the dike wall contact. Spacing of the dike-parallel joints is typically less than 10 cm, and joints could be traced

tens of meters or further from the nearest dike.

Sampling was initiated to collect representative dike rocks throughout the geographic extent of the complex. Where possible, fresh relatively unaltered samples were collected from the centers of the dikes; however, extensive alteration and weathering made systematic sample collecting difficult. Multiple samples (where alteration and weathering were minimal) were collected at a few localities to determine chemical composition of the dike from contact to contact (984SRS-17 through 19 and 98SRS-35 a through c are examples). Sample localities are listed in Appendix 2.

Petrography of the dikes was investigated by using x-ray diffraction (XRD) methods and thin sections. Forty thin sections were examined to determine mineral phases and textural variations. Sample localities are shown on Plate 1. Mineralogy evident in the thin sections is relatively consistent. A detailed petrographic description of each thin section is presented in Appendix 4.

Major elements from eighteen samples were analyzed by x-ray fluoresence (XRF) on a Philips P W 1600 Wavelength Dispersive Simulaneous X-rayed Fluoresence Spectrometry†. Analysts Ardith J. Bartel, K. Stewart, and J. E. Taggart from the Branch of Analytical Chemistry, U. S. Geological Survey, Lakewood, Colorado, did the analysis.

---

†Any use of trade name is for descriptive purposes only and does not imply endorsement by the U.S. Geological Survey.

REGIONAL GEOLOGY

The Colorado Plateau (CP)

The intrusive igneous complex is situated on the northwest edge of the Colorado Plateau. The study area includes a part of the High Plateaus and the Canyonlands physiographic sections of the Colorado Plateau (fig. 3a). The western edge of the Colorado Plateau in Utah, and its physiographic relationship to the intrusive complex, are illustrated in figure 4.

The Colorado Plateau is a relatively coherent uplifted crustal block surrounded to the west and south by the extensional block faulted regime of the Basin and Range Province, and to the east by the Rio Grande Rift (fig. 3a). The tectonic significance and relationship of the large crustal block comprising the Colorado Plateau to the uplifted and extensionally deformed Basin and Range Province and the Rio Grande Rift during the last 20 m.y. is of interest in this study. The apparent rigidity of the Colorado Plateau block may be due to stress-field differences between the block and the surrounding provinces (Thompson and Zoback, 1979); seismicity studies also suggest that the interior is a rigid block, with differential uplift and rotation confined to the edges (Eggleston and Reiter, 1984). Figure 3b illustrates the crustal structure of the Colorado Plateau from seismic reflection studies.

Pre-Cenozoic structures and sedimentation may have determined the tectonic behavior of the plateau. Large monoclinal uplifts and intervening basins or structural terraces characterize the Colorado Plateau. Parts of the Colorado Plateau contain a sporadic distribution of high and rugged laccolithic mountain groups, such as the Henry and La Sal Mountains (fig. 4). The structures of the central plateau largely resulted from Laramide tectonism and igneous activity of Late Cretaceous or Tertiary time. The major uplift of $\sim$1.5 km has occurred since Eocene time, and part of the uplift may have resulted from lithospheric heating and thermal expansion (Bodell and Chapman, 1982). McKenzie (1984) suggests that epeirogenic uplift can result from the intrusion of large thicknesses of basic magma into the lower part of the continental crust. The plateau is underlain by a complex of Precambrian crystalline rocks consisting of a wide variety of granites, gneisses, schists, and mafic intrusive rocks. Paleozoic carbonates, clastics, and evaporites attain an aggregate thickness of 5000 meters (Case and Joesting, 1972). Continental redbeds, marine sandstones, and shales of Mesozoic age are approximately 1500 meters thick. The late Cretaceous or early Tertiary laccolithic mountains are composed of diorite porphyry and related rocks.

In Utah, the plateau is bordered on the west by a zone of thrust faulting, the Sevier orogenic belt, that delineates the eastern edge of the Basin and Range Province. A series of generally flattopped and cliffwalled north-trending mountain masses, the High Plateaus (fig. 4), bisect Utah. The faulting that formed the Wasatch, Fishlake, North and South Sevier, Aquarius, Awapa, Markagunt, and Parinsaugunt Plateaus began as early as late Miocene time and has continued intermittently through Holocene (Anderson and others, 1975). Cenozoic tectonic events that dominated the structural history of the plateau include downwarping in the north and west, broad arching or doming in the center, upwarping of the south and southwestern edge of the plateau, and upwarping and tilting (to the northeast) of the plateau (Hunt, 1956). In southern Utah, erosion, faulting, uplift and igneous activity have produced deeply cut canyons, basins, areas of broad uplift, laccolithic mountains, and dike and sill complexes.

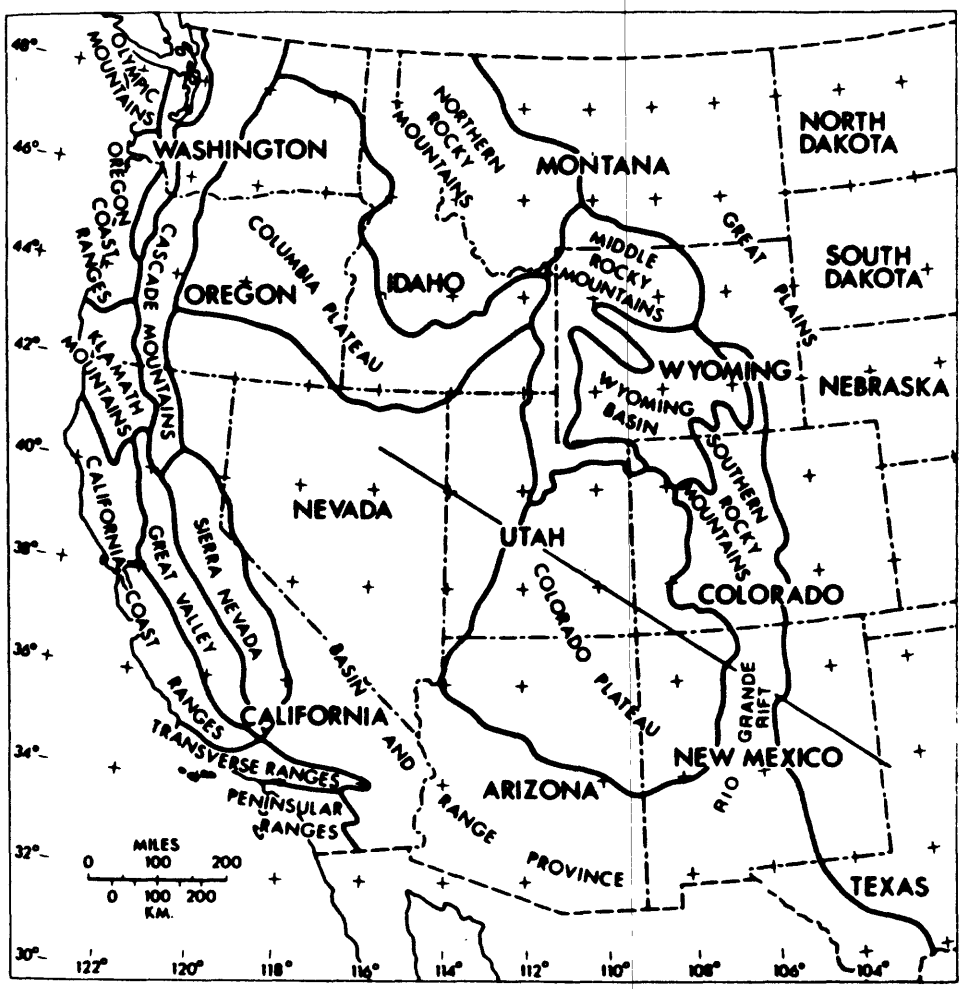

Figure 3a. Location map showing physiographic provinces and section line for figure 3b (from Thompson and Zoback, 1979).

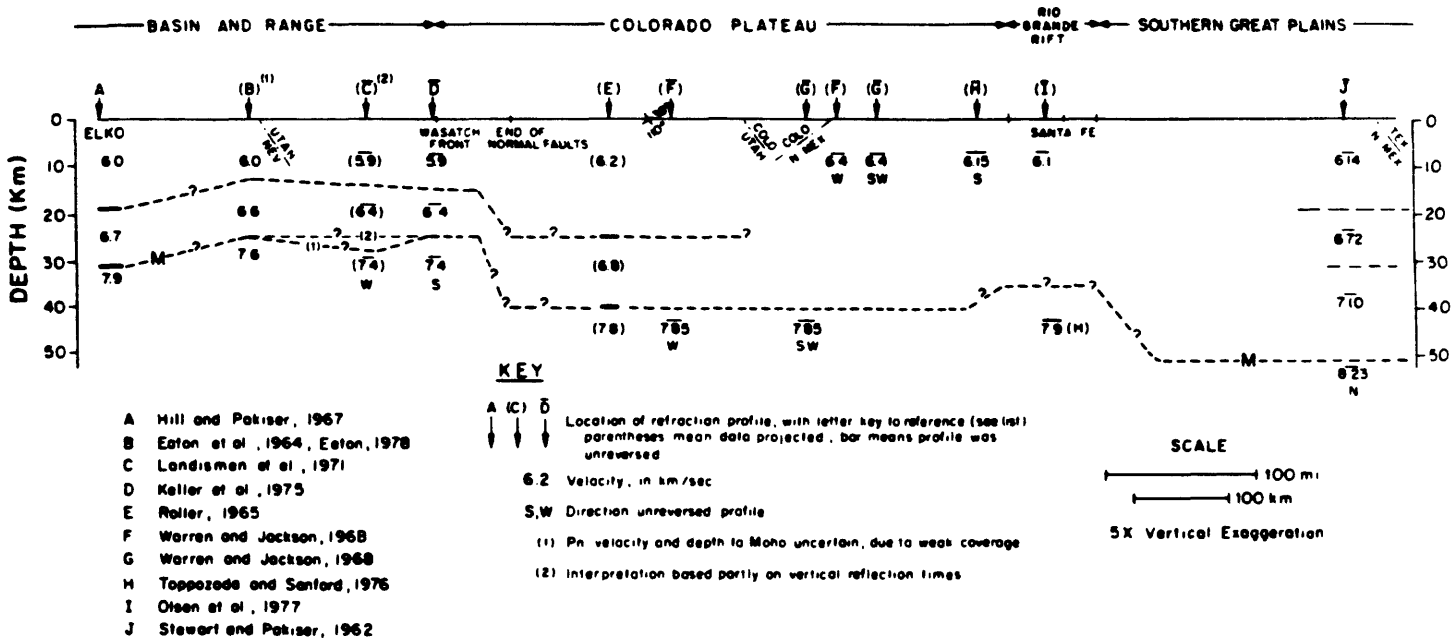

Figure 3b. Crustal structure from seismic reflection data (from Thompson and Zoback, 1979).

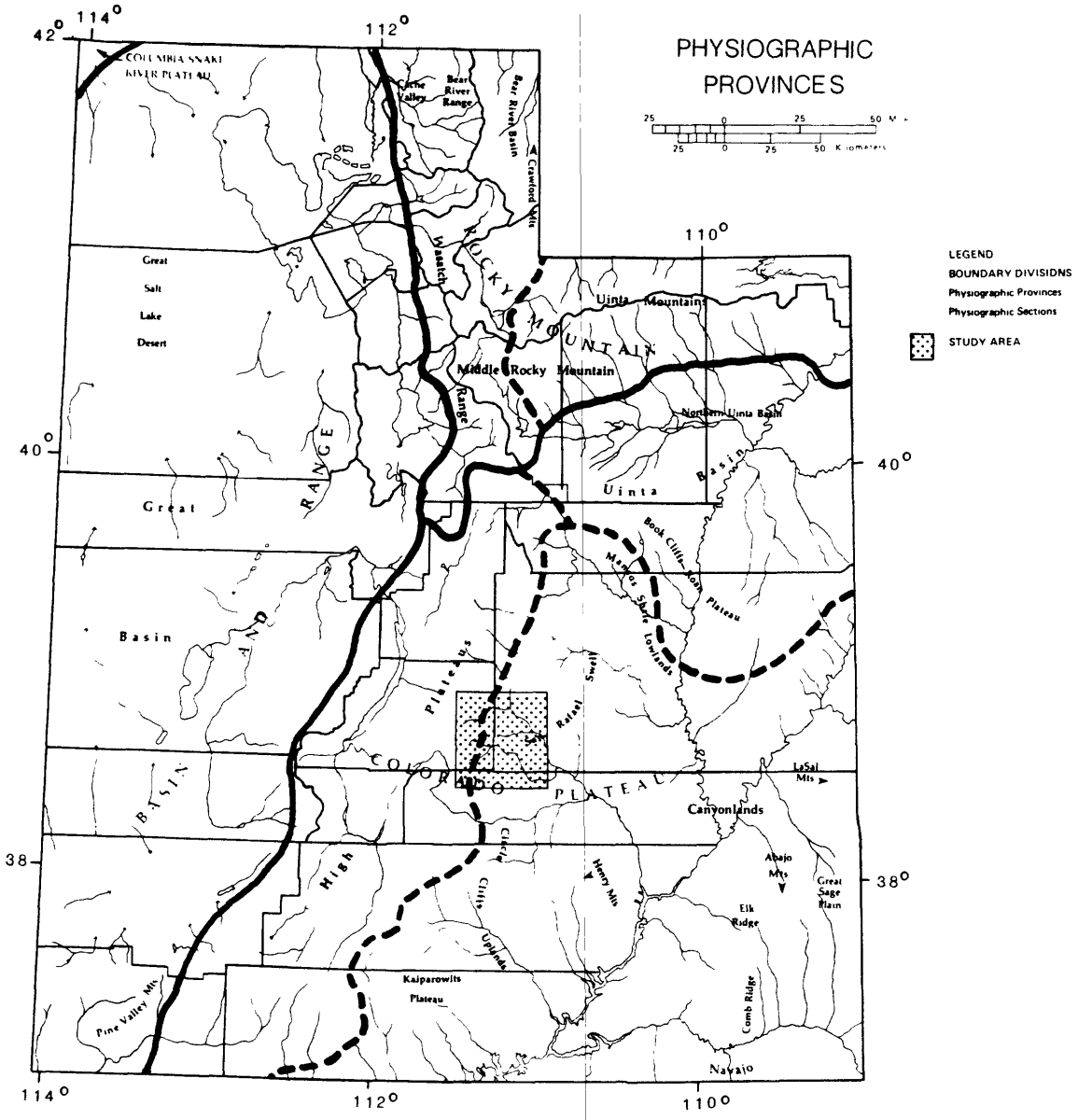

Figure 4. Location and physiographic province map of Utah. Solid lines delineate the major physiographic provinces, and the dashed lines represent the boundary between physiographic sections. The stippled area outlines the location of the study area.

During the Eocene to late Oligocene (Hintze, 1973; Roden and others, 1979), laccolithic intrusions (Henry, Abajo, and La Sal Mountains) were emplaced in the western part of the Colorado Plateau. A period of volcanic quiescence seems to have existed in southern Utah between 24 and 14 m.y.B.P. Younger basalt eruptions in the Colorado Plateau and Basin and Range Province extend from late Miocene through Quaternary time with the most voluminous volcanism between 14 and 10 m.y. B.P. (Anderson and others, 1975). Quaternary intrusives and extrusives seem to be more common in the southern High Plateaus and adjacent areas. The intrusive igneous rocks mapped in the study area have been dated as Pliocene age, 3.8±0.2 m.y. and 4.6±0.4 m.y. (E. H. McKee, written communication). Table 1 is a listing of radiometric ages for selected basaltic rocks in the San Rafael and Capitol Reef areas, Utah.

The San Rafael Swell and Waterpocket Fold

The San Rafael Swell and the Waterpocket Fold, prominent monoclines, are exposed within the Colorado Plateau (fig. 1). The intrusive complex is exposed dominantly in Jurassic sedimentary strata, the San Rafael Group, between the monoclines.

The San Rafael Swell is an asymmetrical, doubly plunging uplift developed during late Eocene or early Oligocene time (Hunt, 1956). Sedimentary rocks ranging in age from Pennsylvanian to Cretaceous are exposed in the anticline (Hunt, 1956; Hawley and others, 1968). The major axis of the structure is sinuous, first trending north-northeast, then swinging east-northeast in the central part of the swell and finally north-northeast (Hawley and others, 1968) and is approximately 135 km long and 56 km wide (Kelley and Clinton, 1960) The central part of the swell is an open, gently domed area about 64 km long and 16 km in average width (Gilluly, 1929). The area, called Sinbad Country, has been breached by erosion and is in most places an area of low relief. The outer area, called the Reef, is a high, nearly vertical escarpment of sandstones of the Glen Canyon Group (Hawley and others, 1968). The strata on the west flank of the swell dip gently to the west, averaging 3° to 8° NW (Lupton, 1913; Gilluly, 1929), but the strata along the east and southeast flanks dip at much steeper angles, ranging from 20° to as great as 85° SE (Hawley and others, 1968) Superimposed on the major domal structures of the swell are a number of irregular folds and faults (Gilluly, 1929).

The second major structural feature of the area is the Waterpocket Fold, one of the largest monoclines of the Colorado Plateau. Gilbert (1877) noted the Waterpocket "Flexure" was formed at the end of the Cretaceous period, but prior to the deposition of the undeformed Eocene strata that cover the earlier strata. This structure extends 160 km from the north end of Thousand Lake Mountain to the Colorado River (Smith and others, 1963). Kelley (1955) described one characteristic aspect of monoclines on the Colorado Plateau as having sinuous trends, and the Waterpocket Fold is marked by a series of short curves of similar lengths. It is called Waterpocket Fold because pockets, eroded into the walls of the gorges, fill and retain water during rain storms. In Capitol Reef area, dips along the fold are about 10° to 35°, with a maximum dip of 70° recorded farther to the southeast (Kelley, 1955).

Table 1. K-Ar radiometric ages of selected basaltic rocks from the San Rafael and Capitol Reef and adjacent areas, Utah (modified after Delaney and others, written communication).

Sample	Lat/Long	Material dated	K_2O(%)	$^{40}Ar^*$ mole/g	$^{40}Ar^*/^{40}Ar^{tot}$	Apparent age m.y.
Diabase from breccia body near cathedral Junction	111° 28′ 06″ 38° 31′ 06″	Whole rock	2.583	1.4015×10^{-11}	11.9	3.8 ± 0.2
Basalt flow near Hogan Pass	111° 28′ 06″ 38° 35′ 57″	Whole rock	1.721	9.3126×10^{-12}	9.0	3.8 ± 0.2
Syenite from sill at The Frying Pan	111° 05′ 47″ 38° 32′ 38″	Biotite	7.68	5.122×10^{-11}	15.3	4.6 ± 0.2
Basaltic andesite from vent on Thousand Lake Mountain	111° 28′ 42″ 38° 25′ 00″	Whole rock	1.367	1.2556×10^{-11}	6.4	6.4 ± 0.4

$\lambda\beta = 4.962 \times 10^{-10}\ yr^{-1}$; $\lambda\epsilon + \lambda\epsilon' = 0.581 \times 10^{-10}\ yr^{-1}$; $^{40}K/K = 1.67 \times 10^{-4}$ mole/mole

UNIT DESCRIPTIONS

The San Rafael Group

The intrusive rocks are exposed in the San Rafael Group and Morrison Formation of Jurassic age. The San Rafael Group consists of the Carmel Formation, the Entrada Sandstone, the Curtis Formation, and the Summerville Formation (Gilluly, 1927; Gilluly and Reeside, 1928; Smith and others, 1963; Hawley and others, 1968; Wright and others, 1979). The Morrison Formation is divided into the upper Brushy Basin Shale Member and the lower Salt Wash Sandstone Member. The majority of the intrusive rocks in the study area are exposed in the San Rafael Group. Formation descriptions will be presented in the following paragraphs. A summary of the stratigaphy and lithology of the units is presented in Table 2.

Carmel Formation (Jc)

The Carmel Formation is the lowest formation of the San Rafael Group and has been traced from southern Utah around the south end of the High Plateaus, along Waterpocket Fold, in the Henry Mountains, along Glen Canyon, and throughout the San Rafael Swell. The Carmel Formation is of diverse lithology; about 75 percent consists of greenish-gray and minor reddish-brown siltstone and shale, and the remainder is limestone interbedded with sandstone, siltstone and claystone, and sandstone and gypsum. The sandstones and limestones at the base of the formation cap the massive crossbedded Navajo Sandstone. Dense and oolitic fossiliferous limestone that characterizes the lower half of the formation forms the resistant crest of the "reef". The Carmel Formation becomes more shaly and more gypsiferous upward, and massive gypsum beds up to 3.6 m thick (O'Sullivan, 1981) occur in the upper two-thirds of the formation (Lupton, 1913). The formation has large lateral changes in thickness and rock types. The uppermost beds of the Carmel Formation are more sandy and grade into the lower part of the Entrada Sandstone.

The Carmel Formation has a maximum thickness of 198 m near the junction of Last Chance and Starvation Creeks (Gilluly and Reeside, 1928); it is 155 m on Salt Wash Creek (Gilluly, 1929), 119 m on the south cliff face of Cedar Mountain (Wright and others, 1979), and 213 m west and southwest of South Desert near the Waterpocket Fold (Smith and other, 1963).

Abundant marine fossils (for complete listing of fossils see Gilluly and Reeside, 1928, page 75) clearly prove the marine origin of the Carmel Formation (Gilluly and Reeside, 1928; Smith and others, 1963). According to Hintze (1973) the Carmel Formation records a shallow seaway of Middle Jurassic time.

Entrada Sandstone (Je)

The Entrada Sandstone consists of a thick sequence of even-bedded earthy fine- to very fine-grained sandstone with subordinate interbedded siltstone and claystone (Gilluly and Reeside, 1929; Smith and others, 1963; Wright and others, 1979). The beds are less resistant than the formations stratigraphically above, and they erode to form valleys, low hills, and steep cliffs. Good examples of such cliffs are exposed in Cathedral Valley along the northeast side of South Desert (Smith and others, 1963).

Table 2[1]. Generalized section of a portion of the sedimentary rocks exposed in the San Rafael and Capitol Reef areas, Utah.

System	Group, Formation, Member	Thickness (m.)		Lithology
	unconformity			
Jurassic	Morrison[2] Formation — Brushy Basin shale member	258	?	Varigated claystone, lesser amounts of siltstone, sandstone, and conglomeratic sandstone lenses.
	Morrison[2] Formation — Salt Wash sandstone member	127	?	lenticular conglomerate and conglomeratic sandstone with siliceous pebbles. siltstone and claystone lenses.
	unconformity			
	San Rafael Group — Summerville Formation	38 - 101		Reddish-brown, thin bedded siltstone and mudstone and fine sandstone, veinlets and thin layers of gypsum.
	San Rafael Group — Curtis Formation	23 - 77		Gray-green thin to thick-bedded sandstone and some siltstone and conglomerate.
	unconformity			
	San Rafael Group — Entrada Sandstone	81 - 277		Reddish-brown thin to thick-bedded sandstone, some siltstone and claystone, weathers to steep cliffs, increasingly less silt eastward.
	San Rafael Group — Carmel Formation	52 - 198		Dense limestone and buff and red (calcareous) sandstone at base, noncalcareous (red to green) siltstone and shale, white gypsum veins and beds.
	unconformity			
	Glen Canyon Group — Navajo Sandstone	134 - 165		White to pale yellow cross-bedded calcareous sandstone, thin local limestone beds.
	Glen Canyon Group — Kayenta Formation[3]	13 - 73		Lenticular beds of white to red-brown fine to medium cross-bedded sandstone, red-brown siltstone, clay-pebble conglomerate.
Triassic	Glen Canyon Group — Wingate Sandstone	108 - 122		Buff to tan, light orange, red-brown very fine cross-bedded sandstone, few lensas of limestone, local red stain.
	unconformity			

[1]Modified from Gilluly and Reeside (1928), Smith and others (1963), and Thompson and Stokes (1970)

[2]Included in Jurassic system after Smith and others (1963) and Thompson and Stokes (1970). Reported by Gilluly and Reeside (1928) as lower Cretaceous.

[3]Reported by Gilluly and Reeside (1928) as the Todilto Formation.

The thickness of the Entrada Sandstone is variable and is 205 m at Starvation Creek 2 km west of the mouth of Last Chance Creek (Gilluly, 1927), 257 m at Muddy River on the west flank of the San Rafael Swell (Gilluly and Reeside, 1928), 238 m in South Desert (Smith and others, 1963), and 114 m on the south cliff face of Cedar Mountain (Wright and others, 1979).

The Entrada Sandstone in the San Rafael Swell and Capitol Reef areas is considered to be of near-shore marine origin, probably in quiet water (Gilluly and Reeside, 1928; Smith and others, 1963; O'Sullivan, 1981).

Stratigraphic position between the Carmel and the Curtis Formation, in which fossils of Late Jurassic age are found, has been used to determine the Late Jurassic age of the Entrada Sandstone (Gilluly and Reeside, 1929). According to Thompson and Stokes (1970), the Entrada Sandstone was deposited between and during late Jurassic marine invasions of the western interior.

Curtis Formation (Jcu)

The Curtis Formation unconformably overlies the Entrada Sandstone, the upper surface of the Entrada Sandstone has been eroded and scoured to various depths. The contact is an erosional unconformity (Gilluly, 1929) and in places an angular unconformity (Smith and others, 1963), and is well exposed in the San Rafael Swell area (Thompson and Stokes, 1970).

The formation consists primarily of gray to green, fine- to very fine-grained glauconitic sandstone and interbedded green siltstone. The sandstone beds are generally persistent and even, ranging from 15 cm to 1.5 m in thickness. There is commonly a conglomerate bed consisting of well-rounded chert pebbles up to 5 cm in diameter at or near the base of the Curtis Formation. The Curtis Formation is exposed on steep or vertical cliffs in many locations, especially along the east side of South Desert, and it caps the "cathedrals" in Middle Desert (Smith and others, 1963).

The formation is of variable thickness, with a maximum of 78 m in the northern San Rafael Swell (Gilluly, 1928), 55 m on the south cliff face of Cedar Mountain (Wright and others, 1979), 23 m at the junction of Last Chance and Starvation Creeks (Gilluly and Reeside, 1928), and 24 m on the east side of the Waterpocket Fold (Smith and others, 1963).

Fossils collected from the Curtis Formation indicate that the formation is of marine origin and probably was deposited in shallow-water as indicated by the coarse basal facies and ripple marks evident throughout the formation (Gilluly and Reeside, 1928). The Curtis Formation has been assigned a Late Jurassic age, based upon the fossils (Gilluly and Reeside, 1928).

Summerville Formation (Js)

The Summerville Formation, a distinctive component of the San Rafael Group, overlies the Curtis Formation and consists of thin beds of red to brown siltstone and lesser amounts of sandstone and shale. The thin, varve-like alternation of light-colored sandstone and dark-colored siltstone or claystone are characteristic of the formation. Thin beds, nodules, and seams of gypsum that cut across bedding are present in the upper part of the Summerville Formation (Gilluly, 1929). There is a transitional contact between the Curtis and Summerville Formations.

The thickness of the Summerville Formation is fairly consistent; it is 50 m in the northern part of the San Rafael Swell (Gilluly, 1929), 51 m on the

south cliff of Cedar Mountain (Wright and others, 1979), and 61 m in most of the Capitol Reef and Waterpocket areas (Smith and others, 1963).

The thin even bedding of the Summerville Formation has been interpreted to be a marginal marine deposit formed in quiet water (Gilluly and Reeside, 1928). A Late Jurassic age has been assigned to the Summerville due to its close relation to the Curtis, which contains fossils of Late Jurassic age (Gilluly and Reeside, 1928).

Morrison Formation (Jm)

The Morrison Formation unconformably overlies the San Rafael Group throughout east-central Utah and is predominantly of non-marine origin. The unconformity is both angular and erosional (Gilluly, 1929). The long period of marine sandstone deposition that gave rise to the Glen Canyon Group (to the east) and the San Rafael Group abruptly ended, and the coarse sandy and conglomeratic sediments of the Morrison Formation were deposited (Thompson and Stokes, 1970). The Morrison Formation consists of two members: the lower Salt Wash Sandstone Member and the upper Brushy Basin Shale Member.

The Salt Wash Sandstone Member (Jms)

The Salt Wash Sandstone Member is composed of lenticular crossbedded channel sandstone and conglomeratic sandstone and lenticular claystone and siltstone (Gilluly, 1929; Gilluly and Reeside, 1928; Smith and others, 1963). The light-colored sequence of sandstones is interbedded with the darker siltstone and mudstone. The stratigraphic sequence differs within short lateral distance due to the lenticularity of the beds and lateral gradation within the unit.

The thickness of the Salt Wash Member generally decreases to the north and northwest part of Utah; over most of the San Rafael Swell and Capitol Reef areas the member is about 61 m thick (Gilluly and Reeside, 1928; Smith and others, 1963).

The depositional environment in which the Salt Wash Member accumulated was marked by energetic transport of large volumes of coarse sediments (conglomeratic sandstone) and quiet water or flood plain deposition (siltstone, mudstone, and claystone). Craig and others (1955) regard the Salt Wash Member as a broad fan-shaped alluvial-plain deposit, with the greatest thickness north of the Utah-Arizona border to the southeast of the Capitol Reef area.

The Brushy Basin Shale Member (Jmb)

The Brushy Basin Shale Member is a series of variegated claystone and lesser amounts of light-gray, almost white siltstone, sandstone and conglomeratic sandstone. The sandstone and conglomeratic sandstone occur in lenses throughout the member. The conglomeratic beds contain clasts up to 5 cm of gray and tan chert, but occasionally red and green chert pebbles have been encountered. Petrified dinosaur bones and wood are common in the Brushy Basin Member (Craig and others, 1955).

The thickness of the Brushy Basin Member varies throughout the study area from 121 m in the San Rafael area (Craig and others, 1955), 49 m in the Capitol Reef area (Smith and others, 1963), and an incomplete 26-meter-thick

section on the south cliff face of Cedar Mountain (Wright and others, 1979).

The sandstones of the Brushy Basin Member indicate that the depositional environment was a quiet, less energetic fluvial system than was the environment of the lower member (Craig and others, 1955; and Smith and others, 1963).

Gilluly (1929), determined the Morrison Formation to be Cretaceous in age, but, Craig and others (1955) and Thompson and Stokes (1970) determined the formation to be of Late Jurassic age. The Late Jurassic age is used in table 2 for the Morrison Formation.

FIELD RELATIONS

Description and Morphology of the Intrusive Complex

A swarm of dikes, related breccia bodies, and sills outcrops to form prominent topographic features in a northeast-trending band between the San Rafael Swell and the Waterpocket Fold (fig. 1). Outcrop patterns of the dikes are en echelon and discontinuous and show offsets perpendicular to the propagation direction. The sills are distributed throughout a 360 km² area southwest of Muddy River and occur mostly in the upper part of the Carmel Formation and in the Entrada Sandstone, although a few are found as high as the Morrison Formation (Gilluly, 1927). The sills are exposed as a band in the middle of the complex. The sills are locally composite and are characterized by syenite lenses, ocelli, and veins, and are enclosed in a fine-grained melanocratic shonkinite (Williams, 1983). The sills, for the most part, show offsets and finger-like septa similar to the dikes.

Gilluly (1927) noted that the sills were localized in a smaller area than the more widely distributed dikes and plugs. The sills appear to be confined in extent to a N. 20° E.-trending band in the middle of the complex. Dike emplacement depth inferred from stratigraphic relations could be as great as 2.5 km, but probably is 0.5 to 1.0 km (Delaney and others, written communication).

The Dikes (Td)

The dikes are narrow, discontinuous bodies, averaging 120 cm in thickness and 135 m in dike segment length, varying in length between 20 m and 1850 m. The average strike of the dikes is slightly west of north (Gilluly, 1927), and the average strike of all mapped dikes (∿153) in the complex is N. 13° W. (fig. 5). The individual dike segments as defined by Delaney and Pollard (1982) have similar strikes, and adjacent segments of one single dike exhibit an en echelon arrangement. The separation of two adjacent segments can range from a few centimeters to several meters, or more.

The local step or propagation direction is not evident on all dikes. A number of the dikes had two or three distinct directions, and this has been noted in the data (#2, #19; Appendix 1). Offset directions were measured on dike walls exposed above the host-rock bedding surface. A number of dikes in the study area form ridges and spines up to 3 m high, thus allowing excellent exposures of the dike contact. Figure 6 is a stereographic plot of all the offset directions available. Appendix 3 is a complete listing of all the offset directions and the locations of the dikes in the study area.

Dike segment length varies considerably over the extent of the complex. Although a few dikes have a continuous outcrop length up to 1.8 km, most average 150-200 m. Figure 7 is a histogram of all lengths of all dike segments found in the complex (total number of segments ∿1200). Minumum segment length that could be shown on the 1:48,000-scale map is ∿25m.

Dike lengths are highly variable and depend on the scale of description employed; i.e. outcrop length and map length may differ. At outcrop scale, dike segments as small as 1 m in length and 5 to 10 cm in thickness can be seen, but when mapping on 1:20,000-scale aerial photographs or 1:24,000-scale orthophoto quadrangle maps the fine detail cannot be descriminated. Such scale-dependent geometries suggest that the concept of fractals and self-similarity may be relevant to patterns of dike distribution (Mandelbrot, 1977, 1982).

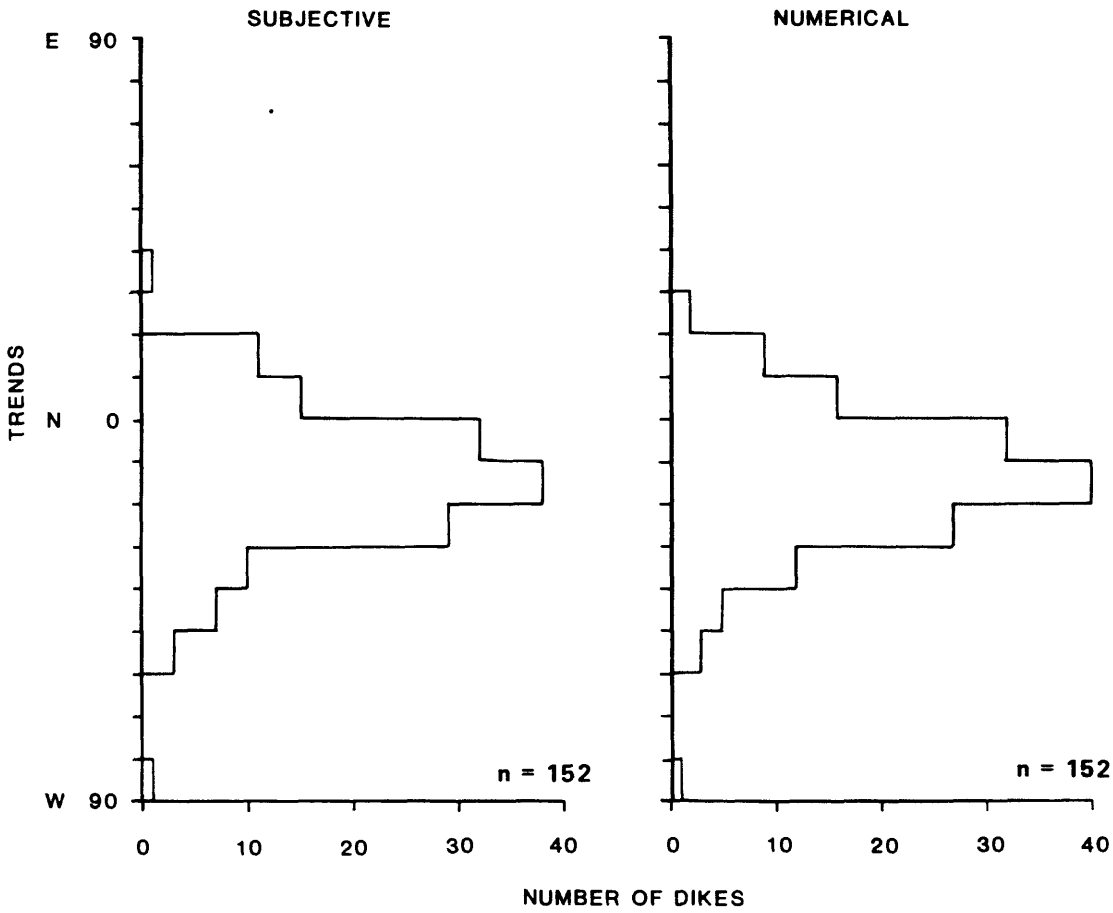

Figure 5. Frequency diagram of 153 dike trends in the study area. (a). The subjective trend was determined by visual inspection of the dike segments on the 1:48,000-scale map, and drawing a line through the segments and measuring the orientation of the line. The average is N. 13° W. (standard deviation 17.1°). (b). The numerical average was determined using a standard averaging program on a desk top calculator. The average trending is N. 14° W. (standard deviation 17.0°).

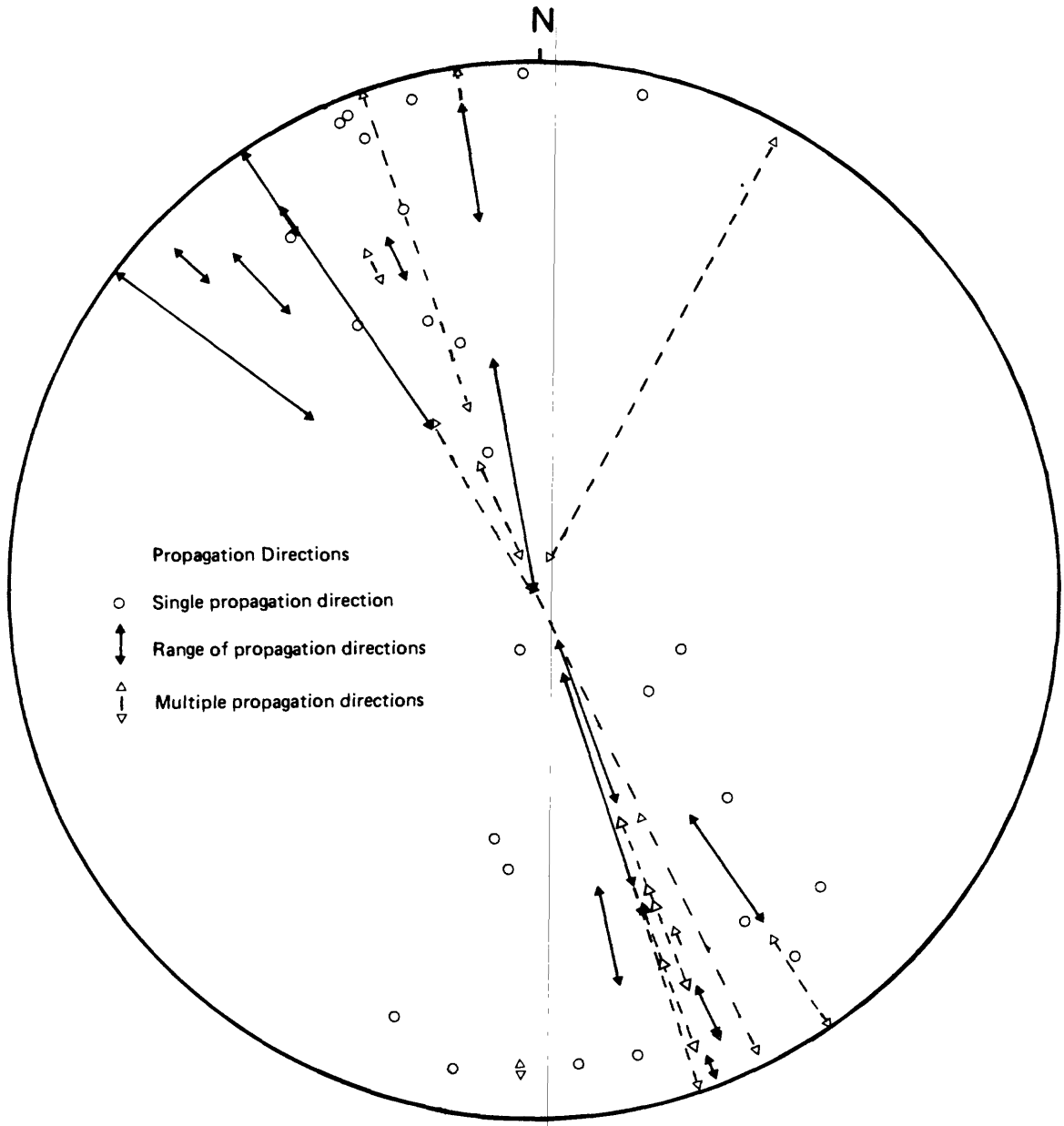

Figure 6. Stereoplot of 98 propagation directions measured on dike wall outcrops in the San Rafael and Capitol Reef areas, Utah. Approximately 50 percent of the propagation directions are between 0° and 25° of horizontal.

The dikes vary in thickness from 500 cm to 10 cm, or even thinner. The very thin dikes can be seen at the end of dike segments and a variety of thicknesses can be measured along a particular dike segment. Several dikes are sinuous and almost constant in thickness; others broaden and narrow in an apparent pinch and swell structure (Gudmundsson, 1984) over the outcrop length. This pinch and swell feature is difficult to represent on the 1:48,000- scale map because a 0.25 mm line on the map represents about 5 m on the outcrop scale. However, the thicknesses can be accurately measured in the field because of the sharp contacts of the dikes with the host rocks. Figure 8 is a histogram of all the dike thicknesses measured in the field. The average thickness of 205 measurements in the study area is 120 cm. Figure 8 does show the average thickness to be ∿120 cm. Thickness is most probably a function of the regional principal stresses in the crust at the time of emplacement and of the pressure and volume of the invading magma (Helgason and Zentilli, 1985).

The contacts between the basalt of the dikes and the host rock are sharp and distinct, with minimal or no metamorphic effects noted. At a few localities narrow zones (up to 20 cm) of contact metamorphism are evident. Hornfelses have been noted at Cathedral Valley at the northwest end of the four breccia bodies (# 119, Appendix 1) and at the south end of the diabase bud on the Moroni Slopes southeast of Cedar Mountain (# 89, Appendix 1). Local induration of the host rock without dike emplacement was found in a few locations in the study area (# 10, 112, Appendix 1).

The dike rock is generally finer-grained adjacent to either contact (up to one-third of the total width) with the host rock, but becomes more coarse-grained near the center. The center of the dike rock is friable and easily broken with a rock hammer. Vesicularity also increases towards the center of the dike. Most of the vesicles are spherical, ranging from 1-5 mm in diameter, but a few larger irregular-shaped vesicles have been found throughout the complex. In a few dikes the vesicles form bands that roughly parallel the dike walls, but in others the vesicles are more evenly distributed throughout the dike. The dike rock exhibits typical cooling structure, with joints or cracks evident both parallel to and perpendicular to the outcrop length of the dike. At one location, columnar joints have been found associated with a large mushroom-shaped plug of dike material. This plug is located east of Factory Butte and west of Last Chance Creek (# 93, Appendix 1). This plug is situated directly adjacent to a dike and is well exposed in a small stream channel. The intrusive rock of the plug contains numerous vesicles filled with calcite. A number of rock samples were collected for thin section and x-ray diffraction analysis of the vesicle filling. Results of the analyses will be discussed in the following section on petrography and chemistry.

Another feature associated with the intrusive complex is the large bulges of the dikes, termed buds (fig. 2) (Wentworth and Jones, 1940), that occur throughout the area. Removal of the dilational component of the overall shape would not allow the adjacent walls of the intrusion to be brought back into contact (Delaney and Pollard, 1981). Examples of buds include a prominent knob, known as Pissant Knoll, southwest of Hebes Mountain (# 26, Appendix 1), and a second topographic feature midway between Cedar Mountain and the Frying Pan on the Moroni Slopes (# 89, Appendix 1). At the second location there are four separate buds of different sizes, but all form oblong cylindrical bodies. The buds are broken into irregular blocks with curved faces, and the largest of the four has host rock associated with it on the west face. The contact is sharp and distinct.

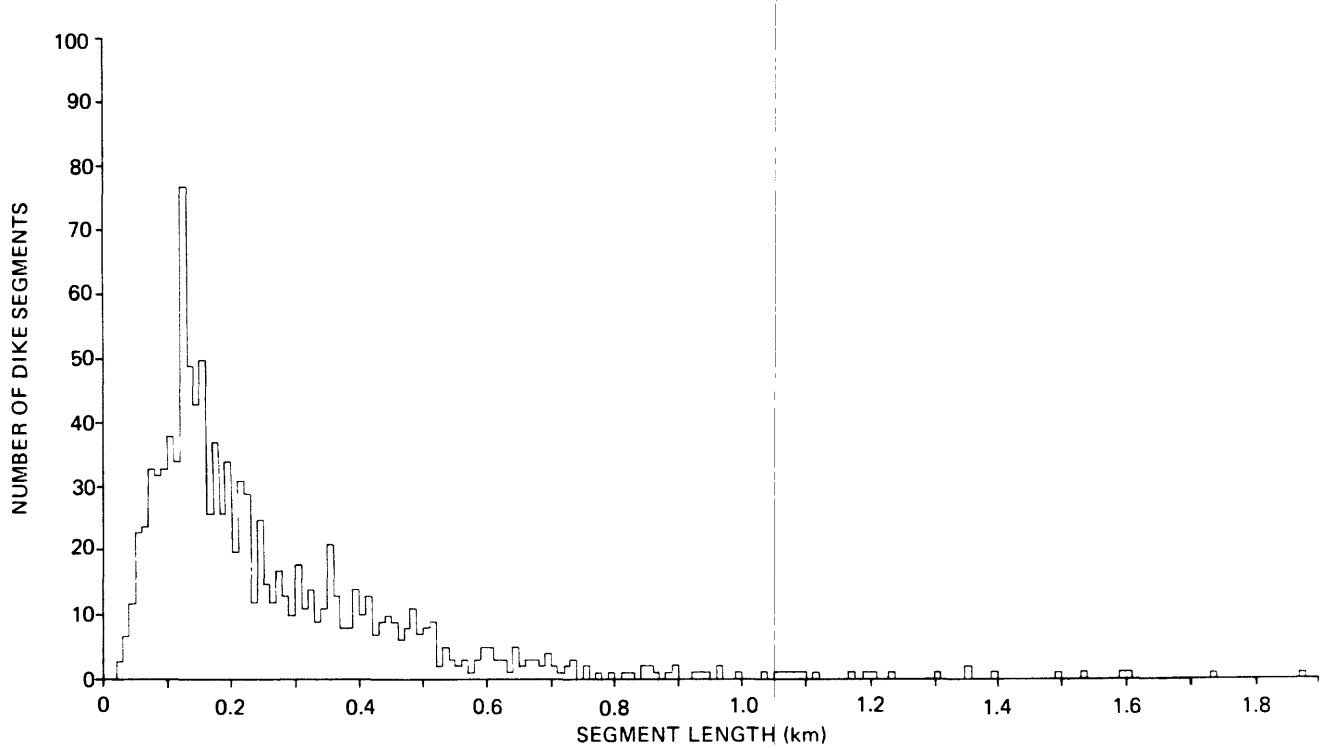

Figure 7. Frequency diagram of ~1200 dike segment lengths in the study area. The average length is about 135 m.

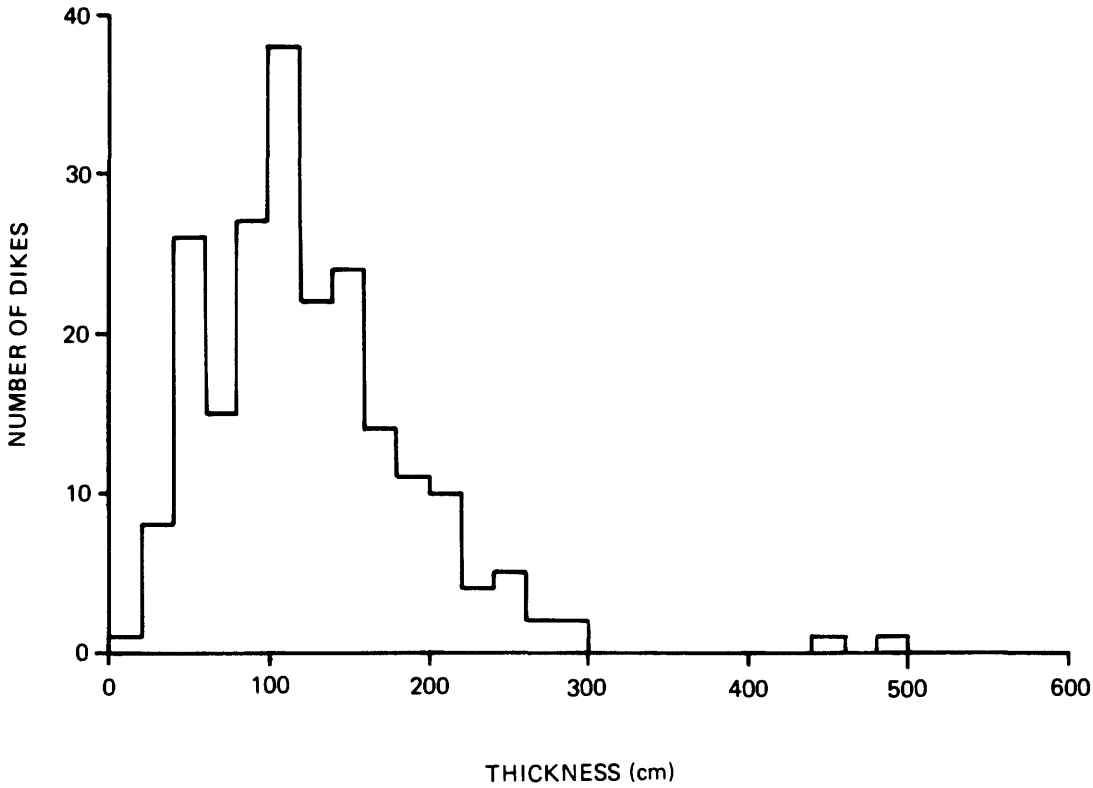

Figure 8. Histogram of 250 dike thickness measurements in the study area. The average thickness is about 120 cm.

Breccia Bodies (br) and Associated Features

The breccia bodies consist of angular, broken fragments of sedimentary host rock and a mixture of the dark-colored dike material. They characteristically form circular to elongate topographic features that trend along the strike of the dikes (fig. 2), and in most cases the dikes either radiate from or cut the bodies.

Breccia bodies are not always spatially associated with dikes at the ground surface. At depth, dikes may radiate from or cut these bodies but can not be seen at ground level. Further erosion of the strata may expose the close relation between the dikes at breccia bodies, but at present only singular breccia bodies are evident. In the study area four examples of singular bodies have been seen. One example of a single brecciated body not associated with a dike is Deadman Peak (# 19, Appendix 1), located northwest of Hebes Mountain. The proportions of brecciated host rock and dike material vary at each location, but approximately 50 percent of the brecciated structures are dike material. Another example includes three small brecciated mounds located to the north of the road on Rock Springs Bench (# 115, Appendix 1). Besides these four singular breccia bodies in the study area, there are approximately 35 breccia bodies associated with dikes. The brecciated material may be associated with the emplacement of the dikes where local thickening of the conduit has occurred (Delaney and Pollard, 1981). About 60 dikes in the study area contain breccia over all or part of the outcrop length; one example of this feature is a dike located due west of Little Black Mountain (# 125, Appendix 1). The dike northeast of Black Mountain (# 96, Appendix 1) is well exposed in the stream channel and contains breccia in the center of the dike with the dike material completely surrounding it.

The Sills (Ts)

Although the main focus and emphasis of this research project has been the dikes in the complex, the location and extent of the sills in the study area also have been mapped (plate 1). Field data collected on the location and extent of the sills were noted on the aerial photographs and orthophoto quadrangle maps and transcribed onto the 1:48,000-scale topographic base map in the same manner as the dikes. Further clarification was obtained from photo interpretation of the 1;24,000-scale color photographs of the lower one-third of the study area and from the 1:62,500-scale map of the Capital Reef National Park and Vicinity, Utah by Billingsley and others (1981).

The sills are generally more resistant to erosion, and are usually exposed high on cliff faces and appear as prominent topographic features throughout the study area. Therefore, access to the majority of the sills in the area is limited. Hebes Mountain, the Frying Pan, and Factory Butte are excellent examples of sills. The sills vary in thickness from 10 cm to a maximum of about 30 m (Williams, 1983). Gilluly (1927, 1929) and Williams (1983) noted that on close inspection of some of the dike-sill contacts, the sill is cut by the dike, and the dike has a chilled border with the sill. This relationship can imply that the dikes were emplaced after the sills were cooled. Where evident and accessible, the chilled margins of the dike and sill are narrow and range from 10 to 15 cm in thickness. Contacts between the dikes and sills also provide evidence that in some cases the sills have been crosscut by the younger dikes; in other cases the dikes appear to terminate at the sills or merge with them. This relationship may illustrate that the dikes have been

feeders for the sills; however, no feeder dikes have been located in the studyarea. More field work at dike-sill contacts would be needed to conclude such a relationship.

Most sills exhibit intermittent offset similar to the dikes (fig. 9) and are especially visible on the cliff faces, such as Cedar Mountain. The dike offsets are in a vertical or near vertical plane, and sill offsets are in a horizontal plane. The sill offsets are propagational and not due to depositional or erosional fluctuations in the host rock beds. Figure 9 illustrates intermittent offset of a sill located on top of a small butte due east of Cedar Mountain. The butte is about 100 m long and 400 m high, and the sill is about 25 m thick. The actual distance of offset of the sills has not been measured in this study. At a few locations, for example a sill south of Little Black Mountain, thin sills form an anastomosing pattern on the exposed rock face. This feature was formed during the emplacement of the sill as the magma was moving along the bedding plane and separating the host rock material into thinner layers. This feature is also seen at the termination of sills, where the magma formed thin fingers as it was being emplaced into the friable beds that it was intruding.

The mafic rock of the sills is similar in composition to that of the dikes. The sills are composite in composition (Gilluly, 1927, 1929; Williams, 1983). Gilluly (1927, 1929) called the darker rock an analcite-biotite diabase and the lighter-colored facies alkaline syenite. Smith and others (1963) concluded that the sills in the Capitol Reef area are similar in composition to the analcite diabase from the San Rafael Swell area as reported by Gilluly (1927). Gilluly (1927) suggested that the syenite was a product of a second injection of magma. Field relations between the dikes and sills support his premise, but further petrologic and geochemical investigations are needed to clarify the precise chronology of evolution and emplacement. Williams' (1983) study of a composite sill at Cedar Mountain shows the sill is characterized by syenite lenses, ocelli, and veins, enclosed in a fine-grained melanocratic shonkonite. Williams (1983) work revealed several variations of the major rock types of Gilluly (1927, 1929). Williams (1983) concluded that the shonkinite magma was intruded as a single event and differentiation occurred in situ with liquid immiscibility and liquid fractionation being the main processes responsible for the igneous rock suite.

The close field association of the dikes and sills and the similarity of composition suggests origin from a similar magma. Detailed major- and minor-element analyses, and geochronology are needed to establish such a relationship.

Relative Age of the Intrusives

Relative ages of a few of the dikes can be ascertained from certain field relations, where one dike is deflected or intruded by another. Figure 10 shows nine examples of dike intersections or deflections and their relative age relation. Based on field relations, six dikes that are trending northeast in the study area have been determined to be younger (figure 10a, b, e, f, h, i). In figure 10c, the northwest-trending dike appears to be younger, but this cannot be stated conclusively from field evidence. The relative ages of the remaining two dike intersections could not be determined (figure 10d, g).

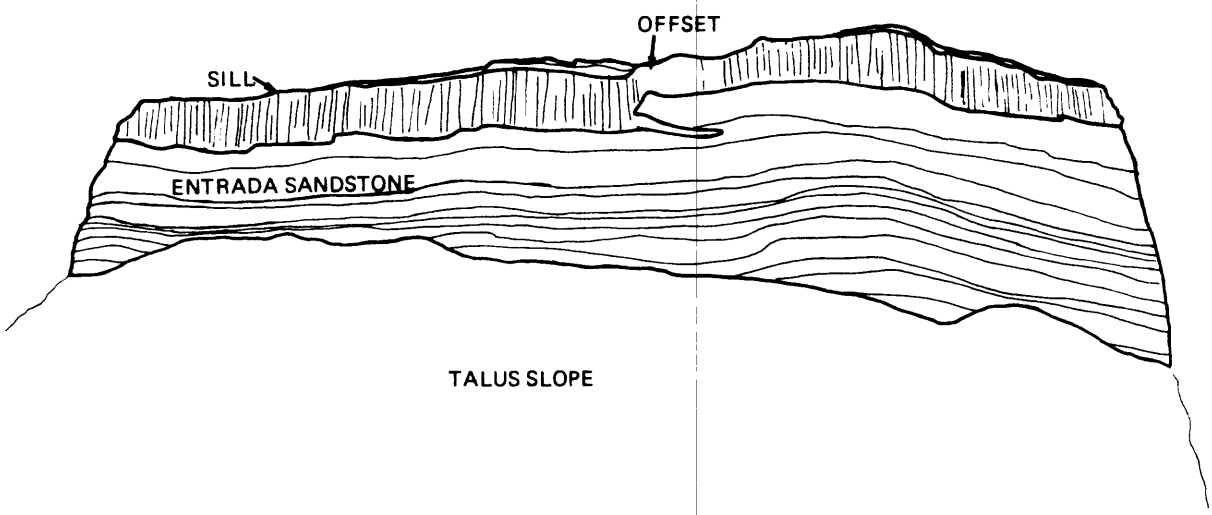

Figure 9. Schematic illustration of intermittent offset of a sill. The sill is located on the top of a small butte due east of Cedar Mountain (fig. 1). The butte is about 100 m wide and 400 m high, and the sill is about 25 m thick.

Joints and Faults

Fracture surfaces along which there has been imperceptible movement arecalled joints. Joints permit adjustments to occur as regional units in which they are found change shape or size during structural movements such as subsidence, uplift, thrusting, expansion and folding (Davis, 1984). Joints can be seen at outcrop scale in most rocks and comprise one of the most abundant structural elements in the earth's crust. The best developed joints are termed systematic joints and are planar, parallel, and evenly spaced ranging from tens of centimeters to tens of meters.

Joints are numerous throughout the study area and are most prominent in the lower shaley member of the Carmel Formation and in the thick massive sandstone units of the Entrada Sandstone and Curtis Formation. Systematic joint-measurement data have been collected throughout the field area and are illustrated as a histogram of number versus strike (fig. 11). Figure 11a is a composite histogram of all joint measurements from the San Rafael Group, and figures 11b-e show each formation of the group individually.

The joints vary greatly in both vertical and horizontal extent through several beds or within a single formation. Some joints in the study area are short, curved, and irregular, and others are long and relatively straight. There is also a great range in the spacing of joints, from a few centimeters to tens of meters. Joint measurement data in the field area were collected when a regular spacing and lateral extent of the joint set could be followed along the outcrop. Relative ages of a small number of joints have been determined and have been noted on plate 1 as N_1 (older), and N_2 (younger).

Kelley and Clinton (1960) compiled a joint and fracture system map for the Colorado Plateau; their investigation concluded that the fracture pattern is dominated by northeastward and northwestward trends. The northwestward trends have much less deviation than the northeastward trends, and NW joint and fracture pattern is suggestive of crustal deformation of the Colorado Plateau and may have provided a pathway for the intrusion of the dike complex. The joints may develop in a number of ways and closely follow deposition of sediments and burial in subsiding basins or shelves (Kelley and Clinton, 1960). Joints can form due to differential compaction or uneven loading during burial. In the study area, massive sandstone beds (Entrada Sandstone) overlie weaker mudstone or clay sediments of the Carmel Formation, and extensive joints have been encountered in the latter formation. In some locations three different systematic joint sets have been found in the highly fissile lower shale member of the Carmel Formation . This feature is seen in the stream channels or canyons where the Carmel Formation is well exposed.

Smith and others (1963) noted that the prominent joint trend along Waterpocket Fold north of latitude 38°13'N ranged from N. 15° E. to N. 15° W., and south of this latitude they trend N. 15° E. to N. 20° W., with most of the dikes intruded along N. 15° E. or N. 15° W.

Kelley and Clinton (1960) divided the Colorado Plateau into a number of tectonic divisions, and their Capitol Reef Fold Belt coincides with the study area in this report. They concluded that the principal fracture trend in the eastern part of the area is N. 20° W., with lesser trends of N. 60°-75° W., and a few northerly ones are present. In the area around the Heep (Hebes) Mountain intrusives, two dominant fracture set trends, N. 20° W. and N. 75° W., are present, and the dikes of this center strike N. 20° W.

The frequency diagram (fig. 11a) reveals information concerning the joint trends in the San Rafael Group. With a total sample population of 588 joint

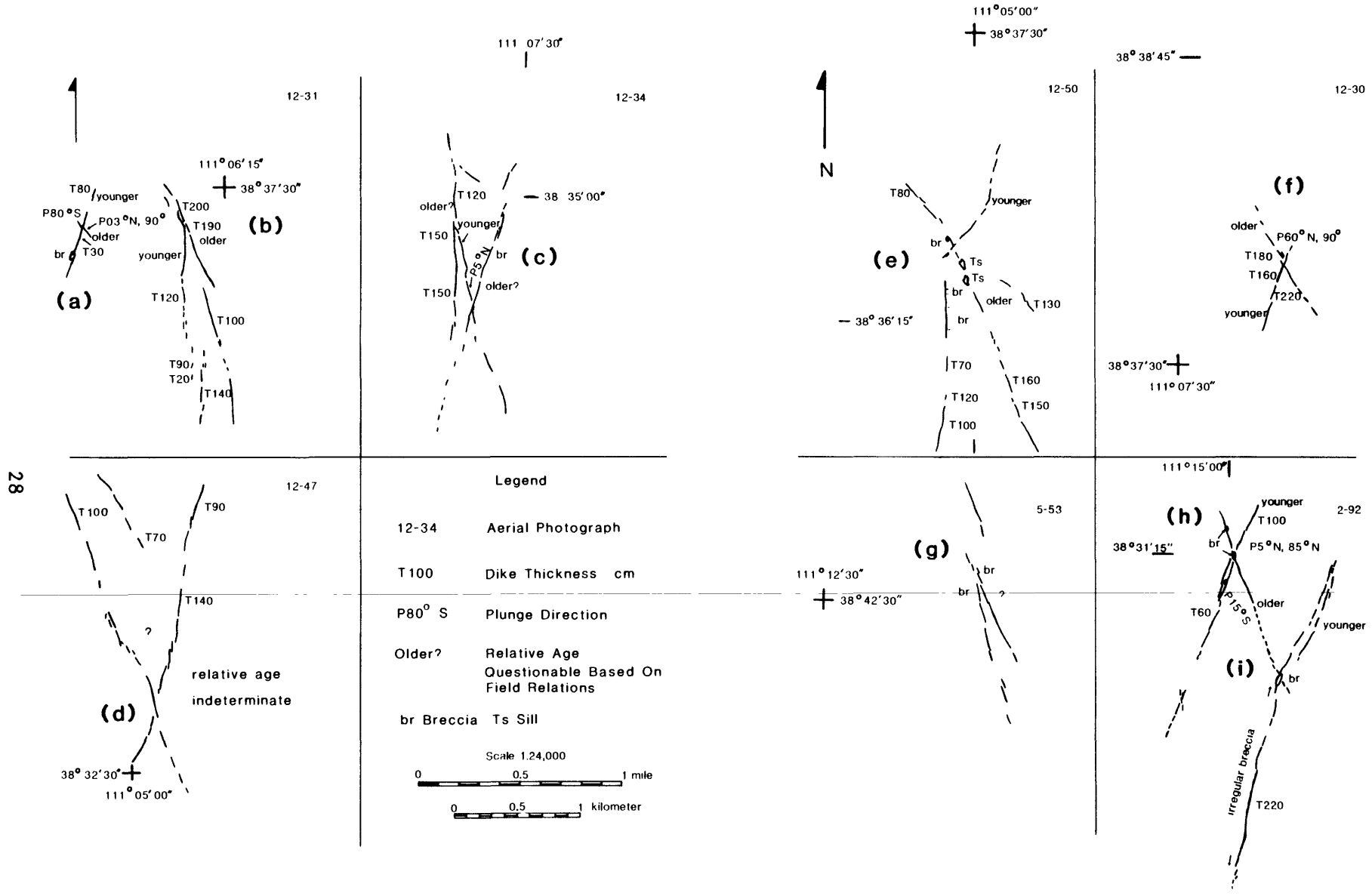

28

Figure 10. Diagram of nine intersections or deflections and the relative ages based on field relations. (a). Excellent degree of confidence, (b) and (c). lower degree of confidence, (d). unable to determine age relations, (e)-(i). excellent degree of confidence.

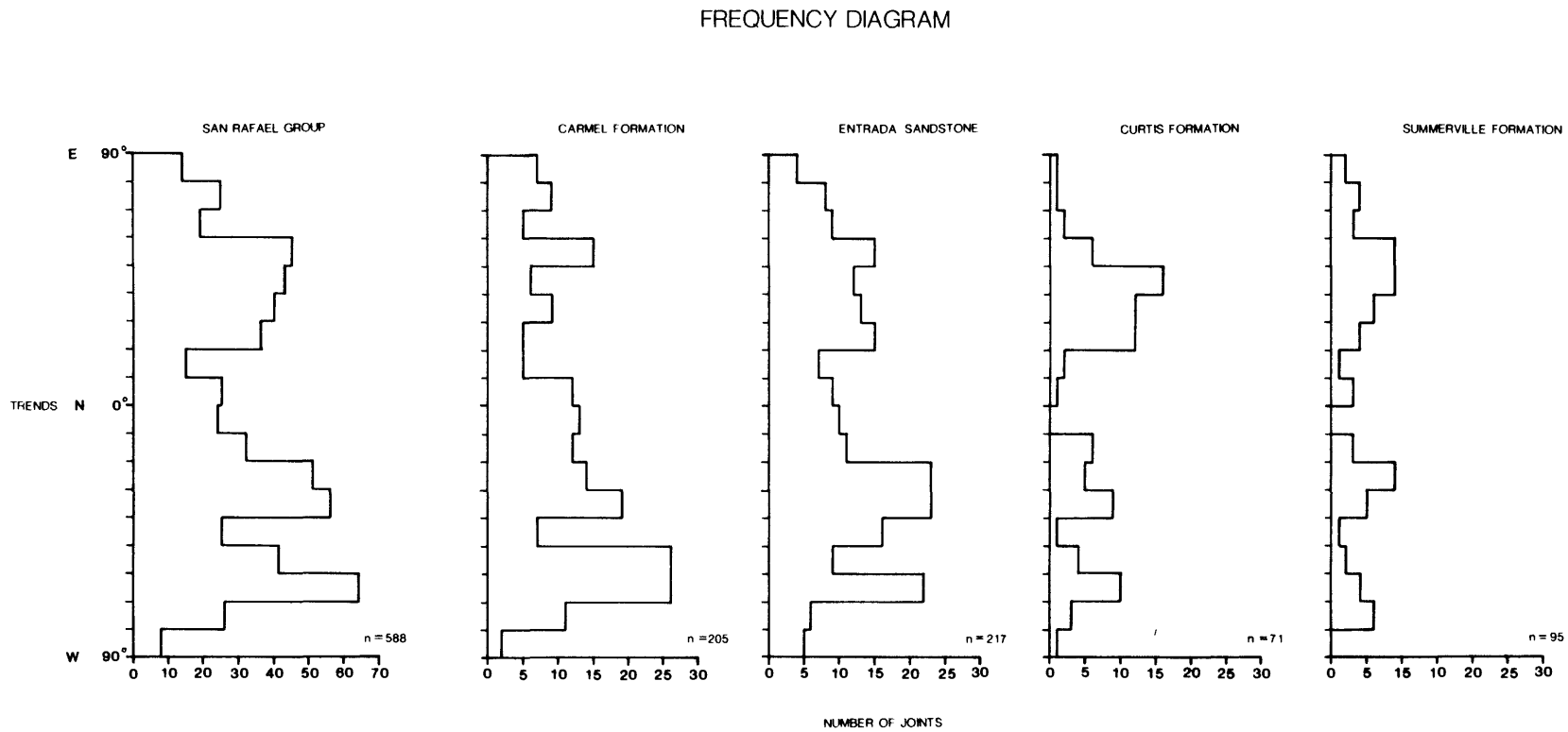

Figure 11. Histogram of joint orientation data (total of 588 measurements) collected for (a) San Rafael Group, (b) Carmel Formation, (c) Entrada Sandstone, (d) Curtis Formation, (e) Summerville Formation.

strikes and trends ranging from N. 90° E. to N. 90° W., two and possibly three trends appear to be dominant. The first trend is N. 65° W.; a second one ranging from N. 20° to 40° W. can be seen on the frequency histogram. A less conspicuous third trend ranging from N. 50° to N. 60° E. is also apparent.The average trend of all the dike segments measured in the field area is N. 13° W. (standard deviation 17.1°).

In the northwest corner of the study area near Willow Wash, one dike, over most of its outcrop length, exhibits the same trend as that of the systematic joint set in the host rock, but at the northern tip the dike trends in a more northerly direction. There is an actual curve to the dike along the outrop. This may indicate that the dike was propagating along the trend of the systematic joint trend of the host rock but changed direction due to changes in the stress field; the dike apparently encountered less resistance as it began to propagate in the northerly direction (Delaney and others, written communication).

A zone of faults is found on the eastern edge of the study area and is associated with the massive sandstone beds of the Navajo Sandstone. A few dikes (to the east of the study area) have been intruded along faults that displace the beds of the Navajo Sandstone. One dike east of Little Black Mountain and Factory Butte (# 92, Appendix 1) has been emplaced along the northern trend of a small fault that is exposed in the Carmel Formation. Smith and others (1963) found evidence of emplacement of dikes along faults in the Waterpocket Fold area. Two dikes (# 78 and #133, Appendix 1) are intersected by the northwestward-trending faults, but the dikes are not offset by the faults and are therefore younger.

PETROGRAPHY AND MINERALOGY

Introduction

The initial field study and petrography of the intrusive rocks of the San Rafael area was conducted by Gilluly (1927). His investigation showed the intrusive complex was composed of two distinct types of igneous rocks: analcite diabase and analcite syenite. In Smith and others' (1963) study of Capitol Reef area, they concluded the dikes and sills were similar in composition to the analcite diabase from the San Rafael Swell area. Wilshire (1967) collected samples of one dike and several sills (Hebes and Cedar Mountains) from the San Rafael area and reported results of rapid rock analyses, CIPW norms and AFM diagrams of the dike and sill samples; however, no interpretative analyses of these data were reported. Williams (1983) completed a detailed petrographic and chemical study of a composite sill at Cedar Mountain (located in the middle of the San Rafael and Capitol Reef areas, Utah). As a result of that study he documented a suite of distinct igneous rocks that include: 1) shonkinite, 2) salite-biotite syenite, and 3)kaersutite syenite. He concluded the sill was produced by differentiation in-situ and the interaction of silicate-liquid immiscibility and liquid fractionation. The present study has shown the dikes, with few exceptions, are composed of olivine basalt. Extensive hydrothermal alteration of the dike material is evident throughout the complex making it difficult to complete extensive interpretative work concerning the crystallization history and petrogenesis.

The dikes are dark colored, locally porphyritic rocks that contain phenocrysts of olivine, augite, biotite, and feldspar set in a dense greenish-black groundmass with numerous biotite flakes and plagioclase microlites (Gilluly, 1927, 1929). Some samples are essentially equigranular, and others have a diabasic texture. The intrusive dike rocks are dark-gray-green, and many contain vesicles and cracks that are filled with secondary minerals, such as quartz (rarely), calcite and zeolites (analcite, thomsonite and rarely natrolite) precipitated from percolating low-temperature groundwater (Best, 1982). Yellowish-brown clinopyroxene is the most prominent phenocryst seen in hand specimen; altered orange-red olivine can also be seen with a hand lens. Phenocrysts of biotite up to 3 mm can be seen in the lighter-gray veins that are found associated with some of the dikes in the complex. The dikes are generally uniform in composition; three dikes, one on the Moroni Slopes to the southeast of Cedar Mountain (# 89, Appendix 1), and two to the west of the Notch on the Waterpocket Fold (# 145 and 146, Appendix 1), show moderate amounts of lighter-colored material either intermingled with the dike material or as veins that cut the dike perdendicular to dike thickness. The second and third dikes contain thin, 1- to 10-cm veins of the lighter-colored material that contains phenocrysts of biotite. Samples of the lighter-colored dike material have been collected for petrologic and mineralogic studies, and the results will be discussed in a later section.

Petrography

Olivine Basalt

The color of the samples varies from medium- to dark-gray-black; the

crystal content ranges from 25-55 percent; mafic minerals include olivine,clinopyroxene, biotite, kaersutite (rare), and iron titanium oxides; felsic minerals include labradorite, orthoclase, and very rare quartz; the groundmass varies from microcrystalline to cryptocrystalline.

The dikes in the study area are composed of medium- to fine-grained basalt and can be classified as olivine basalt on the characteristic ferromagnesian mineral content. The phenocrysts are large; some olivine crystals exceed 3 mm in diameter and occasionally form glomeroporphyritic aggregates. Essential augite is present as phenocrysts up to 1.5 mm in diameter and is the major constituent of the groundmass. Labradorite is the main feldspar present, rarely as phenocrysts, but is an important constituent in the groundmass. Minor amounts of orthoclase (<2 percent) are present as rims on the plagioclase and rarely as euhedral crystals. Occasionally, brown amphibole (kaersutite) has been seen as rims on the augite crystals. Scattered analcite crystals (possibly primary in origin) and more commonly amygdaloidal analcite occur throughout the dike rocks. Thomsonite and natrolite occur as amygdaloidal fillings but not commonly as alteration of plagioclase. Brown biotite occurs throughout the dike rocks, and in 3 locations (# 89, 145, 146, Appendix 1) it is the dominant mafic mineral in thin light-colored veins in the dikes. Detailed petrographic descriptions and selected modal analyses are given in Appendix 4.

Mineralogy

Olivine

Olivine occurs almost entirely as phenocrysts ranging from 0.3 to 3.25 mm in length. The olivine crystals throughout the dike complex exhibit varying degrees of alteration and replacement by serpentine, iddingsite, calcite, and chlorite. Alteration is less extensive in the thicker dikes and buds, and the distance from dike-host rock contact suggests that replacement may have been facilitated by water derived from the surrounding country rock. The crystals are colorless to pale green in thin section and tend to be euhedral to subhedral. In a few thin sections complex skeletal olivine grains with embayments have been noted. Calcite pseudomorphs of the olivines are common in the most extensively altered rocks. Rare simple twinning of the crystals has been noted. Serpentine and iddingsite are common alteration minerals along irregular cracks in the mineral grains and leave only small islands of unaltered olivine.

Pyroxene

Augite predominates over all other mafic minerals and makes up to 50 percent of some rocks. The mineral occurs as crystals that range between 0.1 and 2.5 mm in size. The crystals are pale-green in thin section and are easily distinguished from the olivines. The augite occurs as phenocrysts, euhedral to subhedral grains, characteristically stubby rectangular prisms and square basal sections. Occasionally ragged overgrowths of brown hornblende (kaersutite) has been seen. Some crystals are zoned, with the outer margins showing a brighter-green tint due to the presence of aegirine-augite. Hourglass and oscillatory zoning and simple twinning are evident in most thin sections. However most grains are unzoned and may include poikilitic magnetite, biotite, and apatite. Complex branching augite with subparallel

alignment was noted on one thin section; this sample is from the center of a pyroxene-rich band in the dike. Augite crystals form glomeroporphyritic clots of radiating star-like clusters, and many have cores of magnetite. Some augite grains have been partially replaced by calcite.

Biotite

Biotite occurs mainly in clusters of small plates that range from 0.5 to 2 mm in length. The flakes are shades of brown and are strongly pleochroic. Much of the biotite encloses feldspar and augite poikilitically and is disseminated into cracks of olivine and augite crystals. Some hydrothermal alteration of biotite to chlorite has been noted along cleavages. Oriented grains of biotite similar to flow banding have been noted in the light-colored veins at a few localities. Rare inclusions of magnetite and apatite are present in some biotite grains. Biotite grains are often associated with the olivines and titanomagnetite and may suggest late or post-magmatic reactions.

Hornblende (kaersutite)

Amphibole is rare and appears as ragged imperfect crystals that rim the augite and range in size up to 1.0 mm. Kaersutite-rimmed augite indicates disequilibrium in late magmatic stages. The sections of hornblende present in the sample exhibit the characteristic cleavages at 54° and brown color in thin section.

Feldspars

The plagioclase composition was determined by measuring the extinction angle in the thin section perpendicular to the "a" crystallographic axis (Shelley, 1975). Extinction angles in the plagioclase sections ranged from 28° to 40°. The plagioclase composition of labradorite (An_{43-61}) was confirmed when x-ray diffraction analyses were completed on selected samples. Small miarolites containing plagioclase microlites have been seen in some thin sections and may represent late emission of gas in small quantities towards the end of crystallization. The plagioclase crystals range from 0.05 to 1.0 mm in length, but most are fine microlites contained in the groundmass. The plagioclase grains are corroded and embayed, being penetrated by analcite and thomsonite. Some plagioclase is present as anhedral interstitial matrix and coexists with analcite, clay, and thomsonite in the groundmass. Albite twinning and compositional zoning of the larger plagioclase crystals is common throughout the samples.

The presence of orthoclase was also confirmed by x-ray diffraction analysis techniques. Minor amounts of orthoclase (<3 percent) are present as rims on the plagioclase. Rare anhedral, untwinned orthoclase crystals were seen in thin section. The orthoclase is probably primary, but extensive alteration and replacement has reduced the modal amount substantially. Gilluly (1927) reported 8 percent soda-orthoclase in the modal analyses of the analcite diabase. Alteration and replacement of the orthoclase could explain the minor amounts reported in this study.

Primary Accessory Minerals

Magnetite

Subhedral to euhedral titanomagnetite is present in all dike samples. Rare euhedral unzoned grains are contained as inclusions in unaltered olivineand pyroxene. However, some magnetite has biotite rims and intergrowths. Irregular patches of secondary magnetite have formed in the samples containing olivines extensively altered to serpentine. In many samples the magnetite occurs as fine grains contained in the groundmass.

Apatite and Zircon

Euhedral prismatic crystals of apatite as inclusions in the ferromagnesian minerals are common throughout the dike samples. The crystals characteristically have moderately high relief and weak birefringence and are colorless in thin sections.

Zircon appears as tiny euhedral, tetragonal crystals enclosed in primary biotite. In thin section, the zircon is pale yellow to colorless, with extreme relief and very strong birefringence.

Secondary Minerals

Calcite

Calcite alteration and replacement are common throughout the dikes. Calcite occurs as pseudomorphs of olivine crystals, and as small patches and stringers throughout the dike rocks. Calcite crystals as partial or complete amygdaloidal fillings are prevalent in most dike samples. Distinctive rhombohedral cleavage and strong birefringence characterize the calcite present in the dikes. The calcite is closely associated with the zeolites in these rocks. The presence of calcite indicates late stages of hydrothermal alteration.

Analcite, thomsonite and natrolite

In the dike samples are scattered interstial analcite crystals and patches of analcite associated with plagioclase grains, but most commonly the analcite appears as cavity or vein filling. Analcite in these rocks could have resulted from the replacement of the plagioclase by Na-rich hydrothermal fluids and deposition of secondary analcite at a later time. Isotropic character and no birefringence are distinctive of the analcite in the study area. Occasionally some of the mineral grains have a very low birefringence and may be wairakite, the Ca-analcite. This was not confirmed by XRD.

Thomsonite has been found in many dike samples in the complex. The thomsonite appears as fillings in cavities and is in close association with the other zeolites.

Two occurrences of the fibrous mineral natrolite have been seen in the thin sections and confirmed by x-ray diffraction analyses. The mineral occurs as amygdaloidal filling in association with analcite and thomsonite.

The presence of the zeolites and calcite are indicative of a later stage hydrothermal mineral crystallization in vesicles, cracks, and on the fracture

surfaces of the dikes. Replacement of the plagioclase by possibly Na-rich hydrothermal fluids may have resulted in the formation of the zeolites.

Alteration

Extensive alteration of the dike rock material is evident from field inspection, thin section, and x-ray diffraction work. Zeolitic alteration of feldspar is common, as is amygdaloidal and crack fillings. Calcite alteration and replacement of the ferromagnesian minerals, especially olivine, is present in most samples studied. Iddingsite, chlorite, and serpentine alteration of olivines are also a predominant alteration product. Fine-grained clay alteration of small pools of basaltic glass has been seen in the thin section analyses. The presence of clay minerals was confirmed by x-ray diffraction analyses of selected samples.

Order of Crystallization

The order of crystallization for the dike material is presented as a result of thin section study of mineral intergrowth and crystal margin relations:

1. Olivine
2. Magnetite
3. Apatite and zircon
4. Augite
5. Plagioclase
6. Biotite
7. Hornblende
8. Orthoclase
9. Thomsonite, analcite and natrolite
10. Serpentine, iddingsite, chlorite, and calcite

Introduction

Major-element analyses have been performed on 76 samples from the San Rafael and Capitol Reef areas, Utah. Gilluly (1927) originally reported the results of the analyses; subsequent data sets were taken from Smith and others (1963), Wilshire (1967), Williams (1983) and Gartner (this report). The data sets were edited to include only complete analyses of well-located, well-characterized fresh rocks. Total iron reported as Fe_2O_3 has been converted to FeO using Hughes and Hussey's method (1979) where a correction ratio of Fe_2O_3/FeO equal to 0.25 has been applied. All analyses were recalculated to 100 percent on an anhydrous basis. Williams, (1983) data for shonkinite from Cedar Mountain sill were included on all tables and figures as a comparison to the sample analyses from the study area.

The major-element composition together with calculated CIPW norms of the dike samples are given in Table 3. Analyses of Gilluly (1927), Smith and others (1963) and Wilshire (1967) are also included in Table 3. The average composition of 18 and 16 sample analyses of the basaltic material completed during this study has been included in Table 3 and on all data plots. Figure 12 is the key to the symbols used for the data plotted in figures 13-19. The average 18 includes all samples except 82SRS-7, and the average 16 includes all analyses except 82SRS-1,5, and 7. According to the classification scheme of Irving and Baragar (1971) the basalts plot within the alkali basalts and picrite basalts (fig. 14). On a SiO_2 versus $Na_2O + K_2O$ plot as proposed by Irving and Baragar (1971) (fig. 13), all the basalts plot in the subalkaline field, and the analcite syenite (Gilluly, 1927) plots in the alkaline field. The abundance of alkalies, TiO_2 and P_2O_5 and depletion of SiO_2 are the basis for calling these rocks alkaline. AFM and oxide component diagrams are given in figures 15-19.

Despite the porphyritic nature of most of the intrusive rocks of the San Rafael and Capitol Reef area, Utah, the Harker diagrams display fairly smooth and regular trends. MgO, Fe_2O_3, + FeO (total iron), CaO, and P_2O_5 decrease smoothly and regularly with increasing SiO_2. Al_2O_3, TiO_2, and MnO decrease somewhat less regularly with increasing SiO_2. K_2O and to a lesser extent Na_2O increase with increasing SiO_2.

The chemistry of the intrusive rocks in the San Rafael and Capitol Reef areas is presented in an AFM diagram (fig. 19), in which total alkalies, total iron as FeO*, and magnesia are plotted as relative proportions. The analyses plot as a relatively narrow band, suggesting that they are genetically related. The rocks are calc-alkaline, and plot well below the tholeiitic-calc-alkaline boundary of Irvine and Baragar (1971). The iron depletion that depresses bulk rock compositions into the calc-alkaline field when projected onto an AFM diagram (fig. 19) could represent fractionation of magnetite which depletes the residual melt in iron (Kuno, 1968).

MgO, FeO*, Al_2O_3, and FeO*/MgO

The content of the oxide components MgO, FeO*, and CaO in the intrusive rocks of the area are plotted versus SiO_2 content (figs. 15, 16). Each component behaves in a similar manner and shows a negative correlation with SiO_2. The decrease is regular with some scatter in the data. The data suggest that the rocks share a common origin and evolution.

TABLE 3. Chemical Analyses of San Rafael and Capitol Reef Intrusive Rocks. [Oxides adjusted to sum to 100% without water. CIPW normative numbers are reported in weight % and were calculated using the exact formulae of Washington (1917). SRS samples, the total Fe reported as $FeTO_3$, converted to FeO by: FeO = 0.8 Fe_2O_3 for norm calculations. Sources of data: JG numbers, J. Gilluly (1927); HW numbers, H. G. Wilshire (1967); CM and LS numbers, J. D. Williams (1983); SRS numbers, Gartner (this report); CR numbers, Smith and others (1963); AVG numbers, averaged values of SRS data.]

Sample #	JG1-27A	J62-27C	HW-36	HW-37	HW-38	HW-39	HW-40	HW-41	CM-032	LS-142	LS-143	LS-144	LS-145	CR-132	CR-176	SRS1-84	SRS2-84	SRS3-84	SRS4-84
SiO_2	45.70	51.80	49.23	56.87	46.50	48.39	46.99	48.73	47.89	49.47	48.34	47.29	48.00	44.88	47.16	47.68	47.07	46.92	45.28
Al_2O_3	13.96	18.62	15.77	16.29	15.92	16.27	15.95	15.99	14.63	14.96	15.17	13.45	15.03	14.89	15.08	16.53	14.82	14.38	13.83
Fe_2O_3	4.24	3.16	4.48	2.73	4.32	4.99	4.96	4.62	1.87	1.74	1.91	1.92	1.82	5.80	5.38	1.81	1.92	2.01	2.05
FeO	5.63	3.38	4.69	5.16	4.09	3.69	3.77	3.97	6.27	6.24	6.89	6.92	6.56	5.36	3.88	7.24	7.72	8.03	8.19
MgO	10.81	3.24	8.74	4.35	6.14	7.05	6.49	7.30	10.66	10.31	9.90	12.16	10.65	7.88	6.89	5.22	9.92	10.81	11.88
CaO	11.16	7.34	9.80	6.78	14.78	12.15	14.12	12.02	8.70	7.92	7.88	10.39	8.53	14.89	13.24	13.35	10.16	10.51	11.58
Na_2O	3.23	4.59	2.03	3.24	2.39	2.06	2.05	1.83	2.88	3.91	3.87	3.08	4.11	1.53	2.80	2.60	3.15	3.06	3.16
K_2O	2.17	4.99	2.98	3.04	3.75	3.69	3.67	3.54	3.15	3.33	3.42	2.78	3.08	1.75	2.91	2.48	2.49	1.99	1.52
TiO_2	2.40	2.07	1.28	0.98	1.36	0.96	1.29	1.29	1.35	1.32	1.31	1.24	1.36	1.97	1.40	1.95	1.64	1.31	1.45
P_2O_5	0.60	0.69	0.80	0.40	0.55	0.55	0.53	0.53	0.72	0.64	0.64	0.61	0.67	0.89	1.08	0.98	0.93	0.83	0.91
MnO	0.10	0.10	0.21	0.16	0.20	0.20	0.19	0.19	0.15	0.15	0.16	0.16	0.17	0.15	0.18	0.18	0.17	0.17	0.18
FeO*/MgO	0.87	1.92	0.99	1.75	1.30	1.16	1.27	1.11	0.81	0.77	0.89	0.73	0.79	1.34	1.27	1.70	0.95	0.91	0.84
Q	--	--	--	6.01	--	--	--	--	--	--	--	--	--	--	--	--	--	--	--
Or	12.80	29.51	17.63	17.94	11.37	21.80	20.83	20.93	18.86	19.70	20.21	16.42	18.23	10.35	17.18	14.65	14.70	11.75	8.96
Ab	8.42	20.27	17.13	27.40	21.63	8.09	--	10.68	13.08	14.77	12.99	5.42	9.99	8.11	9.05	10.95	11.60	11.99	7.03
An	17.19	15.47	25.13	20.95	--	24.26	23.51	24.98	17.91	13.41	13.96	14.65	13.43	28.57	19.98	26.12	18.99	19.63	19.19
Lc	--	--	--	--	8.45	--	0.66	--	--	--	--	--	--	--	--	--	--	--	--
Ne	10.24	10.06	--	--	10.94	5.07	9.39	2.58	6.28	9.94	10.69	11.20	13.44	2.63	7.94	5.97	8.16	7.53	10.57
Di	26.99	12.85	14.44	8.20	37.46	25.45	33.78	24.54	16.86	17.36	16.83	26.32	19.63	31.08	30.25	27.57	20.41	21.83	25.96
DiWo	14.31	6.86	7.64	4.22	20.09	13.53	17.99	13.04	8.78	9.06	8.74	13.74	10.23	16.49	16.16	14.09	10.58	11.31	13.48
DiEn	11.38	5.73	5.93	2.58	15.29	11.01	14.81	10.51	6.06	6.31	5.89	9.61	7.09	13.19	13.54	8.01	6.96	7.42	9.03
DiFs	1.29	0.26	0.87	1.40	2.08	0.90	0.97	0.99	2.02	1.99	2.20	2.98	2.31	1.40	0.55	5.48	2.87	3.10	3.45
Hy	--	--	6.93	12.76	--	--	--	--	--	--	--	--	--	--	--	--	--	--	--
HyEn	--	--	6.05	8.26	--	--	--	--	--	--	--	--	--	--	--	--	--	--	--
HyFs	--	--	0.89	4.50	--	--	--	--	--	--	--	--	--	--	--	--	--	--	--
Ol	12.26	1.72	7.97	--	--	5.01	0.97	5.93	19.96	18.30	18.57	19.44	18.50	5.05	2.65	6.15	18.09	19.96	20.48
OlFo	10.89	1.64	6.86	--	--	4.59	0.91	5.37	14.60	13.57	13.16	14.49	13.62	4.52	2.54	3.51	12.43	13.67	14.42
OlFa	1.37	0.08	1.11	--	--	0.41	0.07	0.56	5.36	4.73	5.41	4.94	4.88	0.53	0.11	2.65	5.66	6.29	6.06
Cs	--	--	--	--	--	--	--	--	--	--	--	--	--	--	--	--	--	--	--
Mt	6.15	4.58	6.49	3.96	6.26	7.27	7.19	6.69	2.59	2.52	2.77	2.78	2.64	8.41	7.81	2.63	2.79	2.91	2.97
Il	4.57	3.94	2.43	1.86	2.59	1.81	2.46	2.45	2.59	2.51	2.49	2.35	2.59	3.74	2.66	3.70	3.11	2.48	2.74
Ap	1.42	1.64	1.89	0.94	1.29	1.31	1.25	1.25	1.73	1.52	1.52	1.44	1.59	2.10	2.55	2.31	2.21	1.96	2.16
Alkali	40.15	52.11	59.57	48.39	61.11	64.15	64.15	66.00	52.24	46.00	46.93	47.40	42.85	53.33	50.94	48.85	44.10	39.39	32.50
Felsic	32.59	56.61	33.81	48.06	29.35	32.12	28.80	30.86	40.93	47.79	48.05	36.08	45.76	18.07	30.11	27.55	35.69	32.46	28.66
Mafic	47.73	66.84	51.19	64.46	57.81	55.17	57.45	54.05	44.62	43.64	47.06	42.08	44.06	58.62	57.33	63.40	49.29	48.14	46.27
D. I.	31.46	59.83	34.76	51.35	30.79	34.96	30.87	34.19	38.22	44.41	43.89	33.04	41.66	21.10	34.16	31.57	34.46	31.27	26.55

TABLE 3. Chemical Analyses of San Rafael and Capitol Reef Intrusive Rocks--continued

Sample #	SRS5-84	SRS6-84	SRS7-84	SRS8-84	SRS9-84	SRS12-84	SRS13-84	SRS14-84	82SRS-1	82SRS-2	82SRS-3	82SRS-5	82SRS-7	82SRS-8	82SRS-9	AVG. 18	AVG. 16
SiO_2	45.99	48.07	46.63	47.70	49.47	49.22	48.17	48.08	66.22	47.87	47.01	43.68	79.60	47.93	48.20	48.41	47.32
Al_2O_3	15.05	15.18	14.76	14.57	15.80	15.38	15.56	15.96	14.41	14.92	14.38	12.57	7.71	15.94	15.66	14.98	15.02
Fe_2O_3	1.97	1.87	2.02	1.88	1.73	1.91	1.97	1.90	0.93	1.90	2.00	0.74	0.24	1.83	1.85	1.79	1.84
FeO	7.88	7.49	8.05	7.53	6.93	7.65	7.90	7.52	3.71	7.84	8.01	2.95	0.98	7.34	7.39	7.20	7.36
MgO	7.99	7.83	11.15	8.56	5.74	7.43	9.04	7.29	2.26	8.81	10.68	5.15	2.29	8.20	8.56	8.14	8.47
CaO	12.83	10.96	10.05	12.52	11.38	10.37	9.67	11.46	4.84	10.95	10.68	30.27	4.46	9.60	9.26	11.69	12.16
Na_2O	1.88	3.09	1.84	2.01	2.99	2.45	2.36	2.20	3.85	1.90	2.95	2.71	2.14	3.43	3.74	2.74	2.72
K_2O	3.68	2.86	2.89	3.10	3.97	3.56	3.10	3.30	2.85	3.61	1.98	0.75	2.10	3.07	3.01	2.70	2.73
TiO_2	1.55	1.37	1.51	1.35	1.23	1.24	1.28	1.40	0.65	1.30	1.32	0.77	0.38	1.44	1.26	1.33	1.38
P_2O_5	1.02	1.11	0.94	0.63	0.63	0.66	0.77	0.76	0.25	0.69	0.85	0.30	0.08	1.07	0.91	0.79	0.83
MnO	0.17	0.18	0.17	0.16	0.19	0.15	0.18	0.16	0.03	0.16	0.16	0.09	0.03	0.15	0.16	0.16	0.16
FeO*/MgO	1.21	1.17	0.89	1.08	1.48	1.26	1.07	1.17	2.01	1.09	0.92	0.70	0.52	1.10	1.06	1.08	1.07
Q	--	--	--	--	--	--	--	--	19.46	--	--	--	49.47	--	--	--	--
Or	17.58	16.89	17.08	18.31	23.44	21.01	18.33	19.49	16.85	21.32	11.73	--	12.38	18.48	17.77	16.04	16.15
Ab	--	12.27	9.80	4.55	7.01	11.83	13.31	8.82	32.61	6.24	12.30	--	18.09	12.98	12.99	12.35	6.46
An	21.78	19.18	23.50	21.59	17.99	20.47	22.70	23.94	13.61	21.53	20.04	19.89	5.25	19.01	17.07	22.32	20.69
Le	3.26	--	--	--	--	--	--	--	--	--	--	3.50	--	--	--	--	--
Ne	8.60	7.51	3.11	6.73	9.89	4.80	3.61	5.28	--	5.33	6.86	12.44	--	8.71	10.09	4.27	8.98
Di	28.55	22.74	16.29	29.47	27.85	21.66	16.35	22.69	7.21	22.91	22.12	34.61	12.95	17.48	18.55	24.87	27.67
DiWo	14.70	11.71	8.45	15.21	14.24	11.12	8.44	11.66	3.65	11.82	11.46	18.09	6.83	9.03	9.58	12.84	14.29
DiEn	9.04	7.23	5.62	9.60	8.14	6.68	5.30	7.06	1.88	7.41	7.51	12.81	5.19	5.70	6.06	8.10	9.07
DiFs	4.81	3.81	2.21	4.66	5.47	3.86	2.61	3.97	1.68	3.69	3.15	3.72	0.94	2.76	2.91	3.93	4.31
Hy	--	--	--	--	--	--	--	--	7.09	--	--	--	0.60	--	--	--	--
HyEn	--	--	--	--	--	--	--	--	3.74	--	--	--	0.51	--	--	--	--
HyFs	--	--	--	--	--	--	--	--	3.35	--	--	--	0.09	--	--	--	--
Ol	12.08	13.60	22.27	12.61	7.51	13.57	18.62	12.61	--	15.78	19.58	0.02	--	15.79	16.36	13.19	12.84
OlFo	7.61	8.61	15.53	8.21	4.31	8.29	12.07	7.78	--	10.19	13.39	0.02	--	10.31	10.69	8.60	8.42
OlFa	4.47	4.99	6.74	4.39	3.20	5.28	6.55	4.83	--	5.59	6.19	--	--	5.49	5.67	4.59	4.14
Cs	--	--	--	--	--	--	--	--	--	--	--	26.30	--	--	--	--	--
Mt	2.86	2.71	2.93	2.72	2.51	2.77	2.86	2.75	1.39	2.85	2.91	1.08	0.35	2.65	2.68	2.60	2.67
Il	2.94	2.60	2.87	2.56	2.34	2.35	2.43	2.66	1.23	2.47	2.51	1.45	0.72	2.74	2.40	2.54	2.19
Ap	2.41	2.62	2.21	1.48	1.50	1.57	1.83	1.80	0.59	1.63	2.00	0.72	0.20	2.53	2.15	1.88	1.97
Alkali	66.22	48.05	61.12	60.68	57.05	59.25	56.78	60.04	42.52	65.50	40.21	21.75	49.05	47.20	44.58	53.17	50.09
Felsic	30.22	35.16	31.99	28.97	38.02	36.66	36.11	32.41	58.10	33.46	31.50	10.28	48.67	40.40	42.14	30.30	30.97
Mafic	55.20	54.42	47.45	52.37	60.14	56.25	52.18	56.35	67.27	52.65	48.38	41.78	34.84	39.84	40.85	32.65	31.60
D. I.	29.44	36.67	29.99	29.60	40.34	37.64	35.26	33.59	68.93	32.88	30.89	15.93	79.93	39.84	40.85	32.65	31.60

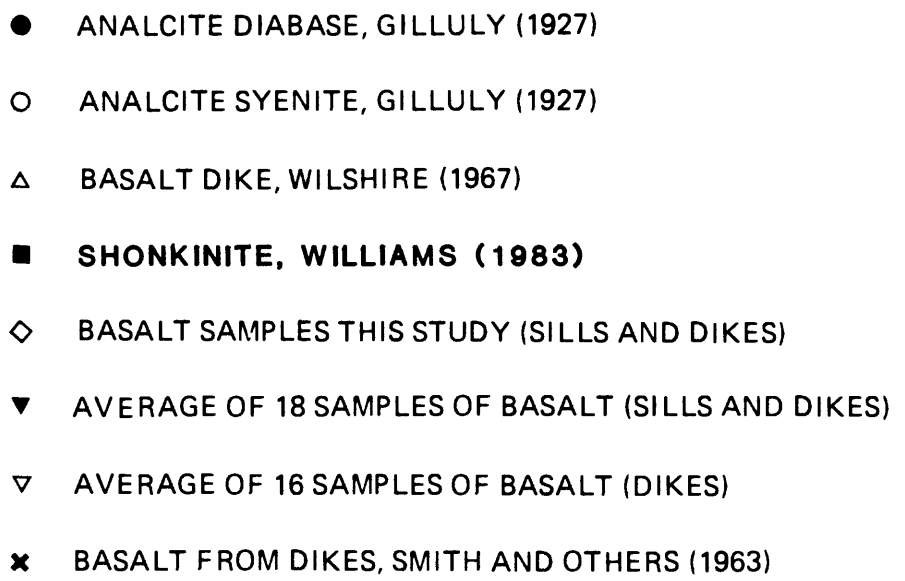

Figure 12. Key to symbols on variation diagrams.

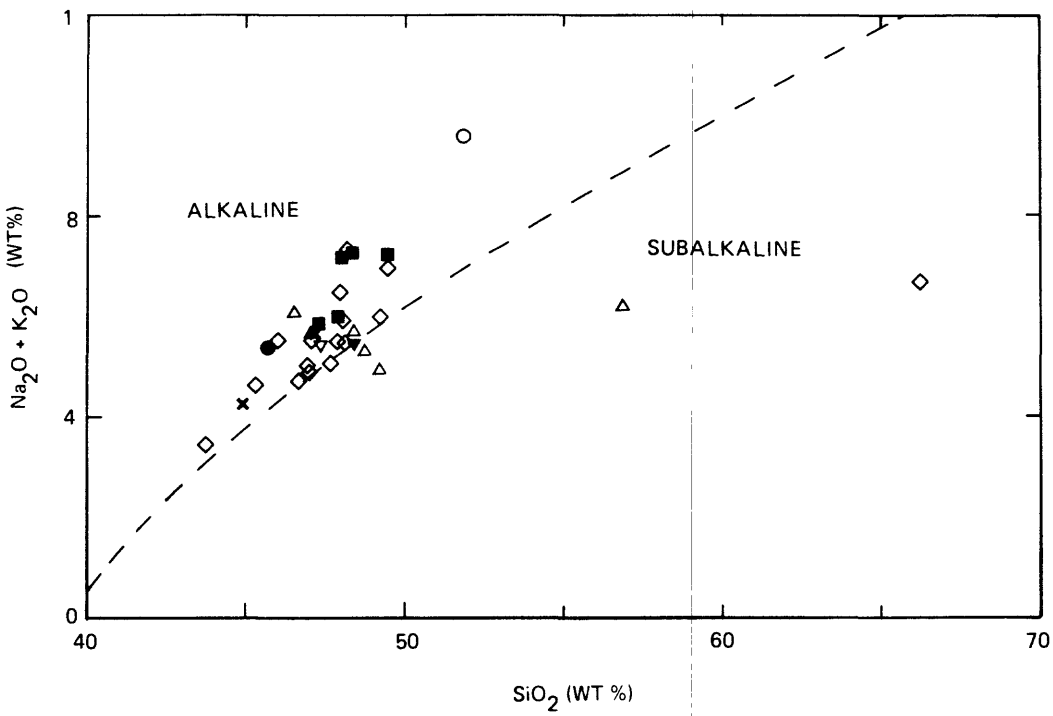

Figure 13. $Na_2O + K_2O$ versus SiO_2 plot for intrusive rocks in San Rafael and Capitol Reef areas, Utah. Dividing line between alkaline and subalkalkine fields proposed by Irvine and Baragar (1971).

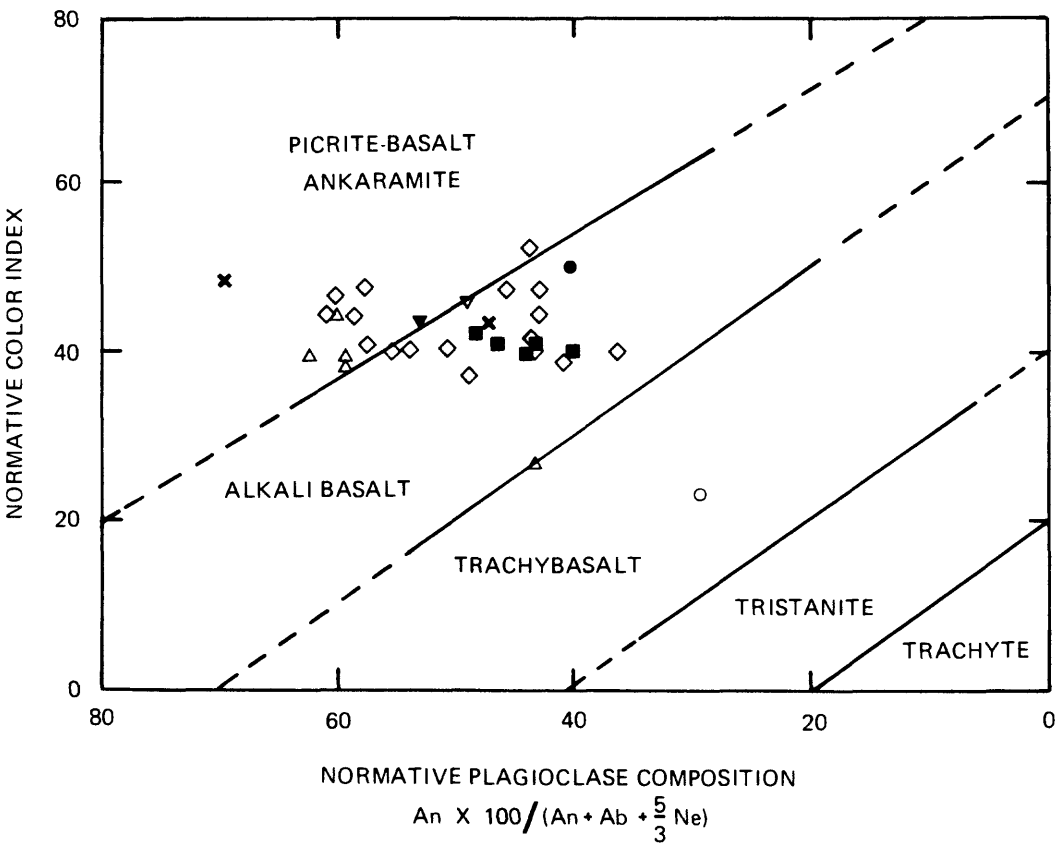

Figure 14. Classification of the intrusive rocks from the San Rafael and Capitol Reef areas, Utah, after Irvine and Baragar (1971).

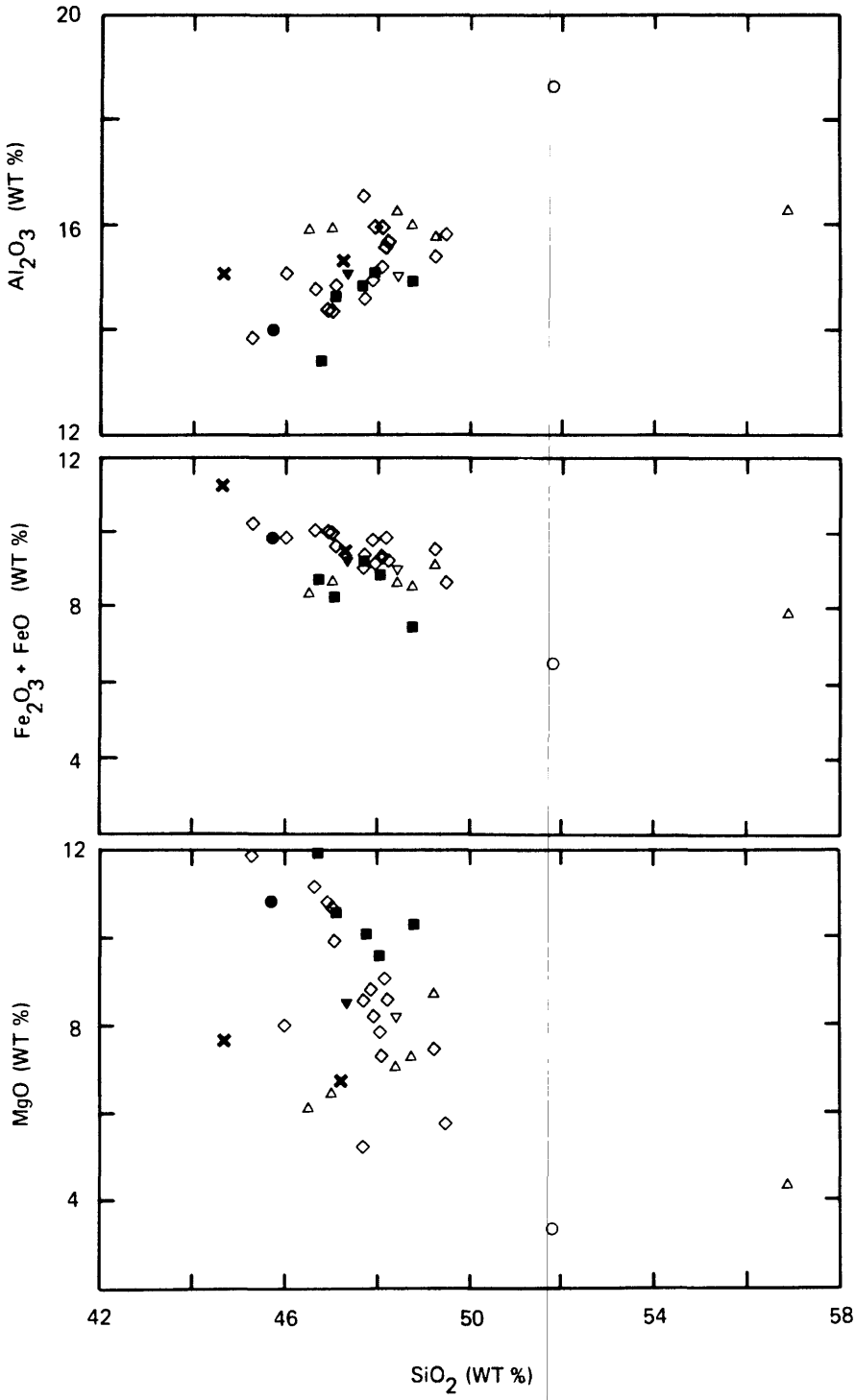

Figure 15. Variation diagrams showing Al_2O_3, Fe_2O_3 + FeO (total iron), and MgO versus SiO_2 for intrusive rocks of the San Rafael and Capitol Reef areas, Utah.

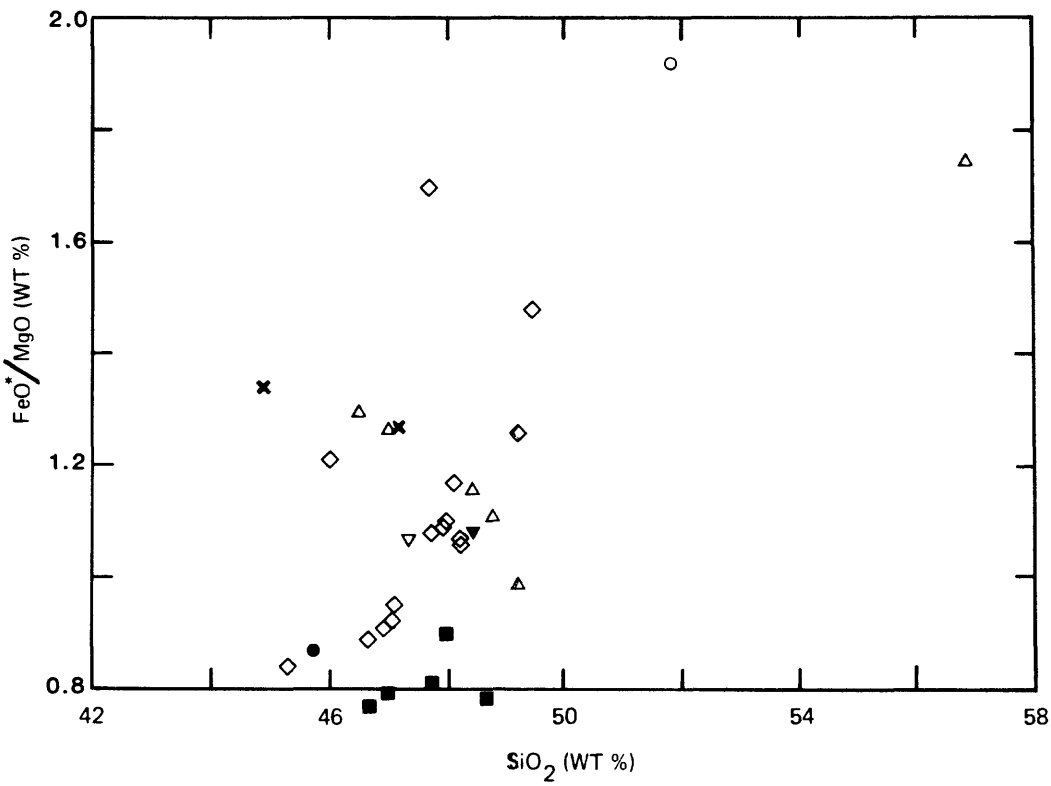

Figure 16. Variation diagram showing FeO*/MgO versus SiO_2 of the intrusive rocks of San Rafael and Capitol Reef areas, Utah.

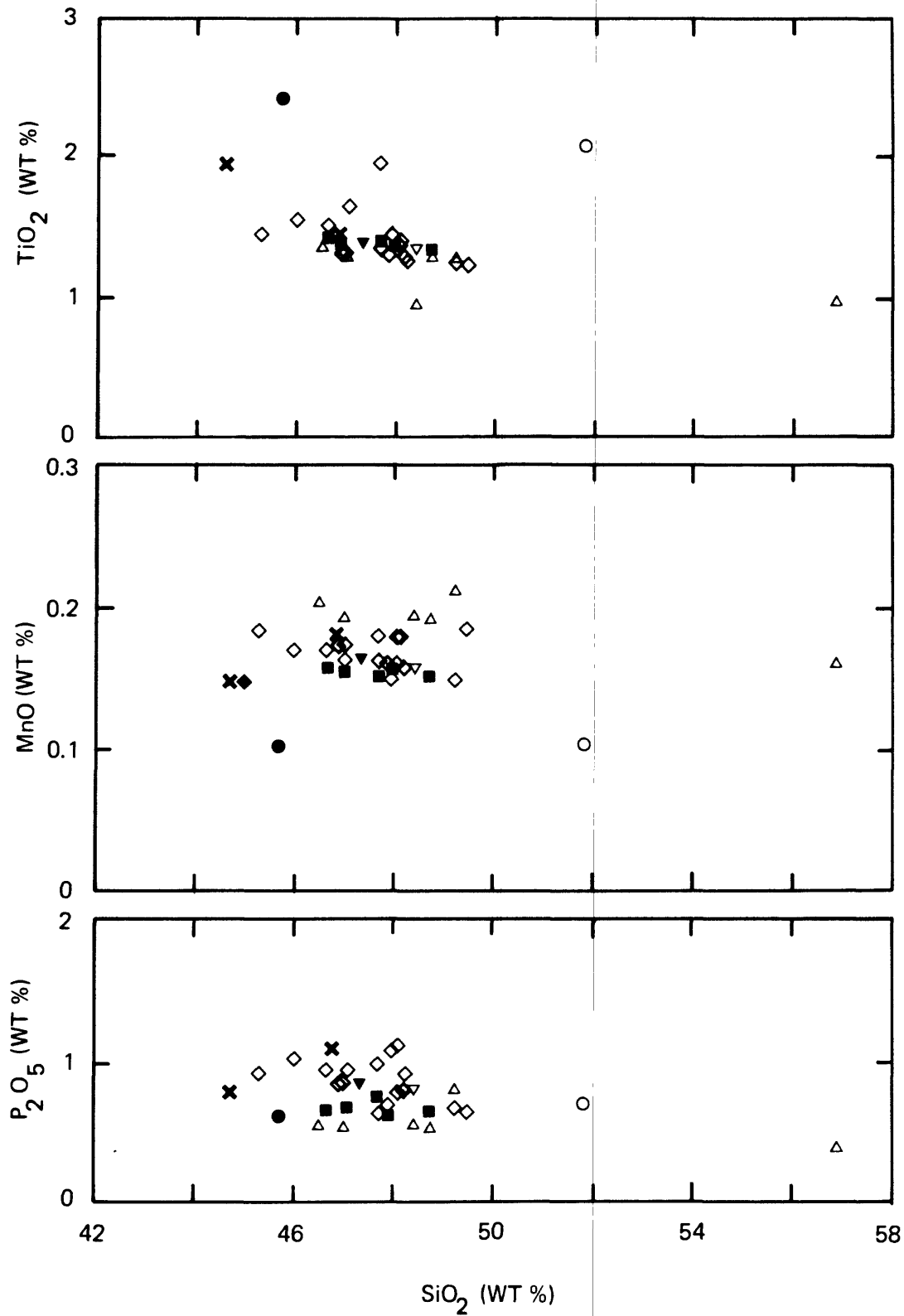

Figure 17. Variation diagrams showing TiO_2, MnO and P_2O_5 versus SiO_2 in the intrusive rocks of San Rafael and Capitol Reef areas, Utah.

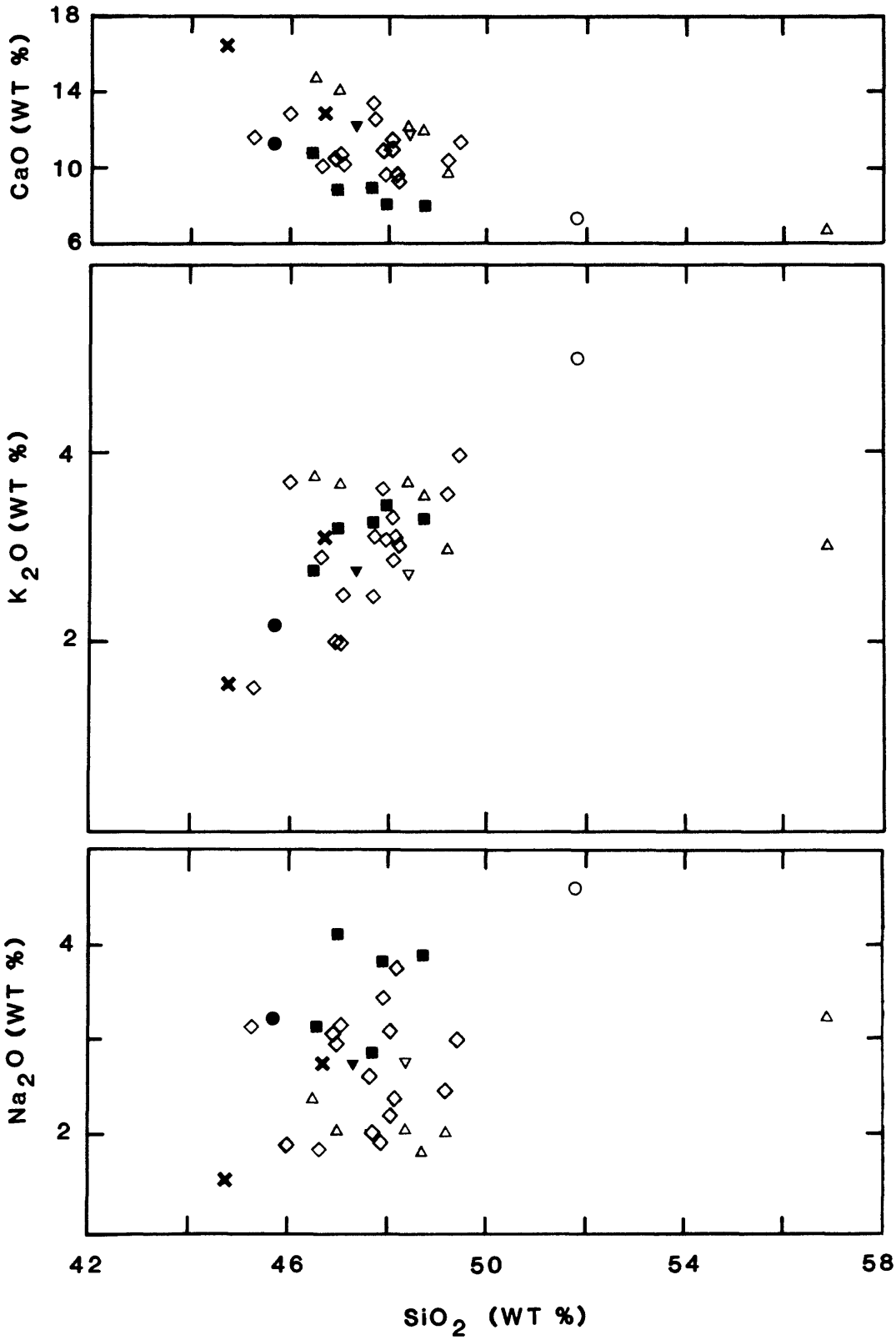

Figure 18. Variation diagrams showing CaO, K_2O, and Na_2O versus SiO_2 of the rocks of San Rafael and Capitol Reef areas, Utah.

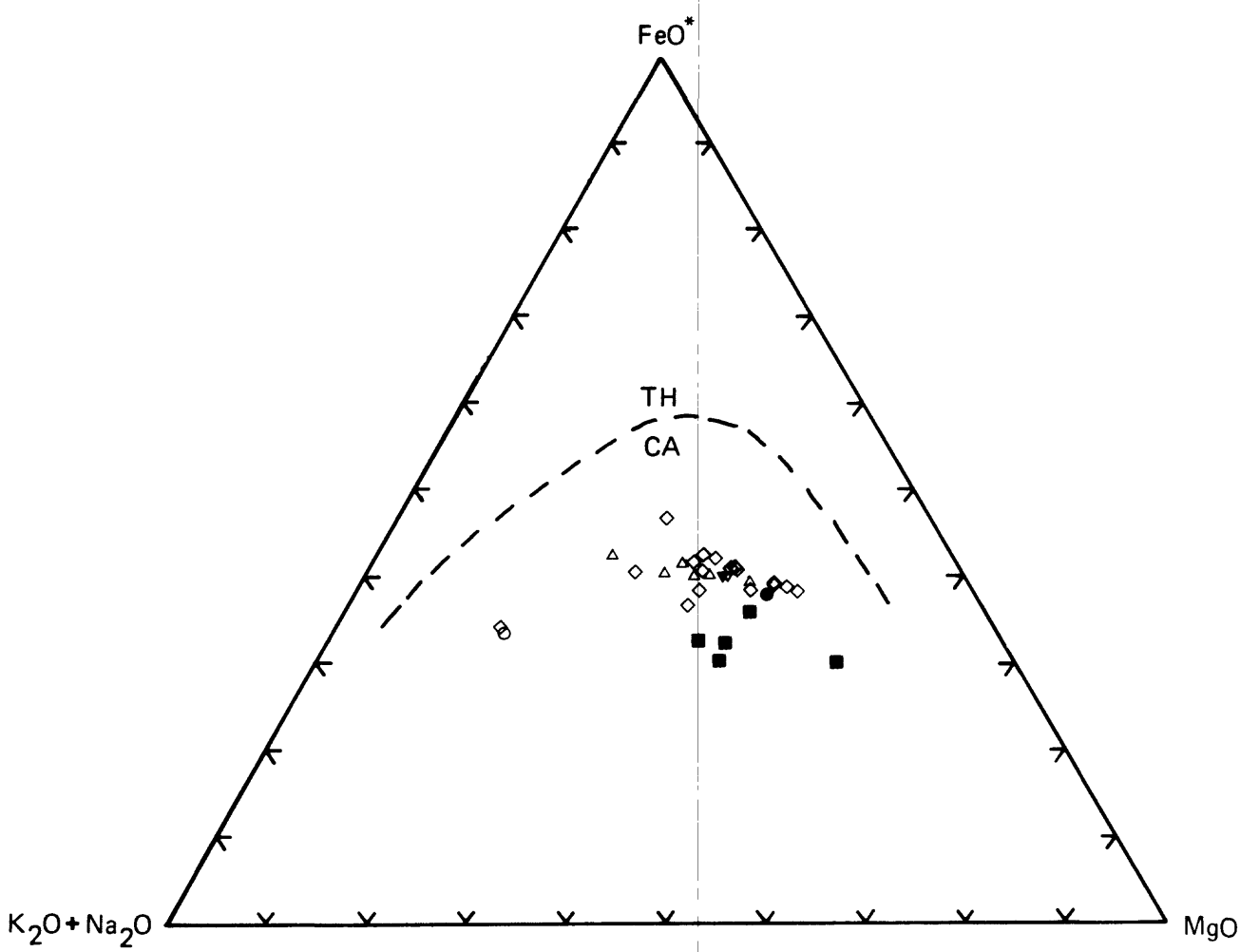

Figure 19. AFM diagram of the intrusive rocks of San Rafael and Capitol Reef areas, Utah. A = total alkalies (K_2O + Na_2O), F = total iron as FeO*, and M = MgO. The criteria of Irvine and Bargarar (1971) were used to delineate the tholeiitic (TH) and calc-alkaline (CA) fields.

MgO content of the intrusive rocks ranges from ∿5 wt. % to ∿12 wt. % (fig. 15). The overall trend of MgO correlates negatively with SiO_2; however, there is some scatter of the data may represent varying degrees of alteration of the samples.

FeO* content of the intrusive rocks range from ∿6 wt. % to ∿12 wt. % (fig. 15), decreasing linearly with increasing SiO_2. The data show little scatter.

Al_2O_3 content (fig. 15) ranges between ∿14 wt. % and ∿17 wt. % with an average of ∿15 wt. %. Most of the intrusive rocks show increasing Al_2O_3 with increasing SiO_2, although there is some scatter of the data at higher SiO_2 content.

FeO*/MgO plotted versus SiO_2 (fig. 16) shows more variability than either MgO or FeO* alone, and the behavior of FeO*/MgO with increasing silica content is more complex. FeO*/MgO ranges from 0.8 to 1.7.

TiO_2, P_2O_2, and MnO

The content of the oxide components TiO_2, Al_2O_3, P_2O_5, and MnO in the intrusive rocks are plotted versus SiO_2 content (fig. 17). The components show less regular correlations and more scatter of the data.

TiO_2 content (fig. 17) of the rocks displays an overall decreasing trend with increasing SiO_2 content, although some scatter is present. The average TiO_2 is about 1.4 wt. %.

P_2O_5 content (fig. 17) shows an overall decrease with increasing silica. There is again some scatter of the data, but an overall negative correlation is not apparent.

MnO content (fig. 17) of the rocks ranges between 0.15 wt. % and 0.18 wt. %, but no negative correlation is evident in the data. Scatter at the higher SiO_2 may be due to small amounts of mafic inclusion material in the groundmass of these rocks.

CaO, K_2O and Na_2O

CaO content ranges from ∿9 wt. % to ∿13 wt. % (fig. 18), decreasing linearly with increasing SiO_2. The data do show some scatter and may represent alteration in the samples.

K_2O content (fig. 18) correlates linearly and positively with SiO_2 content in the intrusive rocks of the study area. There is some scatter of data on the diagram, but the overall trend is positive.

Na_2O content (fig. 18) of the rocks ranges from ∿2 wt. % to ∿4 wt. %, but a positive correlation with increasing SiO_2 is not apparent in the data set. The scatter may be due to the rapid loss of sodium during the weathering process. However, the scatter is not apparent in the Mg and Ca content; elements normally showing similar loss during the weathering process. Hydrothermal alteration may play a role the loss of sodium.

Normative Mineralogy

The CIPW norm represents an idealized anhydrous mineralogy into which a magma with given chemistry would crystallize if formed under an assumed set of uniform conditions. Normative mineralogy is reported for the intrusive rocks of the San Rafael and Capitol Reef area, Utah in Table 3. The intrusive rocks

are nepheline, diopside, and olivine normative.

The normative mineralogy corresponds well with the modal mineralogy. The rocks are high in normative nepheline, but the absence of modal nepheline may suggest that analcite has replaced the nepheline. The rocks are high in normative pyroxene and olivine, and these are phenocrysts present in abundance. The rocks contain between 35 and 52 percent normative plagioclase, and this corresponds fairly well with the plagioclase phenocryst composition. The range of An_{43-61} for rocks of similiar SiO_2 content may also suggest the genetically similar origin. Normative augite is about twice the amount determined by modal analysis, and the Ca in calcite could affect the augite composition. Normative olivine is comparable to the modal content.

DIKE FORMATION AND EMPLACEMENT

Introduction

Intuitively, the cracks occupied by dikes and sills appear to be tension gashes or cracks normal to the principal axis of tensional stress. This may be applicable to dikes that are injected into near-surface rocks, but it would appear that sills can rarely be thought to have formed under regional tension because the vertical stress axis is one of compression resulting from the load of the overlying rocks. At depth, this load exceeds the crushing strength of rock and there can be no principal stress that is tensional under steady stress and therefore, the failure will be due to shear fracture or flow (Hills, 1972). Dikes and sills do represent opening cracks or fractures at depths greater than 3-8 km, at this depth, the crushing strength of granite and other crystalline rock is exceeded, and some factor other than rock strength is involved (Hills, 1972). This appears to be the wedging effects of fluids penetrating the cracks; in some instances there is the possibility of an influence due to shock waves in addition to the steady applied forces, especially in the initiation of cracks (Hills, 1972).

Openings occupied by dikes rarely show evidence of displacement that would indicate that they were active faults at the time the dikes were intruded. Pollard (1973), as well as others, suggested that propagation directions of sheet intrusions are controlled by regional stress orientations, interference from adjacent intrusions, planar discontinuties, and changes in host rock properties. In Hawaii, Fiske and Jackson (1972) suggest that the direction of propagation of the shallow emplaced dikes contained largely within the volcanic edifices is strongly influenced by gravitational stresses and regional structures. On a larger scale, Jackson and Shaw (1975) contend that the volcanoes of the Pacific that form en echelon loci are positioned by changes over time in the stress field in the Pacific lithosphere and that the loci have tracked directions perpendicular to the direction of the least principal stress in the Pacific plate over the last 70-100 m.y. Dike emplacement has been postulated to occur either as magma flow into and dilation of preexisting fractures, or as magma flow into cracks opened by the pressure of magmatic injection. Each hypothesis will be discussed in the following sections.

Magma flow into preexisting cracks

In the first case where the crust may be pervaded by steeply dipping faults, joints, or other planes of weakness, dike orientation and emplacement are controlled by the preexisting structures and should parallel the rock fabric. Wilson (1970) suggested that this relationship may be present in a number of geologic settings, both lunar and terrestrial. Geologic mapping and geophysical studies of the rock fabric, including fractures, fault and joint set analyses can provide valuable information on emplacement mechanisms and likely locations of dikes and fissures. The validity of the emplacement mechanism depends on 3 criteria: the ascending magma must have access to the pre-existing fractures; the magma must exert enough force to dilate the fracture; and sufficient flow of magma must be injected along the distance of the fracture (Pollard and others, 1984). Shaw (1980) suggests that ascent of magma in the earth is a feedback process that combines episodic and incremental magma injections through a self-induced fracture system, which is

governed by the states of stress in the invaded rock and the locally acting fluid pressure of the magma. The magma pressure (P_m) must exceed the compressive stress acting across the fracture plane in order for dilation of the fracture to proceed. According to Pollard and others (1984) this compressive stress may not be a principal stress, and the direction of the principal stress at the time of injection may not have any unique relation to the preexisting crack or the dike.

There are two subhorizontal principal stresses associated with emplacement along a preexisting fracture. The first is designated

$$\sigma_1^r$$

and is the least compressive stress and is of arbitrary orientation α relative to the normal fracture plane; the second may be intermittent or maximum compressive stress,

$$\sigma_2^r$$

(fig. 20 insert). the following equation defines the ratio of stress $\underline{R}$, where tensile stress is positive (Pollard and others, 1984)

$$\underline{R} = (\sigma_1^r + \sigma_2^r + 2\underline{P_m}) \; / \; (\sigma_1^r - \sigma_2^r). \qquad (1)$$

P_m is defined as the pressure of the magma. Figure 20 is a graph of stress ratio R versus angle α. Two distinct regions are defined by Equation (1). In the lower part of the figure, dilation is not possible, and magma would not invade the fracture. However, in the upper part of the graph, dilation is possible for dike formation if the 2 other criteria are met, i.e. access of magma to the fracture and flow of a sufficient distance.

In order to use the condition set in Equation 1 (Pollard and others, 1982; 1984) the following manipulation must be completed to estimate the stress ratio $\underline{R}$. First the pressure of the magma is estimated as

$$\underline{P_m} = \gamma_m \underline{d} \qquad (2)$$

where γ_m is the unit weight of the magma, and $\underline{d}$ is depth. Next the principal regional stresses are estimated as

$$\sigma_1^r = -\underline{m}\gamma_r \underline{d} \quad \text{and} \qquad (3)$$

$$\sigma_2^r = -\underline{n}\gamma_r \underline{d} \qquad (4)$$

where $\underline{m} < \underline{n}$ are constants indicative of the tectonic regime and γ_r is the unit weight of the rock with $\gamma_m \sim \gamma_r$. The stress ratio $\underline{R}$ may range from +1 in some extensional tectonic regimes to approximately -1 for contractional regimes (McGarr, 1982). In the first case $\underline{m} \sim 0.5$ and $\underline{n} \sim 1$, and in the second $\underline{m} \sim 1$ and $\underline{n} \sim 1.5$.

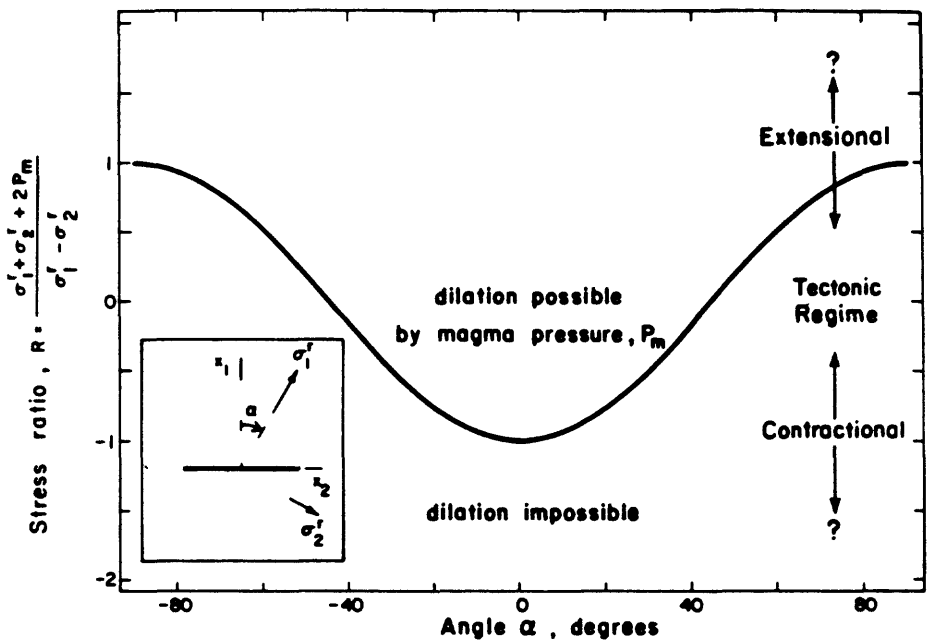

Figure 20. Plot of stress ratio $\underline{R}$ versus angle α between $\underline{x}_1$ axis and direction of remote principal stress σ_1^r. The curve separates the region where dilation of the plane of weakness is possible from the region where dilation is not possible by magma at pressure $\underline{P}_m$ (after Pollard and others, 1984).

Delaney and Pollard (1982) have calculated that for magma (with an initial flow velocity of 1 m/s) flowing distances greater than a few kilometers from an upper crustal source area, dikes 2 m thick could solidify in hours

Magma Flow into Self-generating Cracks

In the second hypothesis, as the magma ascends, dilation generates sufficient tension in the host rock in the front of the dike tip to create new fractures and magma flows into them. Anderson (1938, 1951) showed that at the wedge-like tip of a fluid injection, a large tensional stress which is generally sufficient to extend the crack (fig. 21) is generated by the fluid pressure at right angles to the tip. Griffith's theory of brittle fracture (1921) suggests that these cracks are most likely to be formed in the direction of the maximum stress axis and normal to the minimum stress, whether it is compressive or tensional. Experimental work by Hubbert and Willis (1956), Van Pollen (1957), and Secor (1965) have helped to develop the theories of fluid-induced fractures in rocks. The theory is adequate to account for nearly all vertical dikes injected at depths, where the overburden pressure and the dike forms normal to the minimum compressional stress. Secor (1965, 1969) discussed the mechanical interaction of the rock and the role of fluid pressure that could lead to extension fracturing at depth in the earth's crust. Shaw and Swanson (1970) concluded that at great depth, the greatest and least principal stresses and the fluid pressure must be of a magnitude comparable to the lithostatic (vertical) load to provide the effective stress distribution that could lead to extension fracture. Sills may require magmatic pressures sufficient to lift the overburden; therefore, sills are formed more appropriately at shallow depths. Sill formation is also aided by lateral compression as well as by the presence of preexisting subhorizontal zones of weakness in the bedding plane and unconformities.

If dike propagation is along self-generating fractures, stress field or strain field measurements are important to monitor and to understand the unique relationship between dike orientation and principal stress directions. Work by Delaney and Pollard (1981) at Ship Rock, New Mexico has demonstrated the relationship of preexisting fractures to the paleostress direction. Spence and Turcotte (1984) apply a similarity solution for the two-dimensional propagation of fluid driven cracks. Their solution incorporates both the flow problem within the crack and the fracture problem through the use of a stress factor, γ. This nondimensional stress intensity factor is a measure of the resistance of the medium to the fracture. Spence and Turcotte (1984) then derive expressions for length, width, and driving pressures for a propagating fracture at a constant rate of injection. For example, for magma with viscosity of 10^2 MPa, a dike could be injected at a velocity of 0.5 m/s into a cracking rock length of 2 km and a width of 0.5 m in a period as short as 15 minutes. However, their analysis is only approximate because buoyancy forces and convective cooling have not been considered in the solution.

According to Pollard and others (1984) the mechanics of dike propagation and emplacement involve the interaction of complex processes (fig. 22). Because dikes behave like pressurized cracks Pollard (1973), and Pollard and others (1984) have used the linear elastic-fracture methods of Lawn and Wilshaw (1975) to imply that the near field stress associated with the dike tip involves a concentration of tensile stress that may induce vertical joints. The cooling history of the intrusion, local hydrothermal circulation,

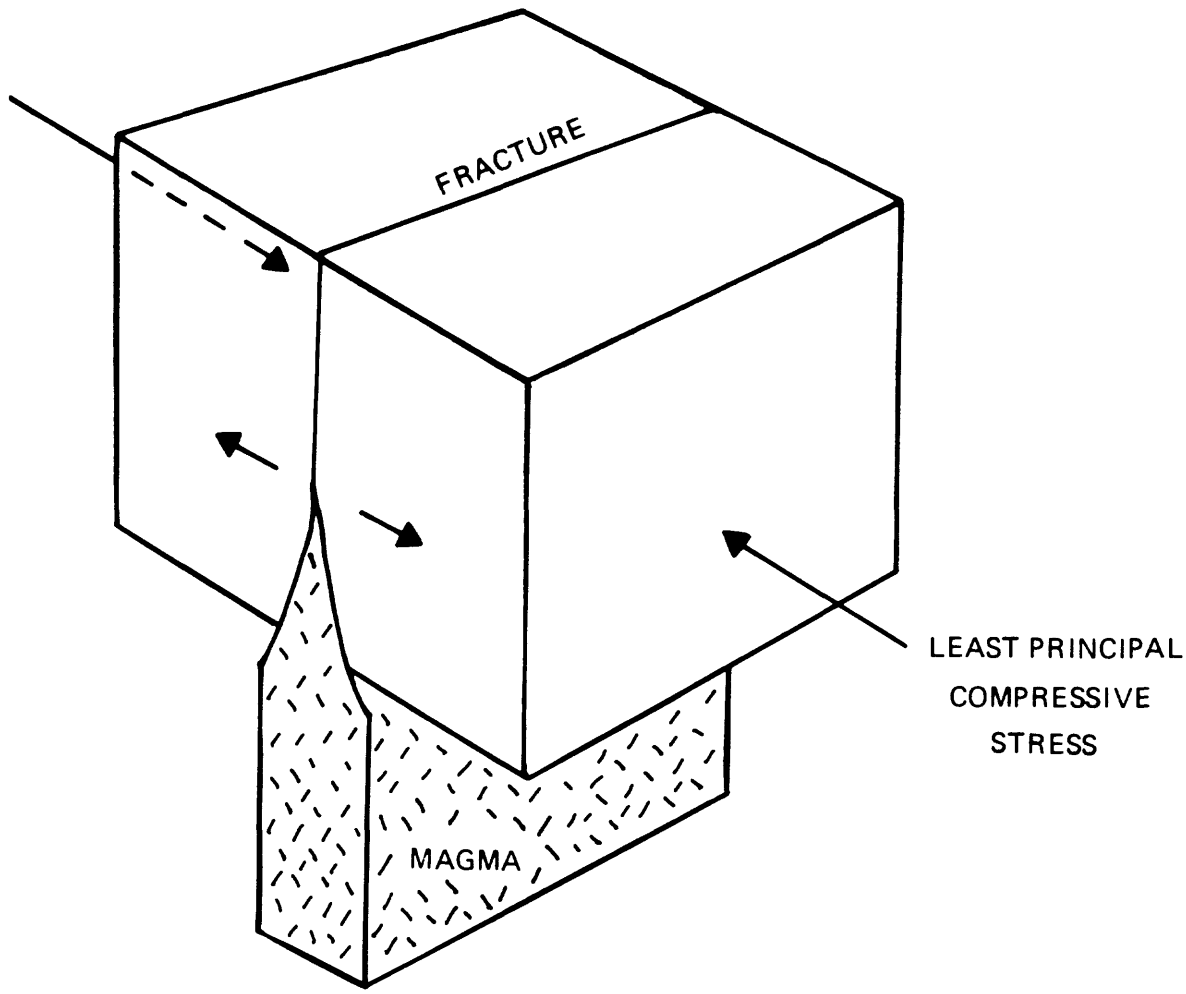

Figure 21. Stress relations for the injection of an igneous dike under high confining pressure (after Hills, 1972).

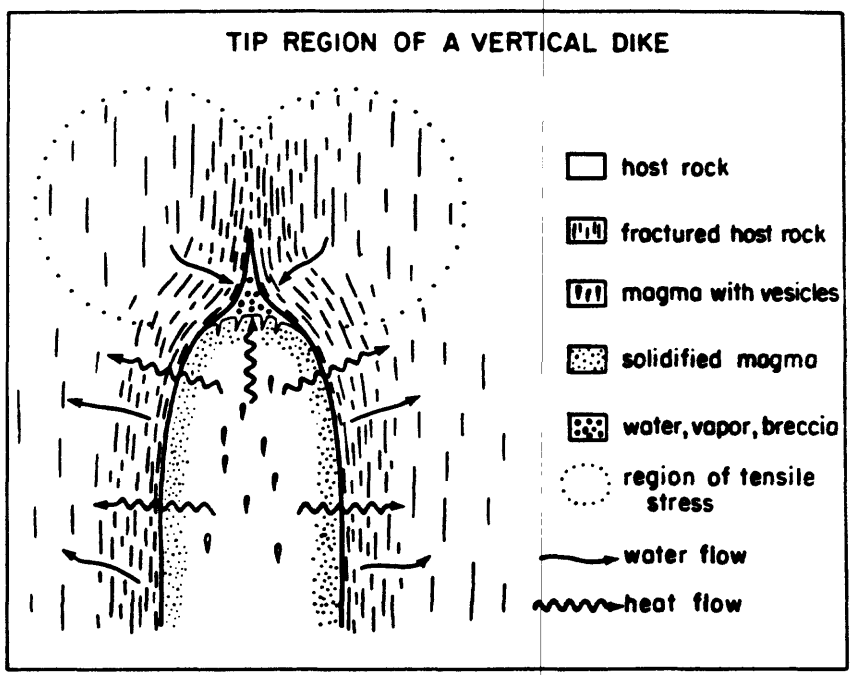

Figure 22. Schematic diagram of the region near the tip of a vertical dike. Dotted curve outlines the region of tensile stress, a zone in which joints become adjacent to the dike contact with continued propagation (after Pollard and others, 1984).

and subsequent magma injection may be affected by the presence of the vertical joints.

Pollard and others (1983) quantitatively analyze dike emplacement by examining the distribution of stress about a pressurized crack in order to understand important features of the stress field. The regional stress field is due to gravitational loading. In the absence of a crack, the lithostatic gradient produces a pressure that increases linearly with depth. Crack dilatation perturbs the field, especially over the top of the dike. A region of tensile stress is defined by contours of maximum principal stress that spread upward and outward from the dike top. Figure 23 illustrates this perturbation of the stress field. Two maxima, one on either side of the dike plane, occur at the surface and are separated by a distance about equal to twice the depth to the top of the dike. There is a decreasing tension beyond the maxima which becomes a compressive stress at a distance greater than the depth to the center of the crack. The resultant configuration of the stress field is dependent on the lithostatic gradient.

In a lunar study, Wilson (1970) suggested that intrusion of en echelon igneous dikes oriented at right angles to the direction of relative tension and which resulted from an intrusion at depth that had worked its way up a major shear zone, would tend to be deflected into the preferred paths opened when the local tensional stress and magmatic pressure overcame the tensile strength in the surrounding rock. Labratory experiments have shown that breakdown into en echelon crack segments occurs when an initial crack, propagating in a principal stress plane, intersects a region where the remote principal stress plane has rotated on an axis parallel to the propagation direction (Lawn and Wilshaw, 1975). These en echelon cracks can then grow along twisting surfaces into a new plane also roughly normal to the minimum principal stress. Pollard and others (1975) applied this concept to igneous dikes in order to interpret en echelon segments. Delaney and Pollard's study (1981) of Ship Rock, New Mexico showed that some dikes are composed of many discrete en echelon segments.

Heat Flow and Dike Cooling

The temperature of basaltic magma ranges between 1050° and 1200°C (MacDonald, 1972; Williams and McBirney, 1979; Delaney and Pollard, 1982), and the magma is commonly considered to be much hotter than the earth's upper crust that it invades. Heat exchange between an invading magma and the wall rock will begin almost immediately. Temperatures near dike margins are well below solidus temperatures, and a layer of cooled solidified magma is present between the wall rock and the uncooled magma flowing in the center of the intrusion. Dike thickness, magma flow rate, distance from the magma source region, temperature difference between the magma and country rock, and the increase in viscosity with decreasing temperature are important factors that affect the heat transport and rate of cooling of the body.

The fluid magma flowing in a channel loses more and more of its heat to the surrounding host rock. Heat is advected downstream by the flow and conducted across the channel by the difference in temperature between the initial magma temperature and that of the surrounding material. At the contact, temperature differences between the magma and the wallrocks may remain below that of the uncooled magma for the duration of heat transfer (Delaney and Pollard, 1982). The lack of contact metamorphic effects near the

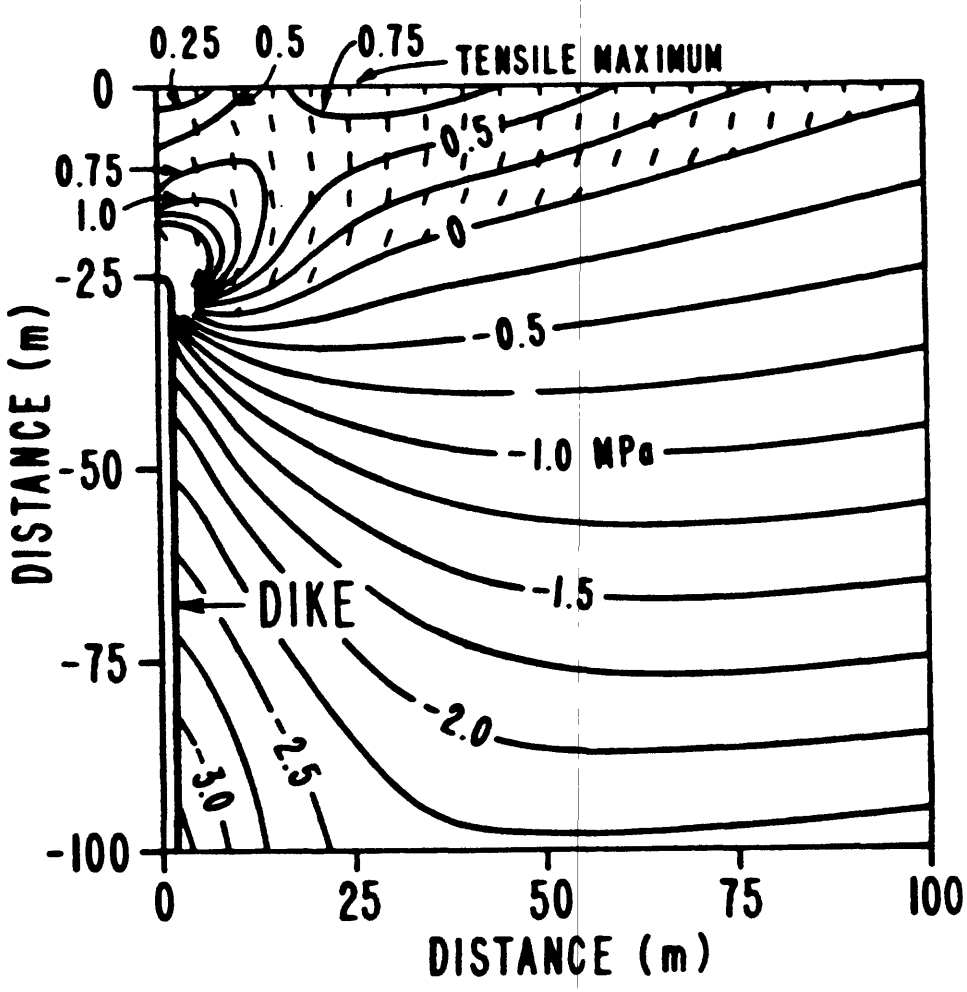

Figure 23. Contour map of maximum tensile stress near the tip of a dike at shallow depth. Magma driving pressure 1 MPa, gravitational gradient is 0.025 MPa/m, and the dike is 100 m high. The dashed lines are perpendicular to contoured stress in the region of tension and indicate orientation of possible secondary cracks (after Pollard and others, 1983 and 1984).

contacts of many dikes can be explained by the short duration of heat transfer and small temperature increases in the wallrock (Delaney and Pollard, 1982). The magma at the center of the dike is moving faster than the magma near the walls. The combination of the growth of the solidification layer inward from the dike wall and the magma flowing in the center of the dike, can result in some compositional and textural variations seen in the dike rock (Delaney and Pollard, 1982). Shaw (1974) suggested that the average heat transfer rate across the vertical boundary layer is a function of two dimensionless variables, the Prandtl number, Pr, and the Grashof number, Gr. The product PrGr is termed the Rayleigh number and is a ratio of internal energy released by the bouyancy force to the kinetic energy sissipated by viscosity. He concluded that the duration of the boundary layer regime under typical plutonic conditions is estimated to be roughly one-fifth of the theoretical solidification time computed from the theory of perfect conduction.

Delaney and Pollard (1981) suggested in their study of Ship Rock, New Mexico that the geometry of the igneous conduit is an important factor in determining magma discharge rate and the convective heat transport rate. Small irregularities in the shape of the dikes and offset may also affect the rate of discharge and cooling.

Flow differentiation in Igneous Dikes and Sills

The more mafic varieties of dikes and sills commonly display gradational variation in the concentration of phenocrysts across the width of the intrusion (Komar, 1972). These intrusions show phenocryst-poor margins followed by a rapid but gradational increase in content to a phenocryst-rich center. Intrusions containing olivine phenocrysts demonstrate these variations particularly well and are most common (Komar, 1972). The largest grains tend to be located toward the center of the intrusion, and progressively smaller grains toward the walls. Classic explanations for such variations are multiple intrusions which form composite dikes and sills or gravity settling of the solid phenocryst grains within the fluid magma. More recently the variations have been postulated to be due to a flow differentiation process operating during the emplacement of the intrusion. Work by Komar (1972) addressed the actual mechanisms that operate during flow to produce the observed differentiation of phenocrysts. He suggests that grain dispersive pressure, gravitational effects, and boundary layer growth are interactive during the emplacement process.

There is a gradational variation in the concentration of olivine and augite phenocrysts across the width of the dikes in the San Rafael and Capitol Reef area, Utah. This is particularly evident in the wider dikes (3-4 m), but has also been seen in thinner dikes (1-2 m). The margins of the dikes are fine-grained and phenocryst-poor, and there is an increase in the phenocryst content towards the center. The size of the phenocrysts also increases towards the center of the dike. Dikes where this feature is evident include #8, #14, #46, #89 and #96 (See Appendix 1).

DIKE SWARMS

Dikes rarely occur alone and are most commonly grouped in dike swarms consisting of hundreds of individual dikes and in regional swarms extending for tens to hundreds of miles. Some are clearly related to local effects, such as those which occur around volcanic centers. Regional swarms are related to major crustal structures and stresses.

Local Dike Swarms

Dike swarms localized about volcanic centers or in the vicinity of stock-like intrusions commonly form radial patterns and are centered on the volcanic neck or stock. This is probably due to up-doming by magmatic pressure giving rise to tension cracks (Hills, 1972). Where local geology is complex, the radial pattern can be modified. An example of this is Spanish Peaks, Colorado where the swarm consists of 500 dikes and has an axis that is normal to the Calebra Range Mountain front, which is taken as the direction of maximum compressional stress.

Regional Dike Swarms

Regional dike swarms are those that tend to follow large-scale crustal structures and stresses.

The Colorado Plateau interior is characterized by west-northwest east-southeast compression; this direction is also approximately the extension direction in the surrounding Basin and Range and Rio Grande Rift Provinces (Zoback and Zoback, 1980). Thompson and Zoback (1979) suggested that the state of compression in the Colorado Plateau interior may be related to its thick "keel" of mantle lithosphere, where the edges are subjected to a static "ridge push" force resulting from density contrasts in the surrounding less dense asthenosphere underlying the Basin and Range Province and Rio Grande Rift. Extensional stress differences in the upper crust along the plateau margins may be predicted from shallow crustal level density differences between the plateau and the surrounding regions. According to Zoback and Zoback (1980), the least principal horizontal stress direction in the Colorado Plateau interior is north-northeast south-southwest, which is perpendicular to the general west-northwest east-southeast least principal stress direction in the surrounding Basin and Range and Rio Grande Rift Provinces. Their data appear to support a radial distribution of least principal horizontal stress orientation perpendicular to the plateau margins. Thompson and Zoback (1979) suggest that the Basin and Range-Rio Grande Rift extensional stress field may extend 100-200 km into the plateau proper, which is consistent with high heat flow, normal faulting, and recent volcanism along the plateau margins. Along the Wasatch fault in Utah, data seem to indicate a more E-W direction that corresponds with modern crustal extension (Zoback and Zoback, 1980).

The prominent regional set of photolineaments in the San Rafael and Capitol Reef areas strike N. 20° W. and N. 75° W. (Kelley and Clinton, 1960). The dike swarm in the Capitol Reef and San Rafael area, Utah trend on average N. 13° W., with the least principle compressive stress direction east-west. This is similar to that of the Wasatch Fault, suggesting that the emplacement of the dikes is roughly consistent with the same stress orientations.

SUMMARY AND DISCUSSION

The exposure of the intrusive complex in the San Rafael and Capitol Reef areas, Utah, provides a unique opportunity for data collection to interpret and understand the dike emplacement mechanisms and magma-tectonic evolution of the western edge of the Colorado Plateau. This study has provided a statistical data base on a regional dike complex, but further work is needed to document the magma-tectonic evolution of the plateau in relation to the surrounding provinces.

The emplacement of an olivine basalt magma as a dike complex composed of discontinuous en echelon segments occurred about 4 m.y. B.P. The extent of vertical emplacement of the magma from depth from the surface determined from stratigraphic relations is a maximum of 2.5 km, but the most likely range is 0.5 to 2.0 km. Field evidence of vesicles in the dike and abundant zeolites and analcite also provide support for shallow depths at the time of solidification.

Heat exchange between the invading magma and wallrocks begins as the magma is injected into the cooler host rock. A layer of cooled, solidified magma forms adjacent to the cooler wallrock, and flow of the less viscous magma continues in the center of the dike. Heat is advected as the magma continues to flow. Estimates for solidification of a dike 2 km in length and between 0.5 to 2 m wide can range from 15 minutes to several hours. Minimal contact metamorphism and thin chilled margins suggest that the intruded magma cooled in a relatively short period of time, probably in a matter of hours for the thinner dikes and up to several days for the thicker ones.

The presence of preexisting fractures or joint sets in the earth's crust may have facilitated the injection of magma as dikes. There is some field evidence, however, that emplacement of magma produced self-generating fractures. The geometry of the complex may have been influenced by the preexisting structures in the host rock, but it was also affected by the proximity to adjacent dike segments in a regionally controlled stress field. Variations in dike thickness may be due to the segmented form of the dike and to brecciation processes with removal and incorporation of wall rock during flow of magma associated with the initial dike dilatation.

The breccias are concentrated where the dike is thickest, suggesting that the final dike form is due to dilation in response to magma pressure and the erosive removal of wallrocks during magma flow. Brecciation of host rocks has been attributed to a variety of mechanisms and is probably due to mechanisms arising from heat transfer such as thermal expansion and pressurzation of pore-fluids and thermoelastic stresses of the wallrocks. Delaney (1982) deduced that fracturing and brecciation may accompany the increased pressure from ground-water expansion during the sudden heating produced by rapid emplacement of an igneous intrusion.

The petrography and major-element chemical analyses suggest that the dikes are composed of a single parent magma, and that there may have been only one episode of magma injection over a relatively short time span possibly < 1 m. y. The episode may have been pulses of magma injection over the entire time span. Further dating is necessary to accurately constrain the time span. The presence of olivine and pyroxene phenocrysts in the chilled margins (in the thicker dikes) indicates that the temperatures of the magma during emplacement were below the liquidus relative to these mineral phases. Samples collected from the narrower dike segments reflect the flow of the earliest magma through the conduits. Flow differentiation is evident in the dike samples collected;

concentration of phenocrysts in the center of the dikes provides evidence of this process. Additionally, the concentration of glomeropophyritic clots of olivine and pyroxene might indicate that the grains grew in place rather than by crystal settling into a specific horizon. A second possible explanation is that the crystals could have nucleated and crystalized at depth and brought up by new pulses of magma injected from the source. Zoning of some of the large phenocrysts in the thicker dikes also provides evidence for growth of the grains in the cooling magma.

Hydrothermal fluids percolated through the complex altering the original chemistry and mineralogy in the majority of the samples. Mineral replacement of interstitial feldspar, especially plagioclase by analcite is common. The presence of other zeolites, thomsonite and natrolite, is also common throughout the complex.

The complex contains a small volume of magma that has penetrated a vast volumetric domain of the crust. Assuming an average width of 120 cm, an extent in emplacement length of 2.5 km (maximum), and a total segment length of all dike segments in the complex of 311 km, the volume is 0.93 km^3. The mimimum magma volume of the dikes, assuming an extent in emplacement length of 0.5 km, is 0.2 km^3. The volume of the magma intruded into the sills has not been included in these calculations, but is important for estimates of the total volume of the basaltic intrusive complex. Assuming the dikes have invaded from mantle depth, the volume would be on the order of 10 km^3.

In Hawaii, this volume of magma is equal to ~100 yr at the maximum generation rate of 0.1 km^3/yr seen in modern basaltic volcanic province (Swanson, 1972; Shaw and others, 1980), and 10^4 yr at minimum rate of 10^{-3} km^3/yr (Shaw and others, 1980). Even if the volume of magma is small, the volume of country rock intruded is large. Using a length of 60 km, a width of 22 km, and a thickness of the lithosphere of the Colorado Plateau as 40 km (Thompson and Zoback, 1979), the volume of country rock intruded would be 5 X 10^4 km^3. The ratio of the volume of magma to the volume of rock intruded is on the order of 10^{-3}. This is similar to the dike fraction of lithosphere beneath Hawaii (Shaw, 1980).

The pattern of dike emplacements provides a reference frame for interpretation of stress fields in the transition region between the Colorado Plateau and the Basin and Range Province during a portion of Pliocene history. Even though the total volume of magma in the complex is small, the mechanics and emplacement history of the dikes and sills may provide data for the magma-tectonic evolution of the Colorado Plateau and crustal dynamics in general.

REFERENCES CITED

Anderson, E. M., 1938, The dynamics of sheet intrusion: Royal Society of Edinburgh Proceedings, v. B-58, no. 3, p. 242-251.

Anderson, E. M., 1951, The dynamics of faulting and dyke formation with applications to Britain: Oliver and Boyd, London, England, 206 P.

Anderson, J. J., Rowley, P. D., Fleck, R. J., and Nairn, A. E. M., 1975, Cenozoic geology of southwestern High Plateaus of Utah: Geologic Society of America Special Paper 160, 88 P.

Best, M. G., 1982, Igneous and Metamorphic Petrology: W. H. Freeman and Company, San Francisco, 630 p.

Bodell, J. M., and Chapman, D. S., 1982, Heat flow in the north-central Colorado Plateau: Journal of Geophysical Research, V. 87, p. 2869-2884.

Billingsley, G. H., Breed, W. J., and Huntoon, P. W., 1981, Geologic map of Capitol Reef National Park and vicinity, Utah.

Case, J. E., and Joesting, H. R., 1972, Regional geophysical investigations in the central Colorado Plateau: U.S. Geological Survey Professional Paper 736, 31 p.

Cox, K. G., Bell, J. D., and Pankhurst, R. J., 1979, The interpretation of igneous rocks: Allen and Unwin, London, 450 p.

Craig, L. C., Holmes, C. N., Cadigan, R. A., Freeman, V. L., Mullens, T. E., and Weir, G. W., 1955, Stratigraphy of the Morrison and related formations, Colorado Plateau Region: U.S. Geological Survey Bulletin 1009-E, p. 125-168.

Davis, G. H., 1983, Structural geology of rocks and regions: John Wiley and Sons, New York, 429 p.

Delaney, P. T., 1982, Rapid intrusion of magma into wet rock: Ground water flow due to pore pressure increases: Journal of Geophysical Research, v. 87, p. 7739-7756.

Delaney, P. T., and Pollard, D. D., 1982, Solidification of basaltic magma during flow in a dike: American Journal of Science, v. 282, p. 856-885

Delaney, P. T., and Pollard, D. D., 1981, Deformation of host rocks and flow of magma during growth of minette dikes and breccia-bearing intrusions near Ship Rock, New Mexico: U. S. Geological Survey Professional Paper 1202, 101 p.

Delaney, P. T., Pollard, D. D., Ziony, J. I., and McKee, E. H., in press, Field relations between dikes and joints: Emplacement processes and paleostress analysis.

Dutton, C. E., 1880, Report on the geology of the High Plateaus, Utah: U.S. Geological Survey of the Rocky Mountain Region Report, 307 p.

Eggleston, R. E., and Reiter, M., 1984, Terrestrial heat-flow estimates from petroleum bottom-hole temperature data in the Colorado Plateau and the eastern Basin and Range Province: Geological Society of America, v. 95, p. 1027-1034.

Fiske, R. S., and Jackson, E. D., 1972, Orientation and growth of Hawaiian volcanic rifts: the effect of regional structure and gravitational stresses: Proceedings Royal Society of London, A-329, p. 299-326.

Gilbert, G. K., 1877, Report on the geology of the Henry Mountains: U.S. Geological Survey of the Rocky Mountain Region Report, 170 p.

Gilluly, James, 1927, Analcite diabase and related alkaline syenite from Utah: American Journal of Science, v. 14, p. 199-211.

Gilluly, James, 1929, Geology and oil and gas prospects of part of the San Rafael Swell, Utah, Part II-Mineral Fuels: U.S. Geological Survey Bulletin 806,p. 69-130.

Gilluly, James, and Reeside, J. B., 1928, Sedimentary rocks of the San Rafael Swell and some adjacent areas in Utah: U.S. Geological Survey Professional Paper 150 D, p. 61-110.

Griffith, A. A., 1921, The phenomena of rupture and flow in solids: Philosophical Transactions of the Royal Society of London, v. A221, p. 163-198.

Gudmundsson, Agust, 1984, Tectonic aspects of dykes in northwestern Iceland: Jökull, v. 34, p. 81-96.

Hawley, C. C., Robeck, R. C., and Dyer, H. B., 1968, Geology, altered rocks and ore deposits of the San Rafael Swell, Emery County, Utah: U.S. Geological Survey Bulletin 1239, 115 p.

Helgason, Johann, and Zentilli, Marcos, 1985, Field characteristics of laterally emplaced dikes: Anatomy of an exhumed Miocene dike swarm in Reydarfjördur, Eastern Iceland: Tectonophysics, v. 115, p. 247-274.

Hills, E. S., 1972, Elements of structural geology: Chapman and Hall Ltd. and Science Paperbacks, England, 502 p.

Hintze, L. F., 1973, Geologic history of Utah: Brigham Young University Geology Studies, v. 20, pt. 3, 181 p.

Hubbert, M. K., and Willis, D. G., 1956, Mechanics of hydraulic fracturing: American Institute of Mining and Metallurgical, and Petroleum Engineers, v. 210, p.153-168.

Hughes, C. J., and Hussey, E. M., 1979, Standardized procedure for presenting corrected Fe_2O_3/FeO ratios in analysis of fine-grained mafic rocks, Neues Jahrbüch für Mineralogie Monatshefte, v. 12, p. 570-572.

Hunt, C. B., 1956, Cenozoic geology of the Colorado Plateau: U.S. Geological Survey Professional Paper 279, 99 p.

Irvine, T. N., amd Baragar, W. R. A., 1971, A guide to the chemical classification of the common volcanic rocks: Canadian Journal of Earth Science, v. 8, p. 523-548.

Jackson, E. D., and Shaw, H. R., 1975, Stress fields in central portion of the Pacific Plate in time by linear volcanic chains: Journal of Geophysical Research, v. 80, p. 1861-1874.

Kelley, V. C., 1955, Monoclines of the Colorado Plateau: Geological Society of America Bulletin, v. 68, p. 789-804.

Kelley, V. C., and Clinton, N. J., 1960, Fracture systems and tectonic elements of the Colorado Plateau: University of New Mexico Publication in Geology, n. 6, 104 p.

Komar, P. D., 1972, Mechanical interaction of phenocrysts and flow differentation of igneous dikes and sills: Geological Society of America Bulletin, v. 83, p. 973-988.

Kuno, H., 1968, Differentiation of basalt magmas, in H. Hess and A. Poldervaart (eds.)Basalt, The Poldervaart Treatise on Rocks of Basaltic composition: John Wiley and Sons, New York, p. 623-688.

Lawn, B. R., and Wilshaw, T. R., 1975, Fracture of brittle solids: Cambridge University Press, Cambridge, England, 204 p.

LeMaitre, R. W., 1976, The chemical variatibility of some common igneous rocks: Journal of Petrology, v. 17, p. 589-637.

Lupton, C. T., 1913, Gypsum along the west flank of the San Rafael Swell, Utah : U.S. Geological Survey Bulletin 530, p. 221-231.

MacDonald, G. A., 1972, Volcanoes: Prentice-Hall, Inc, New Jersey 510 p.

Mandelbrot, B. B., 1977, Fractals; form, chance, and dimension: W.H. Freeman and Company, San Francisco, 365 p.

Mandelbrot, B. B., 1982, The fractal geometry of nature: W. H. Freeman and Company, San Francisco, 460 p.

McGarr, A. M., 1982, Analysis of states of stress between provinces of constant stress: Journal of Geophysical Research, v. 87, p. 9279-9288.

McKenzie, Daniel, 1984, A possible mechanism for epeirogenic uplift: Nature, v. 307, 616-618.

O'Sullivan, R. B., 1981, The middle Jurassic San Rafael Group and related rocks in east-central Utah: New Mexico Geological Society Guidebook, 32nd Field Conference, Western Slope Colorado, p. 89-95.

Pollard, D .D., 1973, Derivation and evaluation of mechanical model for sheet intrusions: Tectonophysics, v. 19, p. 233-269.

Pollard, D. D., Delaney, P. T., Duffield, W. A., Endo, E. T., and Okamura, A. T., 1983, Surface deformation in volcanic rift zones: Tectonophysics, v. 94, p. 541-584.

Pollard, D. D., Fink, J. H., and Delaney, P. T., 1984, Igneous dikes at Long Valley, CA: Emplacement mechanisms and associated structures: in U. S. Geological Survey Open File Report 84-939, Proceeding of workshop XIX, Active tectonic and magmatic processes beneath Long Valley Caldera Eastern California, v. 1, p. 130-145.

Pollard, D. D., Muller, O. H., and Dockstader, D. R., 1975, The form and growth of fingered sheet intrusions: Geological Society of America Bulletin, v. 86, p. 351-363.

Pollard, D. D., Segall, P. and Delaney, P. T., 1982, Formation and interpretation of dilatant echelon cracks: Geological Society of America Bulletin, v. 93, p. 1291-1303.

Powell, J. W., 1875, The exploration of the Colorado River and its canyons: Dover Publications, Inc., New York, 397 p.

Roden, M. F., Smith, D., and McDowell, F. W., 1979, Age and extent of potassic volcanism on the Colorado Plateau: Earth and Planetary Science Letters, v. 43, p. 279-284.

Secor, D. T., 1965, Role of fluid pressure in jointing: American Journal of Science, v. 263, p. 633-646.

Secor, D. T., 1969, Mechanics of natural extention fracturing at depth in the earth's crust, in A. J. Baer and D. K. Norris (eds.), Research in Tectonics: Canada Geological Survey Paper 68-52, p. 3-48.

Shaw, H. R., 1974, Diffusion of H_2O in granitic liquids: Part I. experimental data; Part II. Mass transfer in magma chambers: in A. W. Hofmann, B. J. Giletti, H. S. Yoder, Jr., and R. A. Yund (eds.) Geochemical Transport and Kenetics, p. 139-170.

Shaw, H. R., 1980, The fracture mechanisms of magma transport from the mantle to the surface, in Physics of Magmatic Processes: Princeton University Press, p. 201-264.

Shaw, H. R., Jackson, E. D., and Bargar, K. E., 1980, Volcanic periodicity along the Hawaiian-Emperor Chain: American Journal of Science, v. 280-A, p. 667-708.

Shaw, H. R., and Swanson, D. A., 1970, Eruption and flow rates of flood basalts, in E. H. Gilmour and D. Stradling (eds.) Columbia River Basalt Symposium: 2nd. Proceedings, Chaney, Washington, Eastern Washington State College Press, p. 271-299.

Shelley, David, 1975, Manual of optical mineralogy, Elsevier, Scientific Publishing Company, New York, 239 p.

Smith, J. F., Jr., Huff, L. S., Hinrichs, E. N., and Luedke, R. G., 1963, Geology of the Capitol Reef Area, Wayne and Garfield Counties, Utah: U. S. Geological Survey Professional Paper 363, 102 p.

Spence, D. A., and Turcotte, D. L., 1984, Magma driven propogation of cracks: Journal of Geophysical Research, v. 90, p. 575-580.

Swanson, D. A., 1972, Magma supply rate at Kilauea Volcano, 1952-1971: Science, v. 175, p. 169-170.

Thompson, A. E., and Stokes, W. L. 1970, Stratigraphy of the San Rafael Group, southwest and south central Utah: Utah Geological and Mineralogical Survey Bulletin 87, 53 p.

Thompson, G. A., and Zoback, M. L., 1979, Regional geophysics of the Colorado Plateau: Tectonophysics, v. 61, p. 149-181.

Van Pollen, H. K., 1957, Theories of hydraulic fracturing: Colorado School of Mines Quarterly, v. 52, p.112-131.

Washington, H. S., 1917, Chemical analysis of igneous rocks: U. S. Geological Survey Professional Paper, 1201 p.

Wentworth, C.K., and Jones, A. E., 1940, Intrusive rocks of the leeward slope of the Koolau Range, Oahu: Journal of Geology, v. 48, p. 975-1006.

Williams, H., and McBirney, A. R., 1979, Volcanology: Freeman, Cooper and Co., San Francisco, 394 p.

Williams, J. D., 1983, The petrography and differentiation of a composite sill from the San Rafael Swell Region, Utah: M. S. thesis, Arizona State University, 123 p.

Williams, P. E., and Hackman, R. J., 1971, Geology of the Salina Quadrangle, Utah: U.S. Geological Survey Miscellaneous Investigations Series Map 591-A, scale 1:250,000.

Wilshire, H. G., 1967, New chemical data on alkaline diabase-picrite intrusions from Scotland, New Zealand, and Utah: U.S. Geological Survey Open-File Report 900, 23 p.

Wilson, Gilbert, 1970, Wrench movements in the Aristarchus Region of the Moon: Proceedings of the Geologists' Association, v. 81, p. 595-608.

Wright, J. C., Dickey, D. D., Snyder, R. P., Craige, L. C., and Cadigan, R. A., 1979, Measured stratigraphic sections of Jurassic San Rafael Group and adjacent rocks in Emery and Sevier Counties, Utah: U.S. Geological Survey Open-File Report 79-1317, 157 p.

Zoback, M. L. and Zoback, M. D., 1980, State of stress in the conterminous United States: Journal of Geophysical Research, v. 85, p. 6113-6156.

APPENDIX 1

APPENDIX 1. LISTING OF ALL STATISTICAL DATA COLLECTED ON THE INTRUSIVE COMPLEX IN THE SAN RAFAEL AND CAPITOL REEF AREAS, UTAH.

#*	Strike of segment	Subjective average[1]	Numerical average[2]	Standard deviation	Map length (cm)[3]	Km 1:48000[4]	Propagation[5]	Sample number	Thickness cm[6]	Comments[7]
1	N18,27W	N18W	N20.3W	5.9	0.96	0.46		SRS6-84		Cc, An
	N16W				0.45	0.22			50	
2	N34W	N27W	N28W	8.5	0.43	0.21				
	N22W				0.25	0.12			25	
3	N22W	N21W	N24.7W	10.2	0.65	0.31			40	
	N20W				0.82	0.39			50	
	N35W				0.61	0.29	05°, 40°N		30,150	
	N21W				2.25	1.08	55°-80°S	SRS7-84	145,245,180	local Br
	N19W				1.52	0.73				Cc
	N31W				0.41	0.20				
	N08W				0.56	0.27				
	N43W				1.05	0.50	16°-30°N		145	
	N42W				0.16	0.08				
	N30W				0.09	0.04				
	N31W				0.14	0.07			20	
	N14W				0.37	0.18				
	N14W				0.40	0.19				
	N21W				2.32	1.11			120	Br
	N20W				0.50	0.24				
4	N24W	N21W	N22.5W	2.1	0.61	0.29				
	N21W				1.38	0.66				
5	N08W	N08W	N8.0W	0	0.72	0.35				
6	N10,07,10W	N15W	N10.5W	3.3	0.30	0.14			25	
	N15W				1.02	0.49			80	
7	N02W	N04W	N6.3W	4.5	0.45	0.22				
	N11W				0.37	0.18				
	N06W				0.74	0.36				
8	N13W	N11W	N14.9W	5.2	0.30	0.14				
	N13W				0.28	0.13				
	N10W				2.50	1.20				
	N11W				1.02	0.49			130,100	
	N11W				0.42	0.20				Br
	N13W				0.75	0.36			80	
	N16W				0.32	0.15				
	N25W				0.36	0.17				
	N22W				0.38	0.18				
9	N12,25W	N11W	N15.2W	8.3	2.06	0.99				
	N32W				0.66	0.32				
	N14W				0.29	0.14				
	N22,29W				1.23	0.59				
	N11W				0.90	0.43			95	
	N04W				1.48	0.71				
	N19W				0.26	0.13				
	N13W				0.46	0.22				Br
	N05W				2.48	1.19			200-300	
	N05W				0.28	0.13			85	
	N16,10W				0.31	0.15			260,85,90	

APPENDIX 1. LISTING OF ALL STATISTICAL DATA COLLECTED ON THE INTRUSIVE COMPLEX IN THE SAN RAFAEL AND CAPITOL REEF AREAS, UTAH - Continued.

#	Strike of segment	Subjective average	Numerical average	Standard deviation	Map length (cm)	Km 1:48000	Propagation	Sample number	Thickness cm	Comments
					1.78	0.85				
	N07W				0.66	0.32				diabase float
	N18W				0.24	0.12				indurated ls, sh
	N17W				0.46	0.22				
10	N22W	N23W	N21.0W	2.8	0.38	0.18				
	N17W				0.70	0.34				
	N25W				0.67	0.32			130	
	N23W				0.62	0.30				
	N19W				0.28	0.13				
	N19W				0.98	0.47				
	N22W				1.06	0.51				
11	N07W	N07W	N7.0W	0.0	0.77	0.37			170	
12	N17W	N16W	N17.0W	5.6	0.46	0.22		SRS5-84		Cc, An
	N19W				1.57	0.75			450	
	N12W				1.20	0.58				
	N21W				0.82	0.39				
	N26W				0.25	0.12			140	
	N20W				1.68	0.81				
	N11W				0.25	0.12				
	N10W				0.31	0.15				
13	N09W	N10W	N8.0W	3.9	0.72	0.35				
	N12W				0.39	0.19				
	N09W				0.46	0.22			85	
	N13W				0.83	0.40				
	N07W				0.18	0.09				
	N02W				0.96	0.46				
	N09W				0.19	0.09				
	N02W				1.00	0.48			110	
	N12W				0.79	0.38				
	N10W				0.46	0.22				
	N09W				0.44	0.21			210	
	N09W				0.49	0.24				
	N09W				0.93	0.45				
	N13W				0.44	0.21				
	N06W				0.24	0.12				
	N10W				0.46	0.19				
	N02W				0.44	0.21				br
	N01W				0.09	0.04				diabase float
14	N04W	N05W	N6.7W	4.6	0.83	0.40				
	N12W				0.23	0.11				
	N04W				0.44	0.21				
15	N21W	N22W	N22.8W	6.3	0.27	0.13		SRS8-84	100	Cc
	N25W				0.32	0.15				
	N30W				0.68	0.33				
	N38W				0.22	0.11				
	N22W				0.36	0.17				
	N22W				0.24	0.12				
	N21W									

APPENDIX 1. LISTING OF ALL STATISTICAL DATA COLLECTED ON THE INTRUSIVE COMPLEX IN THE SAN RAFAEL AND CAPITOL REEF AREAS, UTAH - Continued.

#	Strike of segment	Subjective average	Numerical average	Standard deviation	Map length (cm)	Km 1:48000	Propagation	Sample number	Thickness cm	Comments
	N19W				0.36	0.17				
16	N09W	N09W	N9.0W	0.0	0.30	0.14				
	N09W				0.74	0.36			70	
17	N42W	N37W	N39.3W	7.4	0.25	0.12				
	N45W				0.82	0.39				
	N31W				0.43	0.21			110	
18	N24W	N23W	N23.0W	1.0	1.06	0.51	25°, 75°N		95	
	N22W				0.21	0.10				
	N23W				0.72	0.35	70°, 85°N			
19	N02W	N02W	N02W	0.0	0.36X0.19	0.17X0.09				Br
20	N06W	N08W	N11.6W	12.4	0.45	0.22			80	
	N04W				0.28	0.13				
	N04W				0.24	0.12				
	N28W				0.32	0.15				
	N01W				0.81	0.39				
	N16W				0.22	0.11				
	N05W				0.39	0.19				
	N07W				0.43	0.26				
	N08W				1.65	0.79			160,140,120	
	N04W				0.14	0.07				
	N01W				0.28	0.13				
	N02W				0.64	0.31				
	N14W				0.36	0.17			110	
	N06W				0.61	0.29				Br
	N07W				0.57	0.27				
	N07W				0.72	0.35			110	
	N16W				0.42	0.20				
	N45W				0.28	0.13				
	N10W				0.90	0.43			30	
	N40W				0.30	0.14				
21	N90W	N90W	N90W	0.0	1.03	0.49				
	N90W				0.70	0.34				
22	N15W	N18W	N25.2W	11.3	0.80	0.38				
	N19W				0.35	0.17				
	N13W				1.17	0.56				Br
	N18W				0.61	0.29				Br
	N21W				0.39	0.19				Br
	N19W				2.01	0.96			140	Br
	N32W				0.41	0.20				
	N22W				0.47	0.23				
	N28W				0.38	0.18				
	N21W				0.16	0.08				
	N47W				0.20	0.10				
	N49W				0.22	0.11				
	N23W				0.39	0.19				
	N25W	N19W	N17.5W	6.3	0.69	0.33				
	N22W				0.29	0.14				

APPENDIX 1. LISTING OF ALL STATISTICAL DATA COLLECTED ON THE INTRUSIVE COMPLEX IN THE SAN RAFAEL AND CAPITOL REEF AREAS, UTAH - Continued.

#	Strike of segment	Subjective average	Numerical average	Standard deviation	Map length (cm)	Km 1:48000	Propagation	Sample number	Thickness cm	Comments
	N20W				0.55	0.27				
	N26 W				0.46	0.22				
	N20W				0.32	0.14				
	N17 W				0.38	0.18				
	N15W				0.19	0.09				
	N15 W				0.21	0.10				
	N24W				0.27	0.13				
	N13 W				0.41	0.20				
	N13W				0.46	0.22				
	N15 W				0.20	0.10				
	N03W				0.53	0.26				
24	N30W	N14W	N18.8W	8.2	0.68	0.33				
	N15W				0.23	0.11				
	N16 W				0.14	0.07				
	N14W				0.50	0.24				
	N32 W				0.30	0.14				
	N24W				1.13	0.54				
	N12 W				0.20	0.10				
	N11W				0.22	0.11				
	N09 W				0.72	0.35				
	N17W				0.73	0.35	50°N		200	
	N13 W				1.86	0.89	25°-40°S			
	N12W				0.24X0.14	0.12X0.07				Br
	N29 W				0.30	0.14				
	N29W				0.28	0.13				
25	N27,42W	N30W	N30.0W	6.2	1.15	0.55			110	
	N33W				1.07	0.51				
	N24 W				0.29	0.14				
	N24W				0.82	0.39				
	N30 W				0.31	0.15				
	N30W				0.40	0.19				
26	N55W	N29W	N27.8W	14.5	0.25	0.12				
	N30W				0.90	0.43			100	
	N11 W				0.31X0.23	0.15X0.11		SRS4-84		Bud
	N05W				0.02X0.02	0.01X0.01				Br
	N18 W				0.25	0.12			40	
	N14W				0.40	0.19			60	
	N32 W				0.27	0.13				
	N33W				0.22	0.11				
	N22 W				0.17	0.08				
27	N01W	N00W	N1.0W	5.7	0.85	0.41				
	N03 E				0.25	0.12				
	N03E				0.80	0.38			70	
	N09 W				0.85	0.41			40	
28	N22E	N07W	N2.0W	21.)	0.60	0.29				
	N09 W				1.40	0.68			120	
	N18W				0.37	0.18				

APPENDIX 1. LISTING OF ALL STATISTICAL DATA COLLECTED ON THE INTRUSIVE COMPLEX IN THE SAN RAFAEL AND CAPITOL REEF AREAS, UTAH - Continued.

#	Strike of segment	Subjective average	Numerical average	Standard deviation	Map length (cm)	Km 1:48000	Propaga-tion	Sample number	Thickness cm	Comments
30	N20W	N14W	N18.0W	6.2	0.18	0.09				
	N20W				0.63	0.30				
	N16W				0.30	0.14				
	N22W				0.98	0.47				
	N20W				0.43	0.21				br
	N13W				0.98	0.47				
	N10W				0.20	0.10				
	N16W				0.20	0.10				
	N19W				0.35	0.17				
	N16W				0.73	0.35				
	N05W				0.53	0.25				
	N28W				0.35	0.17				
	N27W				0.37	0.18				
	N26W				0.32	0.15				
	N17W				0.28	0.13				
	N13W				0.81	0.39				
31	N03W	N08W	N14.0W	13.7	0.45	0.22				
	N04W				0.17	0.08				
	N10W				1.04	0.50				
	N05W				1.44	0.69				
	N03W				0.58	0.28				
	N09W				0.18	0.09				
	N42W				0.20	0.10				
	N42W				0.22	0.11				
	N09W				0.23	0.11				
	N10W				1.92	0.92			130	
	N22W				0.31	0.15				
	N21W				0.28	0.13				
	N12W				0.25	0.12				
32	N08W	N11W	N9.6W	10.6	0.24	0.12				
	N02W				0.34	0.16				
	N09W				0.31	0.15				Br
	N30W				0.31	0.15				Br
	N10W				0.27	0.13				
	N10W				0.18	0.09				
	N11W				0.10	0.05				
	N08W				0.11	0.05				
	N05W				0.30	0.14				
33	N06W	N05W	N5.0W	1.4	1.05	0.50				Bud
	N04W				0.14	0.07				
34	N09E	N09E	N9.0E	0.0	1.27	0.61				
35	N22W	N12W	N15.4W	5.5	0.34	0.16				
	N13W				0.32	0.15				
	N12W				0.36	0.17				
36	N02W	N04W	N4.7W	2.0	0.44	0.21			100	
	N07W				0.39	0.19			70	
	N07W				0.33	0.16				

APPENDIX 1. LISTING OF ALL STATISTICAL DATA COLLECTED ON THE INTRUSIVE COMPLEX IN THE SAN RAFAEL AND CAPITOL REEF AREAS, UTAH - Continued.

#	Strike of segment	Subjective average	Numerical average	Standard deviation	Map length (cm)	Km 1:48000	Propaga-tion	Sample number	Thickness cm	Comments
	N04W				0.64	0.31				
	N04W				0.20	0.10				
	N04W				0.33	0.16				
37	N06W	N05W	N6.5W	4.5	0.71	0.34				
	N14W				0.11	0.05				
	N12W				0.15	0.07				
	N08W				0.38	0.18			60	
	N04W				0.13	0.06				
	N02W				0.14	0.07				
	N03W				0.14	0.07				
	N03W				0.22	0.11				Br
38	N21E	N28E	N26.5E	7.8	0.32	0.11				
	N32E				0.16	0.08				
39	N05W	N05W	N5.0W	0.0	1.00	0.48				Br
					0.18X0.08	0.09X0.04				
40	N41W	N32W	N32.8W	4.1	0.22	0.11				Older (see # 54)
	N36W				0.25	0.12				
	N31W				0.10	0.05				
	N31W				0.13	0.06				
	N28W				0.44	0.21			180	
	N32W				0.95	0.48	60°N, 90°N		200	
	N34W				0.14	0.07			85	
	N34W				0.16	0.08				
	N28W				0.21	0.10				
41	N01W	N12W	N11.1W	11.4	0.50	0.24			280	
	N08W				0.32	0.15				
	N06W				1.00	0.48			130	
	N08W				0.05	0.02				
	N04W				0.15	0.07				
	N04W				0.15	0.07				
	N06W				0.10	0.05				
	N05W				0.21	0.10				
	N21W				0.14	0.07			150	
	N05W				0.37	0.18				Br
	N05W				0.50	0.24				Br
	N11W				0.30	0.14				Br
	N36W				0.32	0.15	20°N		100	
	N36W				0.14	0.07	15°S			
42	N04W	N12W	N10.5W	9.2	0.32	0.15			50	
	N17W				0.62	0.30				
43	N05W	N10W	N6.1W	6.2	0.20	0.10				
	N02W				1.05	0.50			190	
	N02W				0.32	0.15				
	N02W				0.32	0.15				
	N02W				0.32	0.15				
	N09W, N02E				0.43	0.21				Br
	N08W				0.76	0.36			180	Br

APPENDIX 1. LISTING OF ALL STATISTICAL DATA COLLECTED ON THE INTRUSIVE COMPLEX IN THE SAN RAFAEL AND CAPITOL REEF AREAS, UTAH - Continued.

#	Strike of segment	Subjective average	Numerical average	Standard deviation	Map length (cm)	Km 1:48000	Propaga-tion	Sample number	Thickness cm	Comments
	N10,19W				0.93	0.45			180	
44	N19W	N22W	N21.2W	3.0	0.71	0.34			95	
	N25W				0.18	0.09				
	N19W				0.24	0.12			120	
	N19W				0.98	0.47				
	N22W				0.58	0.28				
45	N44W	N24W	N23.2W	9.2	0.18	0.09				
	N18W				0.92	0.44				
	N07W				0.47	0.23				Br
	N17W				0.36	0.17				
	N18W				0.62	0.30				
	N24W				0.45	0.22				
	N16W				0.26	0.12				
	N17W				0.46	0.22			160	
	N23W				0.26	0.12				
	N20W				0.73	0.35			100	
	N31W				0.33	0.16				
	N31W				0.26	0.12				
	N31W				0.20	0.10				
	N28W				1.30	0.62			185	
46	N30W	N35W	N34.3W	4.2	0.80	0.38				
	N34W				0.83	0.40			120	
	N40W				0.84	0.40				
	N33W				0.84	0.40				
47	N29W	N39W	N35.4W	7.8	0.62	0.30			65	
	N33W				0.33	0.16				
	N44W				0.64	0.31				
48	N46W	N57W	N55.0W	11.7	0.41	0.20				
	N44W				0.22	0.11				
	N63W				0.23	0.11				
	N67W				0.48	0.23				
49	N58W	N56W	N55.0W	5.2	0.28	0.13				
	N58W				0.15	0.07				
	N59W				0.28	0.13				
	N58W				0.16	0.08				
50	N15W				0.54	0.26				
	N16W				0.28	0.13				
51	N13W	N13W	N13.0W	0.0	0.27	0.13				
	N13W				0.86	0.41			100	
	N13W				0.26	0.12				
	N13W				0.73	0.35				
	N13W				0.21	0.10				
52	N03W	N13W	N12.0W	4.4	0.40	0.19				
	N08W				0.75	0.36				
	N19W				0.76	0.36				
	N17W				0.54	0.26				

APPENDIX 1. LISTING OF ALL STATISTICAL DATA COLLECTED ON THE INTRUSIVE COMPLEX IN THE SAN RAFAEL AND CAPITOL REEF AREAS, UTAH - Continued.

#	Strike of segment	Subjective average	Numerical average	Standard deviation	Map length (cm)	Km 1:48000	Propaga-tion	Sample number	Thickness cm	Comments
	N14 W				0.36	0.17				
	N12W				0.26	0.12				
	N12 W				0.31	0.15				
	N12W				0.46	0.22				
	N12 W				0.25	0.12				
	N11W				0.24	0.12				
53	N09W	N05W	N7.3W	2.0	0.67	0.32				
	N08W				0.58	0.28				
	N05 W				0.84	0.40				
54	N06E	N13E	N12.3E	12.5	0.16	0.08				Younger (see # 40)
	N12 E				0.06	0.03				
	N25E				0.38	0.18				
	N16 E				1.03	0.49			160	
55	N05W	N01W	N4.4W	8.4	0.45	0.22				
	N24 W				0.22	0.11				
	N04W				0.89	0.43				
	N02 W				0.32	0.15				
	N-S				0.23	0.11				
	N-S				1.16	0.56			70	
	N-S				0.81	0.39				
	N01 E				0.21	0.10				
	N02E				1.03	0.49				
	N18 W				0.21	0.10				
	N20W				0.23	0.11				
	N02 E				0.33	0.16				
	N03E				0.51	0.24				
	N01 E				0.12	0.06				Br
	N01E				0.23	0.11				Br
	N03 W				0.46	0.22				
	N07W				0.87	0.42				
56	N01W	N03E	N2.0E	4.6	0.21	0.10				
	N01W				0.31	0.15				
	N04 W				0.85	0.41				
	N05E				0.72	0.35				
	N06 E				1.40	0.67			150	
	N07E				3.18	1.53				
57	N23W	N16W	N11.6W	14.6	0.39	0.19				Br, indurated hr
	N31,05 W				1.56	0.75			100	
	N01W				0.38	0.18				
	N02 E				0.38	0.18				
58	N08W	N10W	N11.6W	3.0	0.53	0.25				
	N08 W				0.12	0.06				
	N08W				0.36	0.17				
	N20 W				0.41	0.20				
	N10W				0.12	0.06				
	N12 W				0.30	0.14				
	N12W				0.58	0.28				
	N12 W				0.25	0.12				

APPENDIX 1. LISTING OF ALL STATISTICAL DATA COLLECTED ON THE INTRUSIVE COMPLEX IN THE SAN RAFAEL AND CAPITOL REEF AREAS, UTAH - Continued.

#	Strike of segment	Subjective average	Numerical average	Standard deviation	Map length (cm)	Km 1:48000	Propaga-tion	Sample number	Thickness cm	Comments
	N11W				0.52	0.25				
	N11W				0.37	0.18				
	N11W				0.34	0.16				
	N13W				0.36	0.17				
	N13W				0.28	0.13				
59	N11W	N09W	N9.7W	1.4	0.36	0.17				
	N11W				0.39	0.19				
	N11W				0.40	0.19				
	N09W				0.34	0.16				Br
	N10W				0.56	0.27				Br
	N08W				0.29	0.14				
	N08W				0.46	0.22				
60	N-S	N04W	N1.0W	3.4	0.31	0.15				
	N03E				0.91	0.44				
	N01E				0.46	0.22				
	N04W				0.62	0.30				
	N05W				1.94	0.93				
61	N41W	N41W	N41.0W	0.0	0.51	0.24				
62	N12E	N19E	N16.8E	3.2	1.21	0.58				
	N18E				0.36	0.17				Br
	N18E				0.70	0.34				
	N19E				2.57	1.23			100	
63	N22E	N12E	N14.0E	11.4	0.64	0.31				
	N23E				0.31	0.15				
	N17E				0.35	0.17				
	N20E				1.84	0.88		SRS9-84		Br, Gy, Th
	N20E				0.51	0.24		SRS10-84		
	N01, 14W				2.90	1.39			245	Br
64	N03E	N15W	N13.1W	7.3	0.30	0.15				
	N03E				0.39	0.19			120	
	N01W				0.32	0.15				
	N-S				0.33	0.16				
	N05W				0.39	0.19				
	N10W				0.25	0.12				
	N13, 05W				0.75	0.36				Br
	N10W				0.91	0.44				
	N15W				0.26	0.12				
	N01W				1.46	0.70			145,150,125	
	N11W				0.20	0.10				
	N15W				0.25	0.12	05°N			
	N22W				0.82	0.39				
	N22W				0.28	0.13				
	N09W				0.35	0.17				
	N06W				1.53	0.73				Br
	N18W				2.24	1.08				
	N18W				0.21	0.10				
	N18W				0.11	0.05				
	N18W				0.24	0.12				

APPENDIX 1. LISTING OF ALL STATISTICAL DATA COLLECTED ON THE INTRUSIVE COMPLEX IN THE SAN RAFAEL AND CAPITOL REEF AREAS, UTAH - Continued.

#	Strike of segment	Subjective average	Numerical average	Standard deviation	Map length (cm)	Km 1:48000	Propaga-tion	Sample number	Thickness cm	Comments
	N18W				0.29	0.14				
	N18W				0.23	0.11				
	N13W				0.55	0.26				
	N17W				0.23	0.11				
	N17W				0.43	0.21				
	N17W				0.31	0.15				
	N25W				0.68	0.33				
	N15W				0.29	0.14			50	
	N19W				0.18	0.09				
	N19W				0.44	0.21				
	N23W				0.19	0.09				
	N15W				0.22	0.11			50	
	N27W				0.30	0.14				
	N19W				0.31	0.15				
	N19W				0.21	0.10				
	N14W				0.16	0.08				
	N12W				0.87	0.42				
	N11W				0.33	0.16				
	N07W				0.52	0.25				
	N02W				0.51	0.24				
	N14W				1.45	0.70				
	N11W				0.38	0.18				Br
	N15W				0.51	0.24				
	N13W				0.15	0.07				
65	N11E	N10E	N9.8E	1.3	0.30	0.14			80	Younger (see # 86)
	N10E				0.90	0.43	80°S			Br
	N10E				0.15X0.08	0.07X0.04				
	N08E				0.32	0.15	50°S			
66	N20W	N02W	N2.7W	11.7	0.68	0.33				
	N07W				0.20	0.10				
	N04E				0.20	0.10				
	N04E				0.15	0.07				
	N09E				0.41	0.20				
	N12E				0.40	0.19				
	N14W				0.56	0.27				
67	N15E	N33E	N29.5E	11.7	0.55	0.26				
	N35E				0.36	0.17				
	N26E				0.27	0.13				
	N42E				0.28	0.13				
68	N25W	N06E	N4.0E	10.9	0.30	0.14				
	N05W				0.41	0.20				
	N01W				1.03	0.49			290	
	N03E				1.24	0.60				
	N02E				0.94	0.45				
	N24W				0.17	0.08				
	N17W				0.27	0.13				
	N03E				0.31	0.15				

APPENDIX 1. LISTING OF ALL STATISTICAL DATA COLLECTED ON THE INTRUSIVE COMPLEX IN THE SAN RAFAEL AND CAPITOL REEF AREAS, UTAH - Continued.

#	Strike of segment	Subjective average	Numerical average	Standard deviation	Map length (cm)	Km 1:48000	Propagation	Sample number	Thickness cm	Comments
	N03E				0.25	0.12				
	N08 E				0.39	0.19				
	N03W				0.34	0.16				
	N03 E				0.09	0.04				
	N03E				0.09	0.04				Br
69	N04W	N05W	N6.8W	7.5	0.56	0.27				
	N05E				0.28	0.13				
	N01 W				0.49	0.24				
	N18W				0.19	0.09				
	N18 W				0.29	0.14				
	N04W				0.51	0.24				
	N08 W				0.26	0.13				
	N04W				0.42	0.20				
	N09 W				0.25	0.12				
70	N12W	N16W	N14.8W	4.5	0.53	0.25				Br
	N12 W				0.75	0.36			180	
	N21W				0.86	0.41				
	N12 W				0.91	0.44				
71	N22W	N20W	N21.4W	6.4	0.30	0.14				
	N29 W				0.36	0.17				
	N26W				0.27	0.13				
	N16 W				0.99	0.48				
	N14W				0.72	0.35			80	
72	N03E	N08E	N10.0W	8.5	0.59	0.28				
	N16E				0.53	0.25			120	
	N19 W				0.31	0.15				
73	N14W				1.28	0.61			120	Older (see # 74)
	N02 W				0.12	0.06			110	Younger (see #73)
	N02W				0.11	0.05				
	N03 W				0.12	0.06			90	
	N03W				0.11	0.05				
	N08 W				0.12	0.06				
	N02W				0.11	0.05			10	
	N-S				0.12	0.06				
	N-S				0.13	0.06			140	
	N02 W				0.54	0.26				
	N02W				0.12	0.06	02°N			
	N02 W				0.20	0.10				
	N03W				1.11	0.53				
	N14 W				0.38	0.18				
	N05W				1.22	0.59				
	N13 W				0.50	0.24				
74	N30W	N10W	N11.9W	13.0	0.95	0.46			50,200,185	
	N23 W				1.16	0.56			180,165,150	
	N11W				1.07	0.51			100,100	
	N26 W				0.25	0.12				
	N26W				0.25	0.12				

APPENDIX 1. LISTING OF ALL STATISTICAL DATA COLLECTED ON THE INTRUSIVE COMPLEX IN THE SAN RAFAEL AND CAPITOL REEF AREAS, UTAH - Continued.

#	Strike of segment	Subjective average	Numerical average	Standard deviation	Map length (cm)	Km 1:48000	Propaga-tion	Sample number	Thickness cm	Comments
	N03W				0.81	0.39			100	
	N02W				0.42	0.20			110	
	N02E				0.25	0.12				
	N02E				0.17	0.08				
	N02W				0.29	0.14				
75	N01W	N01W	N1.0W	0.0	0.64	0.31			50	
76	N66W	N23W	N28.0W	25.7	0.28	0.13				
	N21W				1.06	0.51			135	
	N13W				1.00	0.48				
	N12W				1.13	0.54			155	
77	N03W	N03W	N3.0W	0.0	0.38	0.18			120	
	N03W				0.82	0.39			150	
	N03W				0.44	0.21				
78	N35E	N16E	N24.5E	14.8	0.62	0.30			90	Younger (see # 79)
	N28E				0.18	0.09				
	N17E				0.78	0.37				
	N46E				0.14	0.07				
	N38E				0.43	0.21				
	N43E				0.14	0.07				
	N01E				0.81	0.39			70	Br
	N01E				0.31	0.15			90	
	N13E				1.34	0.64			120,100	
	N22E				1.10	0.53			135	
	N25E				0.29	0.14			95	
	N25E				0.32	0.15				
79	N47W	N29W	N27.1W	9.3	0.37	0.18			75	Older (see # 78)
	N47W				0.75	0.36				
	N16W				0.10	0.05				Br
	N25W				0.18X0.15	0.09X0.07		82SRS-1,2		Ts
	N25W				0.14X0.14	0.07X0.07				Ts
	N18W				0.38	0.18				
	N22W				0.30	0.14				
	N23W				0.56	0.27			155	
	N26W				0.29	0.14			150	
	N31W				0.73	0.35				
	N31W				0.12	0.06				
	N31W				0.71	0.34			230	
	N18W				0.43	0.21				
	N23W				1.14	0.55			200	
	N23W				0.31	0.15				
80	N46W	N46W	N46.5W	0.7	0.77	0.37				
	N47W				0.67	0.32				
81	N14W	N20W	N18.6W	3.7	0.40	0.19				
	N14W				0.71	0.34				
	N15W				0.25	0.12				
	N17W				0.40	0.19				
	N23W				0.71	0.36				

APPENDIX 1. LISTING OF ALL STATISTICAL DATA COLLECTED ON THE INTRUSIVE COMPLEX IN THE SAN RAFAEL AND CAPITOL REEF AREAS, UTAH - Continued.

#	Strike of segment	Subjective average	Numerical average	Standard deviation	Map length (cm)	Km 1:48000	Propagation	Sample number	Thickness cm	Comments
	N22W				0.91	0.44				
	N22 W				0.75	0.36				
82	N30W	N35W	N32.0W	6.6	0.54	0.26				
	N25 W				0.97	0.47				
	N39W				0.29	0.14			105	
	N39 W				0.36	0.17				
	N37W				0.67	0.32				
83	N23,10,16E	N15E	N18.3E	6.6	3.60	1.73			60,135	
	N14E				0.97	0.47				
84	N23W	N25W	N25.1W	6.2	0.48	0.23				
	N21W				0.70	0.34			15	
	N24 W				0.69	0.33				
	N24W				0.30	0.14			170	
	N25 W				0.37	0.18				
	N22W				0.86	0.41			95	
	N40 W				0.39	0.19			65	
	N22W				0.87	0.42				
85	N20W	N22W	N17.0W	4.2	0.36	0.17				
	N24W				0.29	0.14				
86	N26W	N26W	N26.0W	0.0	0.34	0.16	03°,80°,90°S		25	Older (see #65)
	N26W				0.10	0.05				
87	N17W	N21W	N19.6W	6.8	0.20	0.10				
	N19W				0.17	0.08				
	N20 W				0.15	0.07				
	N27W				0.08	0.04				
	N20 W				0.19	0.09			35	
	N21W				0.12	0.06				
	N27 W				0.14	0.07				
	N19W				0.18	0.09				
	N08 W				1.06	0.51			175	
	N10W				0.11	0.05				
88	N03W	N04W	N3.8W	2.1	0.14	0.07				
	N06W				0.17	0.08				
	N06 W				0.05	0.02				
	N02W				0.17	0.08			100	
	N02 W				0.14	0.07				
89	N05W	N21W	N18.2W	5.8	0.26	0.12				
	N22 W				0.36	0.17				
	N22W				0.79	0.38				
	N24 W				0.50	0.24		82SRS-3,4,5 SRS3-84 984SRS-17, 17a,18,19,20 21,21a,22,23		Th, Na, An, Gy Bud
	N18 W				0.59	0.28				
	N27W				0.13	0.06				
	N13 W				0.56	0.27				
	N25W				0.72	0.35				

APPENDIX 1. LISTING OF ALL STATISTICAL DATA COLLECTED ON THE INTRUSIVE COMPLEX IN THE SAN RAFAEL AND CAPITOL REEF AREAS, UTAH - Continued.

#	Strike of segment	Subjective average	Numerical average	Standard deviation	Map length (cm)	Km 1:48000	Propaga-tion	Sample number	Thickness cm	Comments
	N14W				0.85	0.41				
	N15 W				0.29	0.14				
	N16W				0.14	0.07				
	N20,35 W				1.01	0.48				
	N10W				0.45	0.22				
	N16 W				0.31	0.15				
	N17W				0.30	0.14				
	N20 W				0.19	0.09				
90	N41W	N26W	N23.3W	7.4	0.76	0.34				
	N20 W				0.45	0.22				
	N20W				0.56	0.24				
	N22 W				0.28	0.13				
	N22W				0.20	0.10				
	N27 W				0.16	0.08				
	N33W				0.18	0.09				
	N26 W				0.17	0.08				
	N26W				0.17	0.08				
	N23 W				0.17	0.08				
	N19W				0.39	0.19				
	N11 W				0.76	0.36				
	N15W				0.18	0.09				
91	N01E	N08W	N6.4W	8.0	0.41	0.20				
	N05E				1.25	0.60				
	N02 E				0.38	0.18			110	
	N-S				0.49	0.24				
	N01 W				0.24	0.12				
	N03W				0.30	0.14			230	
	N02 W				0.24	0.12				
	N02W				0.42	0.20				
	N02 W				0.33	0.16				
	N04W				0.28	0.13				
	N04 W				1.12	0.54				
	N03W				0.44	0.21				
	N01 W				0.09X0.04	0.04X0.02				br
	N02W				0.16X0.07	0.08X0.03				Br
	N-S				0.34	0.16				
	N05W				0.24	0.12				
	N4E,N7W	N08W	N6.4W	8.0	0.79	0.38				
	N10W				0.62	0.30				
	N18 W				0.63	0.30				
	N07E				0.34	0.16				
	N23 W				0.26	0.12				
	N16W				0.29	0.14				
	N12 W				0.35	0.17				
	N08W				0.35	0.17				
	N06 W				0.40	0.19				
	N08W				0.19	0.09				

APPENDIX 1. LISTING OF ALL STATISTICAL DATA COLLECTED ON THE INTRUSIVE COMPLEX IN THE SAN RAFAEL AND CAPITOL REEF AREAS, UTAH - Continued.

#	Strike of segment	Subjective average	Numerical average	Standard deviation	Map length (cm)	Km 1:48000	Propaga-tion	Sample number	Thickness cm	Comments
	N23W				0.40	0.19				
	N06 W				0.44	0.21				
	N18W				0.45	0.22				
	N09 W				0.16	0.08				Br
	N12W				0.46	0.22				
	N06 W				0.85	0.41				
	N08,15W				3.32	1.59				
	N08 W				0.53	0.25				
92	N14E	N03E	N5.2E	3.9	0.17	0.08				
	N12 E				0.14	0.07				
	N05E				0.20	0.10			70	
	N08 E				0.31	0.15				
	N04E				0.17	0.08				
	N05 E				0.22	0.11				
	N08E				0.23	0.11				
	N05,11 E				1.34	0.64				
	N05E				0.60	0.29				
	N06 E				0.16	0.08				
	N03E				0.09	0.04				
	N03 E				0.14	0.07				
	N03E				0.10	0.05				
	N04 E				0.07	0.03				
	N01E				0.07	0.03				
	N01 E				0.07	0.03				
	N01E				0.19	0.09			190	
	N-S				1.86	0.89			190	Cc
93	N23W	N28W	N26.5W	5.2	0.34	0.16			70	
	N25 W				1.02	0.49				Br
	N22W				0.41	0.20				
	N18 W				0.13X0.07	0.06X0.03		984SRS-27		Plug, Cc, An
	N18W				0.69	0.33				
	N25,32 W				1.80	0.86				
	N30W				0.18X0.11	0.09X0.05		984SRS-28		Bud,joints,Cc
	N29 W				1.38	0.66			70	Diabase float
	N32W				2.01	0.96				Diabase float
	N27 W				1.33	0.64				Diabase float
	N32W				0.24	0.12				
	N32 W				0.24	0.12				
94	N12W	N07W	N10.9W	9.0	0.58	0.28		SRS1-84	190	
	N14 W				0.34	0.16				
	N27W				0.25	0.12				
	N19 W				0.22	0.11				
	N19W				0.43	0.21				
	N21 W				0.37	0.18				
	N03W				0.22	0.11				
	N-S				0.34	0.16				
	N03E				0.26	0.12				

APPENDIX 1. LISTING OF ALL STATISTICAL DATA COLLECTED ON THE INTRUSIVE COMPLEX IN THE SAN RAFAEL AND CAPITOL REEF AREAS, UTAH - Continued.

#	Strike of segment	Subjective average	Numerical average	Standard deviation	Map length (cm)	Km 1:48000	Propagation	Sample number	Thickness cm	Comments
	N-S				0.27	0.13				
	N02W				1.04	0.50				
	N05W				0.29	0.14				
	N05W				0.72	0.35		SRS2-84	110	
	N19W				0.49	0.24				
	N17W				0.39	0.19				
	N12W				0.50	0.24			100	
95	N30W	N47W	N35.8W	12.0	0.27	0.13				
	N34W				0.62	0.30			100	
	N26W				0.25	0.12				
	N53W				0.73	0.35				
96	N29W	N41W	N34.7W	7.2	0.62	0.30				
	N28W				0.35	0.17				
	N26W				0.48	0.23				
	N27W				0.56	0.27				
	N27W				0.44	0.21				
	N33W				0.32	0.15				
	N34,27W				1.28	0.61				
	N30W				1.40	0.67				
	N35W				0.31	0.15				
	N30W				2.14	1.03				
	N36W				0.54	0.26				
	N44W				0.36	0.17			100	
	N37W				0.71	0.34			100	
	N35W				0.18	0.09				
	N34W				0.19	0.09				
	N30W				0.30	0.14				
	N30W				0.18	0.09				
	N30W				0.12	0.06				
	N28W				0.20	0.10				
	N28W				0.43	0.21				Br
	N54,44W				3.10	1.49		984SRS-35 a,b,c	100	Br
	N45W				0.48	0.23				
	N36W				0.37	0.18				
	N31W				0.87	0.42				
	N37W				0.97	0.47				
	N38W				0.91	0.44				
	N38W				0.28	0.13				
	N34,51W				1.26	0.60			105	Br
97	N32W				0.16	0.08				
	N32W				0.05	0.02				
	N08W				0.14	0.07				
	N33W				0.13	0.07				
	N37W				0.10	0.05				
	N06W				0.83	0.40				
	N08W				0.17	0.08				
	N-S				0.15	0.07				

APPENDIX 1. LISTING OF ALL STATISTICAL DATA COLLECTED ON THE INTRUSIVE COMPLEX IN THE SAN RAFAEL AND CAPITOL REEF AREAS, UTAH - Continued.

#	Strike of segment	Subjective average	Numerical average	Standard deviation	Map length (cm)	Km 1:48000	Propaga-tion	Sample number	Thickness cm	Comments
	N11 W				0.62	0.30				
	N02W				0.54	0.26				
98	N05W	N01W	N1.5W	1.2	0.16X0.08	0.08X0.04				Br
	N05W				0.93	0.43				
	N02 E				0.35	0.17				
	N03W				0.36	0.17				
	N03 W				0.27	0.13				
	N08E				0.33	0.16				
	N10 E				0.77	0.37				
99	N20W	N20W	N20.0W	0.0	0.96	0.46	25°N			
100	N16E	N16E	N16.0E	0.0	0.44	0.21				
101	N37W	N33W	N30.3W	6.3	0.80	0.38				
	N35 W				0.32	0.15	20°S,0°			
	N26W				0.33	0.16				
	N20 W				0.78	0.37	60°N,0°			
	N32W				0.07X0.02	0.03X0.01				Br
	N32 W				0.04X0.03	0.02X0.01				Br
102	N20W	N13W	N15.6W	14.4	0.48	0.23				
	N29 W				0.24	0.12				
	N39,25W				0.72	0.35				
	N23 W				0.26X0.08	0.12X0.04				Br
	N23W				0.21X0.06	0.10X0.03				Br
	N23 W				0.18	0.09				
	N23W				0.33	0.16				
	N13 W				0.34	0.16			85	
	N06W				0.72	0.35				
	N07 E				1.40	0.67				Br
	N09E				0.85	0.41	08°S			Br
	N05 E				0.83	0.41	45°S		250	
103	N-S	N01E	N2.7E	5.2	0.15X0.08	0.07X0.04				Br
	N05 E				0.91	0.44				
	N02E				0.32	0.15				
	N03 W				0.43	0.21				
	N03W				0.26	0.12				
	N08 E				0.30	0.14				
	N10E				0.78	0.37				
104	N06E	N07E	N6.5E	0.7	0.28	0.13				
	N07E				1.18	0.57				
105	N01W	N01E	N1.7E	1.2	0.58	0.28				
	N01W				0.83	0.40			175	
	N03 E				1.21	0.58				
106	N04E	N04E	N4.0E	0.0	0.98	0.47			105	
107	N02W	N02W	N1.7W	0.5	0.50X0.21	0.24X0.10				Br
	N01W				0.32	0.15				
	N02 W				0.26	0.12				
108	N23W	N02E	N3.0E	11.7	0.40	0.19		984SRS-15		
	N04 E				0.19X0.05	0.09X0.02				Br

APPENDIX 1. LISTING OF ALL STATISTICAL DATA COLLECTED ON THE INTRUSIVE COMPLEX IN THE SAN RAFAEL AND CAPITOL REEF AREAS, UTAH - Continued.

#	Strike of segment	Subjective average	Numerical average	Standard deviation	Map length (cm)	Km 1:48000	Propaga-tion	Sample number	Thickness cm	Comments
	N04 E				0.26	0.12				
	N09E				0.16X0.07	0.08X0.03				Br
	N09 E				0.49	0.24				
	N09E				0.88	0.42				
	N09 E				0.31	0.15				
109	N01E	N09E	N5.6E	5.5	0.50	0.24				
	N12 E				0.38	0.18				
	N06E				0.36	0.17				
	N03 E				0.18	0.09				
	N02E				0.39	0.19				
	N01 E				0.40	0.19				
	N01E				0.35	0.17				
	N02 W				1.42	0.68			210	
	N12E				0.62	0.30	05°N		200,85	
	N13 E				1.08	0.52				
	N13E				0.63	0.30				
110	N11W	N11W	N13.9W	5.8	0.54	0.26			160	
	N09W				1.01	0.48	0°,10°-30°N		125,130,140,80	Cc
	N16 W				1.00	0.48			160,40,200	Cc
	N23W				0.21	0.10				Fe stains
	N20 W				0.25	0.12				
	N09W				0.57	0.27				
	N09 W				0.21	0.10				
111	N23W	N23W	N24.0W	5.9	0.18	0.09	04°N			
	N23 W				0.09	0.04				
	N39W				0.33	0.16				
	N23 W				0.86	0.41	08°-18°S	SRS14-84	100,170	
	N21W				0.28	0.13				
	N21 W				0.20	0.10	02°-04°S			
	N20W				0.04X0.02	0.02X0.01				Br
	N20 W				0.47	0.23				Br
	N20W				0.09	0.04				
112	N21W	N20W	N18.5W	1.6	0.52	0.25				
	N20W				0.39	0.19				
	N17 W				0.27	0.13				
	N17W				0.31	0.15			145	Br
	N18 W				0.45	0.22				Br
	N18W				0.89	0.43				Indurated hr, no diabase, local br
113	N47W	N47W	N47.5W	0.6	0.23	0.11			50-100	
	N47W				0.28	0.13				
	N48 W				0.36	0.17		984SRS-25		
	N48W				0.44	0.21	08°-15°N			
114	N19W	N20W	N20.1W	4.2	0.23	0.11				
	N19W				0.62	0.30	68°N		20,80	
	N18 W				0.25	0.12			45	
	N17W				0.66	0.29			100	

APPENDIX 1. LISTING OF ALL STATISTICAL DATA COLLECTED ON THE INTRUSIVE COMPLEX IN THE SAN RAFAEL AND CAPITOL REEF AREAS, UTAH - Continued.

#	Strike of segment	Subjective average	Numerical average	Standard deviation	Map length (cm)	Km 1:48000	Propaga-tion	Sample number	Thickness cm	Comments
	N17W				0.47	0.23				
	N24W				0.10	0.05				
	N24W				0.08	0.04				
	N24W				0.14	0.07				
	N24W				0.16	0.08				
	N24W				0.37	0.18				
	N23W				0.27	0.13	45°N		80	
	N18W				0.22	0.11				
	N11W				0.99	0.48				
	N20,27W				1.34	0.64			75	Cc
	N16W				0.34	0.16				
	N16W				0.38	0.18			50	
115	N56W	N56W	N56.0W	0.0	0.04X0.04	0.02X0.02				Br
	N56W				0.04X0.04	0.02X0.02				Br
	N56W				0.11X0.04	0.05X0.02				Br
116	N08W	N14W	N13.5W	7.8	0.58	0.28	10°S		85	
	N19W				1.38	0.66				
117	N35W	N32W	N32.5W	13.9	0.19	0.09	25°-45°S		40	
	N32W				0.14	0.07				
	N32W				0.19	0.09				
	N30W				1.11	0.53				
	N12W				0.45	0.22			85	
	N14W				0.15	0.07	00°S			
	N14W				0.56	0.27	00°S			
	N23W				0.90	0.43	25°S		115	
	N25W				0.91	0.44	00°S		175,155	
	N30W				0.31	0.15				
	N30W				0.17	0.08				
	N30W				0.37	0.18				
	N22W				1.50	0.72	8°,25°,35°,65°S			
	N52W				1.02	0.49	65°S			
	N54W				0.46	0.22	00°-45°N			
	N54W				0.16	0.08			110	
	N54W				0.18	0.09				
118	N31W	N33W	N33.0W	1.8	0.38	0.18			35	
	N31W				0.56	0.27			90	
	N33W				0.08	0.04				Br(2)
	N33W				0.09	0.04				Br
	N35W				0.25	0.12	00°-20°N			
	N35W				0.60	0.29			130	
119	N25W	N22W	N25.0W	2.9	0.25	0.12				
	N23W				0.90	0.43	10°,30°S		75	
	N20W				0.09	0.04			80	Br
	N23W				0.11X0.04	0.05X0.02				Br
	N29W				0.29	0.14		82SRS-10,11		Br
	N29W				0.26	0.12	20 ,35°,38°,50°S			
	N24W				2.18	1.65	30°-36°N	984SRS-24	45,50,30	Cc

APPENDIX 1. LISTING OF ALL STATISTICAL DATA COLLECTED ON THE INTRUSIVE COMPLEX IN THE SAN RAFAEL AND CAPITOL REEF AREAS, UTAH - Continued.

#	Strike of segment	Subjective average	Numerical average	Standard deviation	Map length (cm)	Km 1:48000	Propaga-tion	Sample number	Thickness cm	Comments
120	N05W	N32W	N35.5W	14.3	0.30X0.16	0.14X0.08				Br
	N44 W				0.47	0.23				Br
	N31W				0.91	0.44				
	N37 W				0.45	0.22				
	N36W				0.40	0.19				
	N37 W				0.12	0.06				
	N47W				0.13	0.06				
	N60 W				0.27	0.13				
	N28W				0.32	0.15			100	
	N28 W				0.12	0.06				
	N28W				0.46	0.22				
121	N35W	N19W	N24.3W	9.3	0.25	0.12	15°-60°N		130	
	N28W				0.88	0.42				
	N29 W				0.13	0.06				
	N29W				0.41	0.20				
	N29 W				0.14	0.07				
	N29W				0.13	0.06				
	N19 W				0.54	0.26				
	N16,05W				1.50	0.72				
122	N29W	N21W	N24.8W	4.6	0.10	0.05				Older (see # 125)
	N29W				0.09	0.04				
	N29 W				0.09	0.04				
	N20W				2.76	1.30				Br
	N21 W				0.13	0.06				
	N21W				0.23	0.11				
123	N28E	N18E	N18.3E	5.5	1.10	0.53	05°,85°N		95	Younger (see # 124)
	N15E				0.84	0.40			60	
	N18 E				1.71	0.82	15°S			
	N23E				0.10	0.05				
	N23 E				0.14	0.07				
	N23E				1.07	0.51				
124	N12W	N12W	N12.0W	0.0	0.17	0.08				Older (see #123)
	N12W				0.06	0.03				
	N12 W				0.07	0.03				
125	N25E	N18E	N17.7E	5.7	0.68	0.33				Younger (see # 122)
	N25 E				0.58	0.28				
	N25E				0.58	0.28				
	N23 E				0.34X0.11	0.16X0.05				Br
	N23E				0.19	0.09				
	N23 E				1.10	0.53				Br
	N15E				0.79	0.38				
	N16 E				0.57	0.27				
	N10E				0.25	0.12				Br, irregular
	N10 E				1.60	0.77			220	Br, irregular
	N11E				0.11	0.05				Br, irregular
	N15 E				0.16	0.08				
	N14E				0.17	0.08				

APPENDIX 1. LISTING OF ALL STATISTICAL DATA COLLECTED ON THE INTRUSIVE COMPLEX IN THE SAN RAFAEL AND CAPITOL REEF AREAS, UTAH - Continued.

#	Strike of segment	Subjective average	Numerical average	Standard deviation	Map length (cm)	Km 1:48000	Propaga-tion	Sample number	Thickness cm	Comments
	N15E				0.18	0.09				
	N15E				0.24	0.12				
126	N14E	N13E	N8.2E	18.6	0.14X0.11	0.07X0.05				Br
	N10E				0.15	0.07				
	N18E				0.31	0.15				
	N24W				0.28	0.13				Br
	N26E				0.73	0.35				Br
	N10E				0.75	0.36		82SRS-6,7, 8,9	55	Br
127	N05W	N06W	N8.6W	5.0	0.36	0.17				
	N05W				0.24	0.12				
	N05W				0.25	0.12				
	N15W				0.28	0.13				
	N13W				0.39	0.19				
128	N08E	N-S	N3.5E	3.7	0.72	0.35				Br, Cc
	N05E				0.51	0.24				
	N01E				1.06	0.51	08°S,10°S		60	Br
	N-S				0.63	0.30			70	Cc
129	N04E	N05E	N4.8E	1.7	0.10	0.05				
	N03E				0.20	0.10				
	N07E				0.31	0.15				
	N07E				0.56	0.27		9848RS-30	200	Cc, An, Th
	N02E				0.10X0.08	0.05X0.04				Br
	N04E				0.46	0.22				
	N04E				0.11	0.05				
	N05E				0.11	0.05				
	N07E				0.62	0.30				
	N05E				0.59	0.28				
	N05E				0.33	0.16				
130	N01E	N18W	N17.7W		0.41	0.20				Br
	N01W				0.48	0.23				
	N04W				0.65	0.31				
	N13W				0.83	0.40	10°S			
	N13W				0.70	0.34				
	N25,37W				2.28	1.09			130	Cc
	N23W				0.40	0.19			120	
	N44W				0.26	0.12				
131	N01W	N03W	N2.2W	7.3	0.41	0.20				
	N02W				0.36	0.17				
	N10W				0.26	0.12				
	N11W				0.20	0.10				Plug
	N08W				0.53	0.25	08 S			
	N11W				0.57	0.27				
	N07E				0.24	0.12				
	N04E				0.54	0.26				
	N04E				0.67	0.32			70	
	N06E				0.22	0.11				

APPENDIX 1. LISTING OF ALL STATISTICAL DATA COLLECTED ON THE INTRUSIVE COMPLEX IN THE SAN RAFAEL AND CAPITOL REEF AREAS, UTAH - Continued.

#	Strike of segment	Subjective average	Numerical average	Standard deviation	Map length (cm)	Km 1:48000	Propaga-tion	Sample number	Thickness cm	Comments
132	N12W	N08W	N9.3W	7.3	0.58	0.28				
	N02 E				0.25	0.12				
	N10W				1.26	0.60			130	
	N16 W				1.05	0.50			145	Cc
133	N25W	N29W	N25.3W	3.8	1.44	0.69				
	N25 W				0.92	0.44				
	N25W				0.31	0.15				
	N23 W				0.50	0.24			40	
	N24W				0.20	0.10				
	N35 W				0.88	0.42				
	N27W				0.26	0.12			210	
	N27 W				0.11X0.04	0.05X0.02				Br
	N27W				0.67	0.32				
	N23 W				0.12	0.06				
	N23W				0.28	0.13				
	N19 W				0.78	0.37				
134	N07W	N12W	N11.0W	3.6	0.27	0.13				
	N10 W				0.29	0.14				
	N16W				1.22	0.59			150	
	N13 W				1.75	0.84				
	N13W				1.77	0.85				
	N12 W				0.26	0.12				
	N06W				0.43	0.21				
135	N02E	N03W	N3.0W	3.2	0.16	0.08				
	N01E				0.25	0.12				
	N01 E				0.22	0.11			150	
	N05W				1.07	0.51				Br
136	N22W	N19W	N18.1W	7.2	0.64	0.31				
	N32,24W				0.96	0.46			100	
	N30,20 W				1.35	0.65				
	N18W				0.19	0.09				
	N17 W				0.25	0.12				
	N18W				0.18	0.09				
	N19 W				0.19	0.09				
	N16W				0.42	0.20				
	N18 W				0.30	0.14				
	N07W				0.31	0.15				
	N10 W				0.32	0.15				
	N14W				0.31	0.15				
	N07 W				0.28	0.13				
137	N18W	N18W	N18.0W	0.0	0.57	0.27				
138	N17E	N14E	N12.5E	3.5	0.40	0.19				
	N07E				0.48	0.23				
	N06 E				0.24	0.12				
	N01W				0.26	0.12				
	N08 E				0.26	0.12				
	N24,09,15E				2.32	1.11				
	N17 E				0.22	0.11				

APPENDIX 1. LISTING OF ALL STATISTICAL DATA COLLECTED ON THE INTRUSIVE COMPLEX IN THE SAN RAFAEL AND CAPITOL REEF AREAS, UTAH - Continued.

#	Strike of segment	Subjective average	Numerical average	Standard deviation	Map length (cm)	Km 1:48000	Propaga-tion	Sample number	Thickness cm	Comments
	N22 E				0.15	0.07				
	N11E				0.17	0.08				
	N11 E				0.25X0.10	0.12X0.05				Br
	N13E				0.85	0.41				
	N17 E				0.20	0.10				Br
	N14E				0.08	0.04				
	N11 E				0.28	0.13				
	N13E				0.14	0.07				
	N11 E				0.13	0.06				
139	N07E	N01E	N3.1E	3.6	1.35	0.65				
	N02 E				2.21	1.06				Float, alt. hr
	N03E				0.20	0.10				
	N02 E				0.15	0.07				
	N02E				0.12	0.06				
	N01 E				0.07	0.03				
	N03E				0.13	0.06				
	N01 E				0.20	0.10				
	N01W				1.30	0.62			85,200	
	N01 W				0.89	0.43		984SRS-29	260	
	N07E				0.87	0.42			240	
	N11 E				0.39	0.19				
140	N20W	N19W	N19.7W	4.4	0.93	0.45				
	N23 W				1.04	0.50				
	N21W				0.44	0.21				
	N24 W				0.66	0.32	05°N		120	
	N16W				0.25	0.12				
	N13 W				0.40	0.19				
	N14W				0.52	0.25				
	N26 W				0.67	0.32				
	N26W				0.66	0.32				
	N22 W				0.31	0.15	10°N			
	N16W				0.52	0.25				
	N17 W				0.24	0.12				
	N14W				0.26	0.12				
	N21 W				1.22	0.59				
	N22W				0.54	0.26				
141	N28W	N24W	N22.0W	5.0	3.90	1.85	30°,35°N		145,170	
	N20W				1.00	0.48				
	N31 W				0.67	0.32				
	N22W				3.30	1.60				
	N19 W				0.40	0.19			90	
	N25W				0.60	0.29				
	N17 W				0.21	0.10				
	N19W				0.75	0.36	55 , 00°,45-75°S			
	N17 W				0.93	0.45		SRS12-84	90	
142	N06W	N08W	N8.0W	7.6	0.12X0.05	0.06X0.02				Br, Ts
	N06 W				0.12X0.05	0.06X0.02				Br, Ts

APPENDIX 1. LISTING OF ALL STATISTICAL DATA COLLECTED ON THE INTRUSIVE COMPLEX IN THE SAN RAFAEL AND CAPITOL REEF AREAS, UTAH - Continued.

#	Strike of segment	Subjective average	Numerical average	Standard deviation	Map length (cm)	Km 1:48000	Propagation	Sample number	Thickness cm	Comments
	N07 E				0.11	0.05				
	N12W				0.24	0.12				
	N15 W				0.93	0.45			65	
	N18W				0.21	0.10				
	N07 W				0.17	0.08				
	N07W				0.16	0.08				
143	N15W	N12W	N17.0W	5.2	0.12	0.06				
	N16W				0.13	0.06				
	N11 W				0.20	0.10				
	N10W				0.29	0.14			45	
	N10 W				0.18	0.09				
	N10,17W	N15W	N13.5W		1.24	0.60				
	N22 W				1.05	0.51			40	
	N21W				0.20	0.10				
	N21 W				0.16	0.08				
	N23W				0.26	0.12				
	N23 W				0.52	0.25				
144	N20W	N15W	N20.2W	6.5	1.04	0.50		SRS13-84		
	N19 W				0.14	0.07				
	N19W				0.20	0.10				
	N27 W				0.43	0.21				
	N22W				0.24X0.20	0.12X0.10				Plug
	N23 W				0.33	0.16				
	N28W				2.02	1.00				
	N20 W				1.24	0.60				Bud
	N29W				0.17	0.08				
	N16 W				0.53	0.25		984SRS-16		Cc, An, Th, Na
	N14W				0.43	0.21				
	N13 W				0.18	0.09				
	N13W				0.09	0.04				
	N12 W				0.15	0.07				
	N24W				0.24	0.12				
	N12 W				0.24	0.12				
	N33W				0.12	0.06				
145	N16W	N03W	N3.8W	11.1	0.28	0.13			50	
	N14W				0.27	0.13				
	Ni5 W				0.25	0.12				
	N14W				0.24	0.12				
	N14 W				0.23	0.11				
	N34E				0.25	0.12				
	N13 W				0.81	0.39				Br
	N05W				2.44	1.17		984SRS-31, 31a		Br, Qtz, Gl Cc, Bi in vein
	N01E, N12 W				0.90	0.43				
	N-S				0.43	0.21				
	N-S				0.42	0.20				

APPENDIX 1. LISTING OF ALL STATISTICAL DATA COLLECTED ON THE INTRUSIVE COMPLEX IN THE SAN RAFAEL AND CAPITOL REEF AREAS, UTAh - Continued.

#	Strike of segment	Subjective average	Numerical average	Standard deviation	Map length (cm)	Km 1:48000	Propaga-tion	Sample number	Thickness cm	Comments
	N13E,N-S				1.52	0.73				
	N06W				0.93	0.45				
	N06W				0.33	0.16				
146	N28W	N07W	N9.7W	7.2	0.75	0.36				
	N11W				0.44	0.21	55°-90°N		80	
	N28W				0.48	0.23			85	
	N04W				0.42	0.20				
	N12W				0.77	0.37				
	N06W				1.76	0.84				
	N12W				1.95	0.94		984SRS-32	500	Bi in vein
	N01W				0.43	0.21				
	N05W				0.23	0.11				
	N08W				1.31	0.63				
	N07W				2.81	1.35				
147	N16W	N06W	N9.0W	5.4	1.24	0.60		984SRS-33		Cc, Th, An
	N15W				0.43	0.21				
	N12W				0.49	0.24		984SRS-33a		
	N11W				0.36	0.17				
	N10W				0.82	0.39				
	N09W				0.72	0.35				
	N05W				0.64	0.31				
	N-S				1.08	0.52				
	N03W				1.30	0.62				
148	N42W	N40W	N44.8W	6.1	0.18	0.09				
	N42W				1.44	0.69				
	N47W				1.35	0.65				
	N52W				0.33	0.16				
	N54W				0.99	0.48				
	N32W				2.82	1.35				
	N43W				0.28	0.13				
	N45W				0.48	0.23				
	N47W				1.05	0.50				
	N44W				0.53	0.25				
149	N02E	N02W	N2.0E	7.4	0.14	0.07				
	N15E				0.10	0.05				
	N01W				0.31	0.15				
	N02W				0.06	0.03				
	N03W				0.08	0.04				
150	N08E	N-S	N5.0E	3.0	0.44	0.21				
	N02E				0.09	0.04				
	N05E				0.13	0.06				
151	N07W	N17W	N12.4W	7.2	0.15	0.07				
	N17W				0.32	0.15			100	
	N10W				0.35	0.17				
	N23W				0.36	0.17		984SRS-26	140	Cc

APPENDIX 1. LISTING OF ALL STATISTICAL DATA COLLECTED ON THE INTRUSIVE COMPLEX IN THE SAN RAFAEL AND CAPITOL REEF AREAS, UTAH - Continued.

#	Strike of segment	Subjective average	Numerical average	Standard deviation	Map length (cm)	Km 1:48000	Propaga-tion	Sample number	Thickness cm	Comments
	N20W				0.22	0.11				
	N05W				0.36	0.17				
	N07W				0.26X0.06	0.16X0.03				Br
152	N19W	N20W	N31.0W	7.8	0.38	0.18				
	N29W				0.77	0.37				
	N31W				0.34	0.16				
	N37W				0.28	0.13				
	N33W				0.35	0.17				
	N25W				0.23	0.11				
	N43W				0.49	0.24				
153	N16W	N16W	N16W	0.0	0.12X0.09	0.06X0.04				Br
	n = 1178	n = 153 N13.4W S.D 17.1	n = 153 N13.5W S.D. 17.0			n = 1170 average length 135 cm	n =98 50% between 00°-25°		n = 205 average thickness 120 cm	

* Number corresponds to dike on Plate 1.

[1] Subjective average of strike of dike which appears to be a single dike with coherent outcrop length.

[2] Numerical average of strike of dike segments which appear to be a single coherent dike.

[3] Length measured on the 1:48,000 scale map (Plate 1) with LASICO linear measuring probe, resolution and accuracy 0.0385mm or 1.9×10^{-3} km.

[4] Map length converted to km.

[5] Local propogation direction measured on the outcrop wall of the dike with a Brunton compass.

[6] Dike thickness measured in the field perpendicular to the lesser dimension and represents the thickness of a dike segment.

[7] Abbreviations used: An = analcime; Cc = calcite; Th = thompsonite; Na = natrolite; Gy = gypsum; Qtz = quartz; Gl = glass; Bi = biotite; Br = brecciated; diabase float with no evidence of in place dike; indurated host rock but no evidence of diabase; Hr = host rock; Ls = limestone; Sh = shale; Ts = sill; Fe = iron stains

APPENDIX 2

APPENDIX 2. LOCATION OF SAMPLES IN TABLE 3.

SAMPLE NUMBER	LATITUDE NORTH	LONGITUDE WEST	UNIT	SAMPLE LOCALITY DESCRIPTION
82SRS-1	38°36'30"	111°05'06"	Je	Termination of sill
82SRS-2	38°36'30"	111°05"06"	Je	Termination of sill.
82SRS-3	38°34'25"	111°05'42"	Jc	NW corner of bud.
82SRS-4	38°34'25"	111°05'42"	Jc	Host rock near bud.
82SRS-5	38°34'25"	111°05'42"	Jc	Dike-host rock contact.
82SRS-6	38°29'53"	111°14'53"	Je	Anastomosing sillets.
82SRS-7	38°24'00"	111°10'00"	Jmb	25 cm from sill contact.
82SRS-8	38°24'00"	111°10'00"	Jmb	Sill.
82SRS-9	38°24'00"	111°10'00"	Jmb	Sill-host rock contact.
82SRS-10	38°31'05"	111°19'01"	Je	NE lobe of breccia.
SRS1-84	38°31'38"	111°06'22"	Jc	Center of dike.
SRS2-84	38°30'15"	111°06'15"	Jc	Center of dike.
SRS2-84	38°34'23"	111°05'45"	Jc	Center of dike.
SRS4-84	38°40'15"	111°07'15"	Je	E margin of bud.
SRS5-84	38°47'38"	111°06'25"	Jc	Center of dike.
SRS6-84	38°47'05"	111°04'30"	Jc	Center of dike.
SRS7-84	38°46'30"	111°06'00"	Je	Center of dike.
SRS8-84	38°42'58"	111°07'45"	Je	Right margin of dike.
SRS9-84	38°34'30"	111°07'45"	Jc	Center of dike.
SRS10-84	38°31'03"	111°18'30"	Jc	Gypsum bed 25 cm thick.
SRS11-84	38°31'07"	111°19'01"	Je	NW lobe of breccia.
SRS11-84	38°37'15"	111°11'52"	Je	Center of dike.
SRS13-84	38°42'48"	111°11'40"	Js	Center of dike.
SRS14-84	38°39'00"	111°18'45"	Je	Right margin of dike.
984SRS-15	38°42'53"	111°21'30"	Jc	Dike-host rock contact.
984SRS-16	38°42'17"	111°11'29"	Jc	Center of dike.
984SRS-17	38°34'14"	111°05'38"	Jc	dike-vein contact.

APPENDIX 2. LOCATION OF SAMPLES IN TABLE 3--continued

SAMPLE NUMBER	LATITUDE NORTH	LONGITUDE WEST	UNIT	SAMPLE LOCALITY DESCRIPTION
984SRS-17a	38°34'14"	111°05'38"	Jc	Fine-grained vein.
984SRS-18	38°34'15"	111°05'38"	Jc	dike-vein contact.
984SRS-19	38°34'15"	111°05'38"	Jc	Dike-host rock contact.
984SRS-20	38°34'16"	111°05'38"	Jc	West edge of bud.
984SRS-21	38°34'17"	111°05'38"	Jc	Dike-host rock contact.
984SRS-21a	38°34'17"	111°05'38"	Jc	Host rock 3m from contact.
984SRS-22	38°34'13"	111°05'38"	Jc	Altered gypsum/host rock.
984SRS-23	38°34'12"	111°05'38"	Jc	Hornfelsic rock near bud.
984SRS-24	38°31'00"	111°19'01"	Je	Center of dike.
984SRS-25	38°33'15"	111°23'47"	Je	Center of dike.
984SRS-26	38°26'45"	111°22'36"	Je	Center of dike.
984SRS-27	38°30'16"	111°07'38"	Jc	Center of bud.
984SRS-28	38°30'07"	111°07'32"	Jc	West edge of bud.
984SRS-29	38°32'09"	111°11'56"	Jc	Dike and vein.
984SRS-30	38°32'16"	111°13'08"	Jc	Center of dike.
984SRS-31	38°23'10"	111°14'28"	Jc	Center of dike.
984SRS-31a	38°23'03"	111°14'27"	Jc	Dike-vein contact
984SRS-32	38°22'55"	111°14'05"	Jc	Dike and vein.
984SRS-33	38°22'04"	111°12'30"	Jc	Center of dike.
984SRS-33a	38°21'30"	111°12'34"	Jc	Center of dike.
984SRS-35a	38°28'45"	111°05'37"	Je	Right margin of dike.
984SRS-35b	38°28'45"	111°05'37"	Je	Center of dike.
984SRS-35c	38°28'45"	111°05'37"	Je	Left margin of dike.
CR-132	38°16'45"	111°24'39"	Trm	Dike.
CR-176	38°20'30"	111°22'35"	Trc	Dike.

APPENDIX 2. LOCATION OF SAMPLES IN TABLE 3--continued

SAMPLE NUMBER	GEOGRAPHIC LOCATION	UNIT	SAMPLE LOCALITY DESCRIPTION
JG-A-1927	SW part of SRS, 15mi SE Emery UT	?	Mafic part of 30' composite sill.
JG-C-1927	SW part of SRS, 15mi SE Emery UT	?	Salic part of 30' composite sill.
W-36	San Rafael Swell 9mi S Emery Ut HW 10	?	Basalt flow.
W-37	San Rafael Swell Hebes Mtn. area	Je	Termintion of en echelon dike segment.
W-38	San Rafael Swell Hebes Mtn. area	Je	Margin basalt dike.
W-39	San Rafael Swell Hebes Mtn. area	Je	6" from dike contact.
W-40	San Rafael Swell Hebes Mtn. area	Je	4" from contact opposite #39.
W-41	San Rafael Swell Hebes Mtn. area	Je	Center of dike.
WLM-25	Average of 769 samples from the literature		Dolerite
WLM-26	Average of 405 samples from the literature		Diabase
WLM-27	Average of 3594 samples from the literature		Basalt

APPENDIX 3

APPENDIX 3. LISTING OF STRIKES AND PROPAGATION DIRECTIONS MEASURED ON DIKE WALL OUTCROPS IN THE SAN RAFAEL AND CAPITOL REEF AREAS, UTAH.

#	Segment Strike	Segment Propagation	Map dike Number	Aerial photo Number	Symbol[1]
1	N35W	40°NW	3	12-21	O
2	N43W	16°-30°NW	3	12-22	▲
3	N24W	70°,85°NW	18	5-20	Δ
4	N17W	50°NW	24	12-28	O
5	N13W	25°-40°SE	24	12-28	▲
6	N32W	60°NW,90°NW	40	12-30	Δ
7	N36W	20°NW	41	12-31	O
8	N36W	15°SE	41	12-31	O
9	N15W	05°NW	64	12-34	O
10	N10E	80°SW	65	12-32	O
11	N08E	50°SW	65	12-32	O
12	N02W	02°NW	73	12-33	O
13	N26W	50°,03°,90°SE	86	12-31	Δ
14	N20W	25°NW	99	2-89	O
15	N35W	20°,00°SE	101	2-89	Δ
16	N20W	60°,00°NW	101	2-89	Δ
17	09E	08°SW	102	2-90	O
18	N12E	05°NE	109	Map	O
19	N09W	00°,10-30°NW	110	Map	Δ,▲
20	N23W	08°-18°SE	111	2-82	▲
21	N21W	02°-04°SE	111	2-82	▲
22	N19W	68°NW	114	2-85	O

APPENDIX 3. LISTING OF STRIKES AND PROPAGATION DIRECTIONS MEASURED ON DIKE WALL OUTCROPS IN THE SAN RAFAEL AND CAPITOL REEF AREAS, UTAH--continued.

#	Segment Strike	Segment Propagation	Map dike Number	Aerial photo Number	Symbol[1]
23	N23W	45°NW	114	2-85	O
24	N48W	08°-15°NW	113	2-86	▲
25	N35W	25°-40°SE	117	2-86	▲
26	N22W	65°SE	117	2-88	O
27	N54W	00°-45°NW	117	2-88	▲
28	N35W	00°-20°NW	118	2-92	▲
29	N23W	10°,30°SE	119	2-87	Δ
30	N24W	30°-36°NW	119	2-87	▲
31	N35W	15°-60°NW	121	2-92	▲
32	N28E	05°,85°NE	123	2-92	Δ
33	N18E	15°SW	123	2-92	O
34	N01E	08°,10°SW	128	14-73	Δ
35	N13W	10°NW	130	14-73	O
36	N24W	05°NW	140	5-48	O
37	N22W	60°NW	140	5-48	O
38	N28W	30°,35°NW	141	5-48,50	Δ
39	N19W	00°,40°-75°SE	141	5-48	Δ,▲
40	N11W	55°-90°NW	146	Map	▲
41	N21W	55°-80°SE	3	12-22	▲
42	N05E	45°SW	102	2-90	O
43	N23W	04°NW	111	2-83	O

APPENDIX 3. LISTING OF STRIKES AND PROPAGATION DIRECTIONS MEASURED ON DIKE WALL OUTCROPS IN THE SAN RAFAEL AND CAPITOL REEF AREAS, UTAH--continued.

#	Segment Strike	Segment Propagation	Map dike Number	Aerial photo Number	Symbol[1]
44	N22W	08°,25°,35°SE	117	PD-1	▲
45	N08W	10°SE	116	PD-1	O
46	N24W	20°,35°,38°,50°SE	119	PD-1	▲
47	N14W	00°	117	PD-1	O
48	N35W	25°SE	117	PD-1	O
49	N52W	65°SE	117	PD-1	O
50	N30W	00°	117	PD-1	O
51	N14W	00°	117	PD-1	O

[1] O Single propagation direction measured on a dike wall outcrop

Δ Range of propagation directions measured on a dike wall outcrop

▲ Multiple propagation directions measured on a dike wall outcrop.

APPENDIX 4

APPENDIX 4. DETAILED PETROGRAPHIC DESCRIPTION OF THE INTRUSIVE ROCKS, SAN RAFAEL AND CAPITOL REEF AREAS, UTAH.

Sample: SRS1-84
General description: Fine grained olivine basalt containing miarolitic and amygdaloidal cavities.

Mineralogy	Mode	
Augite	45%	Large, miarolitic cavities lined with small labradorite grains in calcite matrix. Alteration extensive, skeletal olivine crystals replaced by serpentine and iddingsite along fractures. Amygdules (up to 4mm in diameter) filled with calcite, clays and serpentine. Augite (up to 0.5mm) contained as phenocrysts with some altered to hornblende.
Plagioclase	35%	
Olivine	tr	
Biotite	5%	
Magnetite	5%	
Calcite	5%	
Chlorite	tr	
Clay	3%	
Serpentine	tr	
Iddingsite	tr	
Apatite	tr	

Sample: SRS2-84
General description: Medium-grained olivine basalt with seriate and subophitic textures.

Mineralogy	Mode	
Augite	50%	Alteration minimal, olivine replaced by chlorite and serpentine along fractures. Large phenocrysts of augite and olivine (up to 1.5mm) in a microcystalline matrix of augite, biotite flakes and plagioclase microlites. Olivine rarely twinned; sector and hourglass zoning of augite. Glomeroporphyritic clots of augite and olivine. Apatite inclusions in augite phenocrysts.
Plagioclase	20%	
Olivine	15%	
Biotite	5%	
Magnetite	5%	
Chlorite	tr	
Serpentine	tr	
Calcite	tr	
Clay	3%	

Sample: SRS4-84
General description: Medium-grained olivine basalt with seriate and subophitic texture.

Mineralogy	Mode	
Augite	40%	Phenocryst of olivine with minimal alteration of serpentine along fractures. Glomeroporphyritic clots of augite, with some small patches of altered brown glass. Hourglass zoning of some augite phenocrysts. Serpentine alteration along small fractures in the slide. Minimal alteration of plagioclase to analcite.
Plagioclase	20%	
Olivine	20%	
Biotite	20%	
Magnetite	10%	
Serpentine	tr	
Analcite	tr	
Apatite	tr	

Sample: SRS5-84
General description: Olivine basalt with porphyritic texture.

Mineralogy	
Augite	Extensively altered thin section. Altered olivine, euhedral augite and biotite flakes contained in a cryptocrystalline matrix. Skeletal olivine almost totally altered to calcite and serpentine. Small areas of iddingsite also seen in fractures of olivine. Augite phenocrysts are twinned and have simple and hourglass sector zoning. Irregular patches of analcite. Euhedral grains of titanomagnetite as inclusions in augite and in the matrix.
Plagioclase	
Olivine	
Biotite	
Magnetite	
Calcite	
Clay	
Iddingsite	
Serpentine	
Analcite	

Sample: SRS6-84
General description: Fine-grained olivine basalt with seriate and glomeroporphyritic textures.

Mineralogy	
Augite	Extensive alteration of olivine, skeletal phenocrysts remaining, completely replaced by calcite, serpentine, chlorite and occassionally iddingsite. Augite extensively zoned-sector and oscillatory; containing fine-grained brown glass, magnetite and augite inclusions. Glomeroporphyritic clots of augite, biotite, plagioclase and magnetite. Irregular patches of analcite and calcite.
Plagioclase	
Magnetite	
Biotite	
Analcite	
Serpentine	
Calcite	
Iddingsite	

Sample: SRS7-84
General description: Vesicular olivine basalt with seriate and glomerophyritic textures.

Mineralogy	Mode	
Augite	35%	Extensive alteration of olivines, olivine pseudomorphs of chlorite, serpentine, iddingsite and small patches of calcite. Irregular vesicles, some have serpentine rims and partially filled with calcite. Glomeroporphyritic clots of augite, less alteration than previous sample, sector and oscillatory zoning. Phenocrysts range from 0.01 to 0.6mm. Small patches of clay alteration present throughout thin section. Plagioclase phenocrysts highly embayed and contain small grains of biotite and augite.
Plagioclase	25%	
Olivine	5%	
Biotite	10%	
Magnetite	10%	
Calcite	3%	
Serpentine	5%	
Iddingsite	5%	
Clay	5%	

Sample: SRS8-84
General description: Medium-grained olivine basalt with seriate and glomeroporphyritic textures.

Mineralogy	Mode	
Augite	30%	Very extensive alteration of olivine to
Plagioclase	20%	pseudomorphs of serpentine, iddingsite and
Olivine	5%	calsite, very rare anhedral grains of orig-
Biotite	15%	inal olivine. Glomeroporphyritic clots
Magnetite	7%	of augite, plagioclase and titanomagnetite
Iddingsite	5%	Small patches of brown glass altered to clay.
Serpentine	10%	Augite phenocrysts up to 0.5mm with sector
Calcite	5%	and oscillatory zoning.
Clay	3%	

Sample: SRS9-84
General description: Fine-grained olivine basalt with porphyritic and glomeroporphytic textures, containing vesicles.

Mineralogy	
Augite	Highly vesicular sample, up to 15% of thin-
Plagioclase	section, irregular shaped with some cal-
Olivine	cite. Very small % of original olivine
Biotite	phenocrysts remain, now calcite pseudo-
Magnetite	morphs. Glomeroporphytic clots of augite
Calcite	and plagioclase. Biotite as patches and
Thomsonite	flakes with some chlorite alteration along
Hornblende	cleavage. Rare augite phenocryst altered
Chlorite	to hornblende. Matrix cryptocrystalline.
Serpentine	Grains of titanomagnetite as fine peppering
Clay	throughout matrix. Plagioclase minimally
	altered to thomsonite. Small patches of
	clay alteration in the matrix.

Sample: SRS10-84
General description: Gypsum-fibrous type from bed in the Carmel Formation.

Mineralogy	
Gypsum	20cm thick gypsum bed. Sample analysed by
	x-ray diffraction.

Sample: SRS11-84
General description: Peperite containing olivine basalt and quartz sandstone.

Mineralogy	
Quartz	Consists of patches of altered basaltic material and host rock. Approximately 50% of the thin section is microcrystalline quartz grains and fine grained clay alteration. Basaltic material is extensively altered, olivine pseudomorphs, augite phenocrysts embayed and contain inclusions of magnetite and biotite.
Augite	
Olivine	
Plagioclase	
Apatite	
Serpentine	
Clay	
Magnetite	

Sample: SRS12-84
General description: Fine-grained olivine basalt with porphyritic texture containing amygdaloidal cavities.

Mineralogy	
Augite	Extensive alteration of olivine, skeletal olivine crystals replaced by calcite, with iddingsite and serpentine along fractures. Amygdules up to 0.25mm filled with calcite, and serpentine. Plagioclase, biotite, augite matrix altered to clay and serpentine patches. Alteration of biotite to chlorite along cleavage.
Biotite	
Olivine	
Plagioclase	
Chlorite	
Clay	
Magnetite	
Calcite	
Iddingsite	

Sample: SRS13-84
General description: Fine-grained olivine basalt with porphytitic and glomeroporphyritic textures, with vesicular amygdaloidal cavities.

Mineralogy	
Augite	Highly altered olivine phenocrysts to pseudomorphs of calcite, clay and serpentine. Subhedral augite phenocrysts show sector and oscillatory zoning and rare penetration twins, Rare phenocrysts of aegirine rimmed augite. Approximately 25% cryptocrystalline matrix, containing patches of clay mineral alteration. Rare analcite alteration of plagioclase. Glomeroporphyritic clots of augite and olivine. Vesicles up to 0.5mm; amygdules partially filled with analcite and calcite crystals.
Plagioclase	
Olivine	
Biotite	
Magnetite	
Calcite	
Analcite	
Serpentine	
Clay	

Sample: SRS14-84
General description: Olivine basalt with porphyritic texture, containing amygdaloidal cavities.

Mineralogy	Mode	
Augite	40%	Amygdules, irregularly shaped ranging from
Plagioclase	20%	0.3 to 3.25mm, rimmed with serpentine and
Olivine	3%	filled with calcite; total number of 25 on
Biotite	5%	the thin section. Calcite pseudomorphs of
Calcite	10%	of olivine, rare anhedral olivine grains.
Serpentine	5%	Microphenocrysts of augite, plagioclase and
Iddingsite	2%	biotite in the matrix, partially altered to
Magnetite	7%	to clay. Rare iddingsite and chlorite
Clay	3%	alteration of olivine.
Chlorite	tr	

Sample: 984SRS-15
General description: Medium-grained olivine basalt with seriate and glomeroporphytic textures, containing vesicular and amygdaloidal cavities.

Mineralogy	Mode	
Augite	45%	Varying degree of alteration, simple and
Plagioclase	15%	complex skeletal phenocrysts up to 3mm in
Olivine	10%	length, some show alteration to iddingsite
Biotite	10%	and serpentine along fractures. Spherical
Analcite	2%	vesicles up to 1.0mm in diameter and amyg-
Serpentine	5%	dules up to 0.2mm partially filled with cal-
Iddingite	5%	cite and thomsonite. Plagioclase partially
Apatite	tr	altered to analcite and thomsonite. Glom-
Thomsonite	2%	eroporphyritic clots up to 3.0mm of euhedral
Magnetite	5%	and branching augite grains containing al-
		tered brown glass, biotite and magnetite.
		Some sector zoning of the augite.

Sample: 984SRS-16
General description: Fine-grained olivine basalt containing amygdaloidal cavities.

Mineralogy	
Analcite	No thin section. Cavity filling analysed by
Thomsonite	x-ray diffraction. Cavities up to 5cm in
Calcite	diameter.
Clay	
Natrolite	

Sample: 984SRS-17
General description: Olivine basalt with seriate and subophitic textures.

Mineralogy	Mode	
Zircon	tr	Varying degree of alteration of olivine
Augite	40%	phenocrysts to iddingsite, cholite and
Plagioclase	25%	serpentine. No sharp crystal faces on
Olivine	10%	plagioclase. Patches of alteration up to
Biotite	15%	3.0mm in diameter where plagioclase is
Magnetite	5%	altered to thomsonite and analcite.
Iddingsite	3%	Biotite grains show chlorite alteration
Serpentine	4%	along cleavage. Clay alteration also
Chlorite	tr	present on the thin section along small
Clay	tr	fractures.
Alamcine	tr	
Thomsonite	tr	

Sample: 984SRS-17a
General description: Microcrystalline olivine basalt with porphoritic and glomeroporophyrtic textures containing vesicular and amygdaloidal cavities.

Mineralogy	
Augite	Olivine pseudomorphs containing iddingsite
Plagioclase	along crystal faces and fractures, partially
Olivine	altered to serpentine with some original un-
Biotite	altered olivine ramaining. Unfilled ves-
Magnetite	icles up to 1.0mm in diameter. Amygdules
Thomsonite	partially filled with calcite, serpentine, and
Analcite	natrolite. Patches of plagioclase partially
Apatite	altered to thomsonite and analcite. Glomero-
Iddingsite	porphyritic clots of augite, biotite, plagio-
Serpentine	clase and magnetite. Matrix cryptocrystalline.
Natrolite	

Sample: 984SRS-18
General description: Olivine basalt with seriate and glomeroporphyritic textures, containing veins of cryptocrystalline basaltic material and miarolitic cavities with amygdaloidal cavities.

Mineralogy	Mode	
Augite	35%	Varying degree of alteration of olivine
Plagioclase	30%	phenocrysts to iddingsite and serpentine,
Olivine	10%	some anhedral olivine present in each
Biotite	10%	phenocryst. Large patches (up to 4.0mm)
Serpentine	5%	of thomsonite, serpentine and clay through-
Iddingsite	5%	out thin section. Plagioclase altered to
Clay	2%	thomsonite and analcite. Biotite as patches

Magnetite	7%	and flakes with small amounts of chlorite
Analcite	tr	along cleavage. Miarolotic cavities lined
Thomsonite	1%	0.01mm labradorite needles. Natrolite in the
Natrolite	tr	the amygdules range 0.01 to 0.5 mm in diameter.

Sample: 984SRS-19
General description: Contact margin of olivine basalt dike.

Mineralogy	Mode	
Augite	45%	Margin of dike, thin section contains very
Plagioclase	20%	fine-grained augite grains that represent
Biotite	15%	the contact of the dike and makes up 75% of
Olivine	10%	thin section, remaining 25% is composed of
Magnitite	5%	olivine, augite, and biotite phenocrysts.
Serpentine	3%	Olivine shows varying degee of alteration
Iddingsite	2%	to iddingsite and serpentine, zircon in-
Zircon	tr	clusions in some of the least altered
Analcite	tr	olivine. Patches of plagioclase altered to
Clay	tr	anaclite. Rare small patches of brown glass altered to clay.

Sample: 984SRS-19a
General description: Cryptocrystalline basalt.

Mineralogy	
Augite	Cryptocrystalline equant grains of augite
Clay	with patches and stringers of clay and cal-
Calcite	cite alteration. 90% of the thin section is augite the remaining 10% is alteration.

Sample: 984SRS-20
General description: Olivine basalt with banded and subophitic textures.

Mineralogy	
Augite	Layered sequence of fine-grained and medium
Plagioclase	grained augite titanomagnetite, plagioclase,
Biotite	calcite, biotite and various alteration of
Magnetite	the constituents. Contact between the two
Olivine	is very distinct and grades from medium to
Iddingsite	finer grains. One large crack on thin
Serpentine	section filled with thomsonite, analcite,
Analcite	serpentine and ? clay minerals. A second
Thomsonite	crack is filled with brown glass, no al-
Hornblende	teration of glass evident. Several large phenocrysts of anhedral augite converted to brown hornblende

Sample: 984SRS-24
General description: Olivine basalt with seriate and subophitic textures, containing vesicular and amygdaloidal cavities.

Mineralogy	Mode
Augite	35%
Plagioclase	25%
Olivine	tr
Biotite	10%
Calcite	10%
Magnetite	10%
Analcite	tr
Iddingsite	tr
Serpentine	10%

Amygdules, up to 2.0mm, partially or completely filled with calcite and analcite and rimmed with serpentine; total of 25 on the on the thin section. Spherical vesicles up to 0.5mm also present but less abundant than amygdules. Skeletal olivines almost totally altered to serpentine, iddingsite and calcite. Augite phenocrysts show rare twinning, simple sector and hourglass zoning. Large patches up to 3.0mm of palgioclase altered to euhedral analcite crystals.

Sample: 984SRS-25
General description: Extensively altered olivine basalt with porphyritic texture, containing vesicles and partially filled amygdules.

Mineralogy	Mode
Calcite	30%
Augite	25%
Plagioclase	20%
Biotite	10%
Serpentine	5%
Chlorite	tr
Magnetite	10%
Apatite	tr
Analcite	tr

Very extensive alteration of the sample, calcite alteration pervasive throughout entire slide. One large vesicle 5cm in the center of thin section. Amygdules up to 0.7mm partially and completely filled with calcite. Biotite flakes partially altered to chlorite along cleavage. Skeletal olivine completely altered to calcite and serpentine. Plagioclase curved and partially altered to analcite.

Sample: 984SRS-26
General description: Olivine basalt with seriate and glomeroporphyritic textures.

Mineralogy	Mode
Augite	35%
Biotite	15%
Plagioclase	20%
Magnetite	10%
Olivine	3%
Analcite	3%
Serpentine	2%
Thomsonite	tr
Calcite	10%
Chlorite	tr

Glomeroporphyritic clots of augite, biotite and magnetite. Skeletal olivine now calcite, serpentine and chlorite pseudomorphs. Augite twinned and zoned (hourglass and simple). Biotite flakes bent with minimal chlorite alteration. Plagioclase embedded in analcite and thomsonite. Patches of clay and serpentine alteration. Small hornblende surrounding anhedral augite.

Sample: 984SRS-27
General description: Altered olivine basalt with seriate, intersertal and subophitic textures, containing amygdaloidal cavities.

Mineralogy	Mode	
Augite	35%	Olivine altered to serpentine, clay and chlorite. Amygdules up to 1.25mm partially filled with calcite. Plagioclase embedded in analcite. Augite phenocrysts have sieve texture, corroded, sector zoning, contain pools of brown glass. Pools of brown glass altered to clay minerals. Microlites of plagioclase throughout slide.
Plagioclase	20%	
Biotite	10%	
Analcite	5%	
Calcite	12%	
Serpentine	5%	
Magnetite	7%	
Clay	3%	

Sample: 984SRS-28
General description: Olivine basalt with seriate texture contains large calcite vein on one edge of the thin section and amygdaloidal cavities.

Mineralogy	Mode	
Calcite	20%	Large 3cm wide calcite vein on top edge of thin section, small amount of basaltic material incorporated in the calcite vein. Amygdules up tp 3mm filled with calcite and analcite, most rimmed with serpentine. Olivine phenocrysts almost totally altered to serpentine, with some small patches of calcite. Augite highly corroded, with a sieve texture, some sector zoning presnt.
Analcite	3%	
Serpentine	10%	
Augite	40%	
Plagioclase	15%	
Biotite	5%	
Magnetite	7%	

Sample: 984SRS-29
General description: Olivine basalt containing a 4mm wide vein of finer grained biotite and plagioclase.

Mineralogy	Mode	
Augite	35%	Vein of bent biotite flakes and plagioclase bisecting the thin section, rare augite crystal set in a cryptocrystalline matrix, with small patches of brown glass. Skeletal olivine altered to serpentine but some anhedral olivine remains. Plagioclase curved and altered to analcite and thomsonite. Augite show sector and oscillatory zoning.
Plagioclase	25%	
Olivine	3%	
Serpentine	10%	
Biotite	10%	
Calcite	5%	
Magnetite	8%	
Analcite	2%	
Thomsonite	1%	

Sample: 984SRS-30
General description: Olivine basalt with a seriate, glomeroporphyritic and intersertal textures.

Mineraloogy	Mode
Augite	45%
Olivine	10%
Plagioclase	5%
Biotite	15%
Iddingsite	3%
Analcite	2%
Thomsonite	1%
Magnetite	10%
Serpentine	5%

Olivine phenocrysts show minimal alteration along fractures to iddingsite and rarely serpentine. Plagioclase extensively altered to analcite and thomsonite. Patches of murky brown glass with some alteration to to clay. Clots of augite, biotite and magnetite.

Sample: 984SRS-31
General description: Margin of olivine basalt dike with seriate and intersertal textures.

Mineralogy	Mode
Augite	30%
Biotite	10%
Plagioclase	10%
Magnetite	10%
Calcite	5%
Quartz	20%
Glass	5%
Clay	tr

Margin of brown glass and large 8cm anhedral quartz crystal with small amounts of calcite and clay alteration along fractures of the grain. Remainder of slide contains relict olivine crystals, augite, biotite, plagioclase and magnetite.

Sample: 984SRS-31a
General description: Olivine basalt with seriate, glomeroporyphitic and intersertal textures.

Mineralogy	Mode
Augite	40%
Olivine	5%
Iddingsite	10%
Serpentine	3%
Chlorite	tr
Biotite	10%
Plagioclase	20%
Magnetite	10%
Analcite	3%

Olivine phenocrysts partially altered to serpentine and iddingsite along fractures. Clots of augite, altered glass and magnetite. Small patches up to 0.5mm of murky brown glass. Augite phenocrysts zoned and twinned. Plagioclase embedded in analcite.

Sample: 984SRS-32
General description: Olivine basalt with two distinct sections of the thin section, one cryptocrystalline and the second microcrystalline.

Mineralogy	
Augite	Slide composed of two distinct sections.
Olivine	The first part contains olivine pheno-
Chlorite	crysts in a cryptocrysatlline matrix.
Serpentine	Olivine altered to chlorite, serpentine,
Iddingsite	and iddingsite. Rare euhedral augite
Thomsonite	present. The second half of slide is
Plagioclase	composed of a microcrystalline olivine
Magnetite	where olivine is altered the same as previously described. Plagioclase is curved and embedded in thomsonite. Biotite flakes and patches present. Contact between two is very sharp.

Sample: 984SRS-33a
General description: Olivine basalt with a porphyritic and glomeroporphyritic textures, containing amygdaloidal cavities.

Mineralogy	
Augite	Olivine and augite phenocrysts set in a
Olivine	cryptrocrystalline matrix of plagioclase
Magnetite	augite and biotite. Olivine partially
Biotite	altered to serpentine and iddingsite along
Calcite	fractures. Irregular patches of calcite
Analcite	and analcite, plagioclase embedded in anal- cite. Augite phenocrysts up to 0.5mm with a sieve texture of glass inclusions. Skel- etal olivine up to 1.25mm. Amygdules up to 1.5mm partially filled with calcite and analcite, rimmed with serpentine.

Sample: 984SRS-33
General description: Fine-grained olivine basalt from center of the dike, with porphyritic and glomer- oporphyritic textures, containing amygdaloidal cavities.

Mineralogy	
Augite	Altered sample with skeletal olivine (up to
Olivine	1.25mm) partially altered to iddingsite and
Analcite	serpentine along fractures. Augite up to
Magnetite	0.5mm, twinned phenocrysts with sector and
Serpentine	oscillatory zoning. Plagioclase embedded in
Plagioclase	analcite. Amygdules up tp 1.0mm rimmed with
Biotite	serpentine and partially filled with anal- cite and calcite. A number of euhedral

analcite grains throughout the thin section. Clots of augite, palgioclase, biotite and magnetite.

Sample: 984SRS-35a
General description: Microcrystalline olivine basalt with seriate texture.

Mineralogy

Augite	Skeletal olivines completely replaced by calcite, serpentine and chlorite. Microlites of plagioclase, biotite, augite and magnetite show a crude flow texture or an orientation of the grains. Small stringers of plagioclase laths and biotite flakes exhibit a flow-like structures. Small patches of analcite and serpentine noted throughout the slide.
Biotite	
Plagioclase	
Magnetite	
Analcite	
Serpentine	
Calcite	
Chlorite	

Sample: 984SRS-35b
General description: Olivine basalt with seriate texture, containing vesicular and amygdaloidal cavities.

Mineralogy

Augite	Right 1/3 of slide has similiar texture and mineralogy as previous slide. Relict olivines totally replaced by calcite. Laths of plagioclase, augite, magnetite and biotite flakes compose the remaining 2/3 of the slide. Plagioclase phenocrysts up to 1.25 mm in length are curved and branch possibly in the direction of flow. Amygdules up to 0.5mm partially filled with calcite and rimmed with serpentine.
Biotite	
Plagioclase	
Magnetite	
Calcite	
Serpentine	

Sample: 984SRS-35c
General description: Basalt with subophitic texture, containing vesicular and amygdaloidal cavities.

Mineralogy

Augite	Augite phenocrysts (up to 3.0mm) make up approximately 80% of the slide. Augite is curved and branching and is in subparallel alignment. The remainder of the slide is made up of microlites of plagioclase, biotite flakes, and magnetite. A few vesicles up to 0.3mm are also present. Amygdules up to 0.5mm are partially filled with calcite and partially altered brown glass
Biotite	
Plagioclase	
Calcite	
Magnetite	

Sample: Cathedral Plug
General description: Olivine basalt with seriate, subophitic, and glomeroporphyritic textures.

Mineralogy	Mode	
Augite	50%	Fresh, minimally altered sample.
Zircon	1%	Euhedral olivine phenocrysts up to
Olivine	20%	3.25mm with minimal iddingsite and
Plagioclase	20%	chlorite alteration along fractures,
Biotite	4%	contain euhedral zircon inclusions,
Magnetite	5%	embayed and filled with plagioclase
Chlorite	tr	laths, biotite flakes and augite.
Iddingsite	tr	Rare patches of murky brown glass.
		Augite phenocrysts, up to 0.25mm, twinned (simple penetration) with sector (hourglass) and oscillatory zoning present. Clots of olivine.

Sample: 82SRS-2
General description: Olivine basalt with seriate and intersertal textures, containing vesicular and amygdaloidal cavities.

Mineralogy	Mode	
Augite	40%	Skeletal olivine partially replaced by cal-
Plagioclase	15%	cite with some serpentine and iddingsite
Olivine	10%	along fractures. Small anhedral grains of
Biotite	10%	olivine remain. Augite (up to 0.6mm) phen-
Magnetite	tr	ocrysts show sector and oscillatory zoning.
Calcite	15%	Amygdules up to 0.2mm partially filled with
Clay	2%	calcite and rimmed with serpentine. Small
Serpentine	tr	pools (up to 0.03mm) of brown glass partial-
Magnetite	5%	ly altered to clay. Spherical vesicles up
Iddingsite	tr	0.1mm throughout thin section.

Sample: 82SRS-3
General description: Olivine basalt with subophitic and glomeroporphyritic textures.

Mineralogy	Mode	
Augite	40%	Fresh, relatively unaltered sample, with no
Olivine	20%	secondary zeolitic alteration present.
Biotite	8%	Olivine phenocrysts up to 3.0mm with rare
Plagioclase	25%	iddingsite and chlorite alteration along
Magnetite	5%	fractures. Few olivines embayed with
Clays	tr	magnetite, augite and plagioclase inclusions.
Iddingsite	tr	Augite phenocrysts up to 0.5mm, containing
Serpentine	tr	inclusions of brown glass and magnetite;
Chlorite	tr	some sector and oscillatory zoning of
Horneblende	tr	crystals. Glomeroporphyritic clots of ol-
		vine and augite phenocrysts. Rare hornblende noted on the crystal faces of augite.

Sample: 82SRS-8
General description: Extensively altered olivine basalt with seriate and glomeroporphyritic textures.

Mineralogy	Mode	
Augite	50%	Skeletal olivines now calcite pseudomorphs, with some chlorite and serpentine alteration along fractures and crystal faces. Patches of magnetite in the olivine phenocrysts. Clots of augite throughout the slide. Phenocrysts of augite up to 0.7mm containing fine-grained magnetite and glass inclusions, also exhibit hourglass zoning and twinning. Minimal alteration of biotite flakes to cholrite along cleavage.
Plagioclase	15%	
Olivine	5%	
Biotite	5%	
Magnetite	5%	
Calcite	5%	
Chlorite	2%	
Serpentine	3%	

Sample: 82SRS-9
General description: Olivine basalt with seriate and glomeroporphyritic texture.

Mineralogy	Mode	
Augite	35%	Olivine phenocrysts up to 1.2mm with some iddingsite and serpentine alteration along fractures, some phenocrysts embayed and filled with magnetite and augite grains. Biotite flakes, some bent and show minimal chlorite alteration along cleavage. Augite zoned and twinned, and contain small inclusions of magnetite and augite. Small grains of analcite noted on the slide.
Plagioclase	25%	
Olivine	10%	
Biotite	5%	
Calcite	1%	
Magnetite	10%	
Iddingsite	2%	
Serpentine	2%	
Analcite	tr	